SPECIAL HANDLING

SHC65-9015-314/2
Copy No. 10

VOLUME TWO
PROJECT 9015
FINAL REPORT
1960 - 1964

June 1965

SPECIAL HANDLING

Approved For Release 2000/04/12 : CIA-RDP67B00657R000300150001-1

Abstract

This volume contains the appendixes to the 9015 Project Final Report*. Most of the appendixes are reports written on the project. The reports have not been updated to include later results or to reflect current thinking, but they have been reviewed and found to be essentially correct.

The dates of the original work are as follows:

Appendix I	-------
II	March 1961
III	December 1964
IV	February 1963
V	-------
VI	December 1964
VII	November 1964
VIII	February 1963
IX	May 1963
X	February 1964
XI	-------
XII	June 1963
XIII	September 1964
XIV	February 1964
XV	December 1964

*Itek Document Number SHC65-9015-314/1, Volume One.

LIST OF APPENDIXES

Appendix I

DOCUMENTS

Appendix I

DOCUMENTS

This is a list of the documents generated at Itek on the 9015 project.

Project Reports

Model 9015 Processor Final Report	May 1964	SHC64-9015-310
9015 Project Final Report, Volume I	June 1965	SHC65-9015-314/1
Appendixes, Volume II	June 1965	SHC65-9015-314/2
9015 Project Report, Jan-June 1965	June 1965	SHC65-9015-315

These four volumes cover all phases of the project up to June 1965. The Processor report is often referred to in the Project report as reference 1. The latest report covering the period January to June 1965 covers specific studies on noise and stray light.

Progress Reports

Progress Report	November 1961	SHC61-9015-158G
Progress Report	December 1961	SHC62-9015-08
Progress Report	January 1962	SHC62-9015-57
Progress Report	February 1962	SHC62-9015-77
Progress Report	March 1962	SHC62-9015-176
Progress Report	April 1962	SHC62-9015-172
Progress Report	May 1962	SHC62-9015-195
Progress Report	June 1962	SHC62-9015-237
Progress Report	July 1962	SHC62-9015-238

Progress Reports (continued)

Progress Report	Aug/Sept 1962	SHC62-9015-331
Progress Report	October 1962	SHC62-9015-359
Progress Report	November 1962	SHC62-9015-384
Progress Report	December 1962	SHC63-9015-42
Progress Report	January 1963	SHC63-9015-77
Progress Report	February 1963	SHC63-9015-103
Progress Report	March 1963	SHC63-9015-159
Progress Report	April 1963	SHC63-9015-190
Progress Report	May 1963	SHC63-9015-250
Progress Report	June 1963	SHC63-9015-312
Progress Report	July 1963	SHC63-9015-342
Progress Report	August 1963	SHC63-9015-385
Progress Report	September 1963	SHC63-9015-433
Progress Report	October 1963	SHC63-9015-478
Progress Report	November 1963	SHC63-9015-535
Progress Report	Dec/Jan 1964	SHC64-9015-81
Progress Report	Feb/March 1964	SHC64-9015-219
Progress Report	April 1964	SHC64-9015-267
Progress Report	May 1964	SHC64-9015-329
Progress Report	June 1964	SHC64-9015-432
Progress Report	July 1964	SHC64-9015-441
Progress Report	August 1964	SHC64-9015-503
Progress Report	September 1964	SHC64-9015-582
Progress Report	October 1964	SHC64-9015-666
Progress Report	November 1964	SHC64-9015-770

Progress Reports (continued)

Progress Report	December 1964	SHC65-9015-30
Progress Report	January 1965	SHC65-9015-120
Progress Report	February 1965	SHC65-9015-138
Progress Report	March/April 1965	SHC65-9015-241
Progress Report	May 1965	SHC64-9015-278

Proposals

Proposal 6B -- Basic proposal submitted by [redacted] 25X1A

25X1A

Proposal 3155 July 1960
Itek proposal to cover work on 6B proposal

Added Task Submission June 1962 SHC61-9015-157
Change to processor necessitated by system changes.
Auxiliary facilities and equipment.

Proposal 3320 August 1961 SHC-209-61
Addendum October 1961 SHC61-9015-271
Test and Simulation Program

Proposal 3334 August 1961 SHC61-9015-209
F101 Flight Test Support

Added Scope Proposal January 1962 SHC62-9015-04
Revision January 1962 SHC62-9015-24
New Optical System to accommodate system changes.
Film Drive modifications.
Interface Engineering

Program Recommendations June 1962 SHC62-9015-194
Added Scope Proposal July 1962 SHC62-9015-215
Further Test and Simulation Effort
Special Purpose Optical Bench Processor
Continuation of F101 Flight Test Support

Follow-on Proposal April 1963 SHC63-9015-161
Installation of TV Viewing Station
Continuation of F101 Flight Test Support
Interface Engineering
Experimental Processor
Special Purpose Optical Bench for field use

Proposals (continued)

9015 Follow-on Proposal Field Service Test Support Correlator Modifications and Detail Correlator System Theory and Experiment Improved Correlator	March 1964	SHC64-9015-168

In addition, the following proposal was initiated in connection with this program; but it covered work concerned primarily with the recorder.

Proposal for Optimum Parameters	February 1962	SHC62-9015-38

The following proposals and work statements involved separate projects, but they are an outgrowth and continuation of the work on the 9015 system.

Statement of Work Proposed Study and Experimentation Efforts to further "Exploitation of Radar Imagery"	July 1964	SHC64-3529-388
Detail Correlation Configuration and Performance	September 1964	SHC64-3529-506
Project 9015 Statement of Work	January 1964	SHC65-9015-53

Miscellaneous Documents

Preliminary Specification	November 1960	SHC9015-60-1R
Instruction Manual Volume I	February 1963	not classified
Instruction Manual Volume II	February 1963	SHC63-9015-102
Final Report, Test and Simulation Program (Note: This document is superseded by the Project Final Report where the entire contents of SHC63-9015-143 is up dated and reproduced)	April 1963	SHC63-9015-143
Effect of Film Exposure on Recorder/Correlator Performance (This work is included in this volume as Appendix XII)	June 1963	SHC63-9015-544
Letter to Peter Hall Subject: "Relocation of Correlation Activity"	September 1964	SHC64-9015-505

Appendix II

INVESTIGATION INTO LIQUIDS SUITABLE FOR IMMERSION PRINTING

Appendix II

INVESTIGATION INTO LIQUIDS SUITABLE FOR IMMERSION PRINTING

In the selection of liquids to be considered, it was important that the following be taken into consideration:

(1) Liquid must have an index of refraction close to 1.50, in that the cellulose tri-acetate films will average close to 1.48, with the estar base types averaging close to 1.58.

(2) Liquid must be safe to handle, insofar as personnel are involved, or, non-toxic.

(3) Liquid must not be flammable.

(4) It must not affect the film adversely, neither emulsion nor base, during or after the immersion.

(5) It should have sufficient viscosity to maintain the film in the center of passage.

(6) Liquid must dry quickly and easily, and leave no residue.

(7) It should be readily obtainable.

(8) Liquid cannot be absorbed into, either base or emulsion.

In the SMPTE Journal of October 1957 a group of twenty solutions were listed. Inasmuch as many of these liquids could not be used for various

reasons, such as dissolving the film plasticizers, being toxic or flammable, the following list was compiled. Several other compounds were tried also.

(1)	Trichlorethane	Index 1.48
(2)	Orthodichlorbenzene	1.55
(3)	Methanol (Methyl Alchohol)	1.33
(4)	Carbon Tetrachloride	1.460
(5)	GE Refractasil	1.46
(6)	Tetrachlorethylene	1.504
(7)	O-xylene	1.505

Preliminary tests consisted of soaking 1" x 10" strips of both the acetate and mylar films in small containers of the liquid, then drying normally, (drain and by air) and then also utilizing an improvised pair of rubber rollers, producing a squeegee effect. Following are the results.

1.0 Trichlorethane

This solution was discarded immediately, in that it is a solvent for the film plasticizer, particularly with the Mylar types. It also raised havoc with the plexiglass breadboards. Produced extreme curl and disfiguration of the film.

2.0 Orthodichlorbenzene

Although there was no apparent damage to the films, the liquid is most unpleasant to use and would require extreme venting. Dried normally in about 3 minutes, in about 30 seconds when roller squeegee was used. The film seems to retain the odor for an hour or longer following drying.

3.0 Methanol

Viscosity seems low, and the liquid is flammable. Dries very quickly

and produced no bad effects other than slight curl following drying with the roller squeegee.

4.0 Carbon Tetrachloride

Dried very rapidly, both normally and with roller squeegee. Viscosity is low and would anticipate problem in complete wetting of the film. This solution also has property of slightly charging the film, thereby enhancing its dust gathering capabilities.

5.0 Refractasil

Dried very slowly by air methods, but quite rapidly by roller squeegee. However, the rollers do take up a considerable amount of the solution, which over a long length of film could conceivably affect its ability to remove the refractasil, a bath of carbon tetrachloride immediately following the refractasil bath speeded up drying markedly with the roller squeegee system, and did not load up the rollers as badly. Printing properties are excellent, with no adverse affects of any kind.

6.0 Tetrachlorethylene (Perchlorethylene)

This solution has been used with success by the technicolor corp., in a similar application, and results of tests here proved this to be worthy of serious consideration. No apparent ill effects on the films were noted, its viscosity is very good, it produces no curl or softening and dries most rapidly.

7.0 Summary

On the basis of these findings, the refractasil and the tetrachlorethylene were selected as the two most outstanding, and the following tests were conducted, now using the breadboard platen.

Brass shims of .005", .0075" and .010" were prepared to be used as separators in the platen.

The .005" was quickly discarded as it did not provide adequate spacing, even with the .004" Mylar film. With the .010" shim it appeared that more bubbles occurred between negative and platen surfaces, so the .0075" shim was used for following tests.

$9\frac{1}{2}$" aerial film was used and it was quickly apparent that the best method of using this platen is to push the negative through the solution, with the sections firmly bolted together. Trying to close the platen with either the refractasil or the tetrachlorethylene resulted in definite bubble formations that are virtually impossible to remove. Air trapped between the faces of the platen is responsible for this. Either a sliding system or an immersed hinge affair might solve this, but threading the negative through the slot definitely eliminates bubbles. Previous experience with this type of printing has proved that it is most difficult to remove bubbling by a sandwich pressure system. Apparently too much separation between faces can add to bubble trouble, while too little will bind. These tests seem to indicate that an approximate clearance of .0025" is adequate, for the .005" films.

This report, originally written early in 1960, was reviewed in May 1965. No new materials or methods are available and the continued use of tetrachlorethelene is recommended.

Appendix III

EFFECTS OF FINITE BANDWIDTH IN THE LIGHT SOURCE

Appendix III

EFFECTS OF FINITE BANDWIDTH IN THE LIGHT SOURCE

1.0 Introduction

The focusing property of a hologram is dependent on the wavelength of the light, the focal length being inversely proportional to the wavelength. Thus a diffraction limited image can only be obtained with monochromatic light, such as that from a laser or a low pressure gas discharge lamp.

An incandescent source such as a carbon arc produces white light which must be filtered before it can be employed for the correlation of holograms. For practical reasons light obtained from a filtered "white" source is never completely monochromatic. The fractional bandwidth $\frac{\Delta\lambda}{\lambda}$ may be small (0.4% in the present system) but is nonetheless an important factor in the performance of an optical correlator.

1.1 Resolution Without Compensation

The resolution obtained for a given value of $\Delta\lambda$ depends on the highest hologram frequency.

If δ_1 = image diameter due to filter bandwidth alone.

δ_2 = image diameter due to hologram bandwidth alone.

δ_3 = image diameter due to all other causes, assumed constant.

Then if the image functions are approximately Gaussian in form,

overall resolution is

$$\delta_T = \sqrt{\delta_1^2 + \delta_2^2 + \delta_3^2}$$

We will hold δ_3 constant, and will determine δ_1 and δ_2 in terms of

filter wavelength λ millimicrons

filter bandwidth $\Delta\lambda$ millimicrons

hologram bandwidth W cycles/inch

(half power bandwidth of Guassian passband)

Diffraction angle $\theta = f_H \cdot \lambda$

where f_H = hologram frequency.

Thus, $\Delta\theta = f_H \cdot \Delta\lambda$

If F is hologram focal length

M is (azimuth) magnification

Then in the absence of any chromatic correction δ_1 and δ_2 can be approximated by

$$\delta_1 = \frac{F}{M} \cdot \Delta\theta = \frac{F \cdot f_H \Delta\lambda}{M}$$

$$\delta_2 = \frac{1}{MW}$$

Figure 1 shows these quantities for

$\Delta\lambda = .004\ \lambda$

f_H = (50 + w) i.e. 50 c/inch offset.

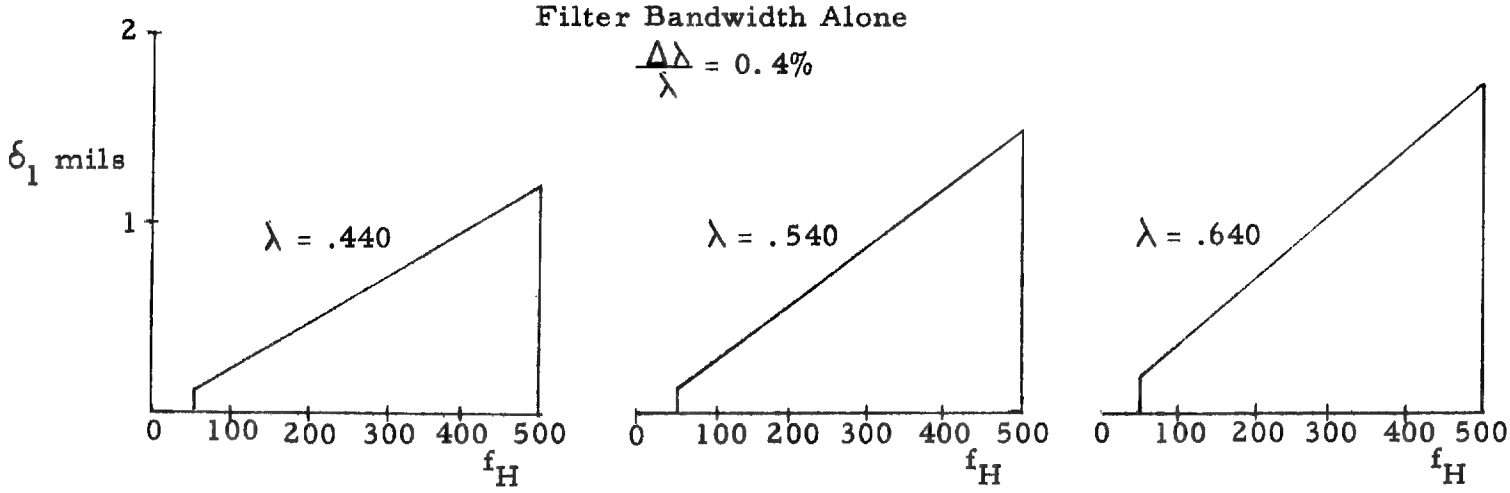

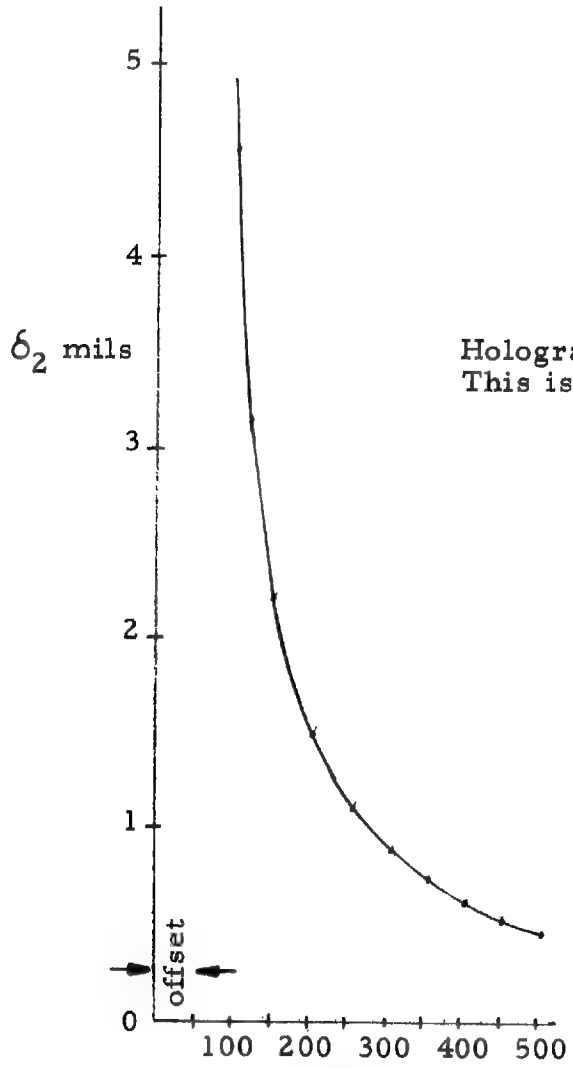

Hologram Aperture Effect.
This is constant once W is fixed.

Figure 1

Variation of Resolution With Light Wavelength and Hologram Frequency

If the aperture is now limited, i.e. f_H is limited, then δ_1 improves and δ_2 gets worse. This is shown in Fig. 2, where the best overall resolution is obtained when the aperture is limited to 300 cycles/inch. The actual resolution obtained here depends on δ_3 and is drawn for $\delta_3 = 0$, but the position of the minima along the frequency axis does not change if δ_3 is independent of the hologram aperture and light wavelength.

2.0 Prism Compensation

A possible method of compensating for the finite bandwidth of light is to insert a prism with controlled dispersion in the optical system. We have seen that the angular spread of light due to finite bandwidth is

$$\Delta\theta = f_H \cdot \Delta\lambda.$$

Thus the angular spread $\Delta\theta$ varies across the hologram getting progressively larger toward the high frequency end of the hologram. A prism inserted in the optical system will necessarily deviate all light of the same wavelength through the same angle. In this case, the best we can do is to design the prism to correct the angle exactly in the center of the hologram, and accept some over-correction at the low frequency end and an equal amount of under-correction at the high frequency end. This is equivalent to correcting the "lateral" spread and leaving some longitudinal spread along the axis through the center of the hologram. This is shown in Fig. 3.

If f_c is the center frequency of the hologram then

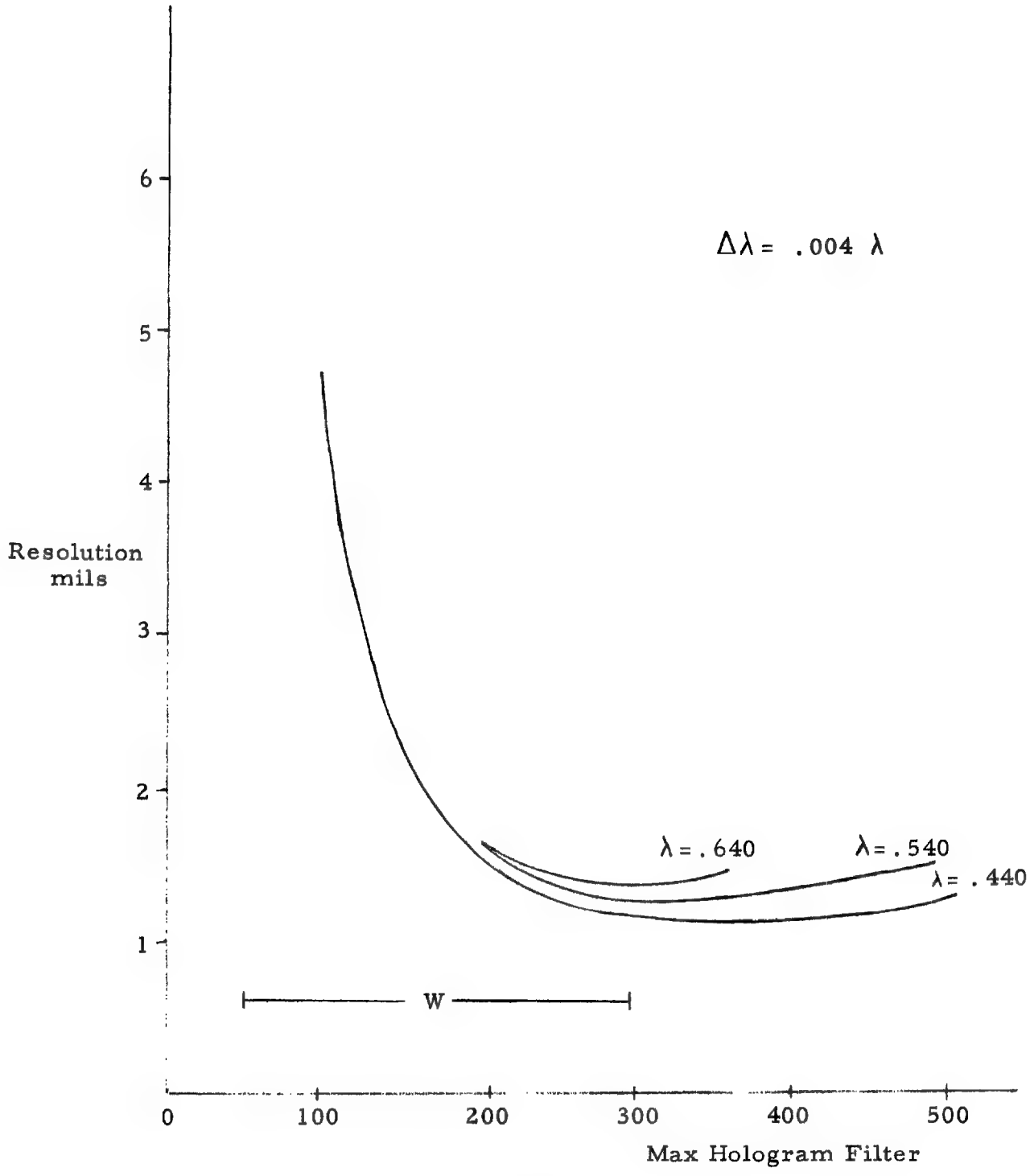

Figure 2

Resolution Versus Aperture No Prism

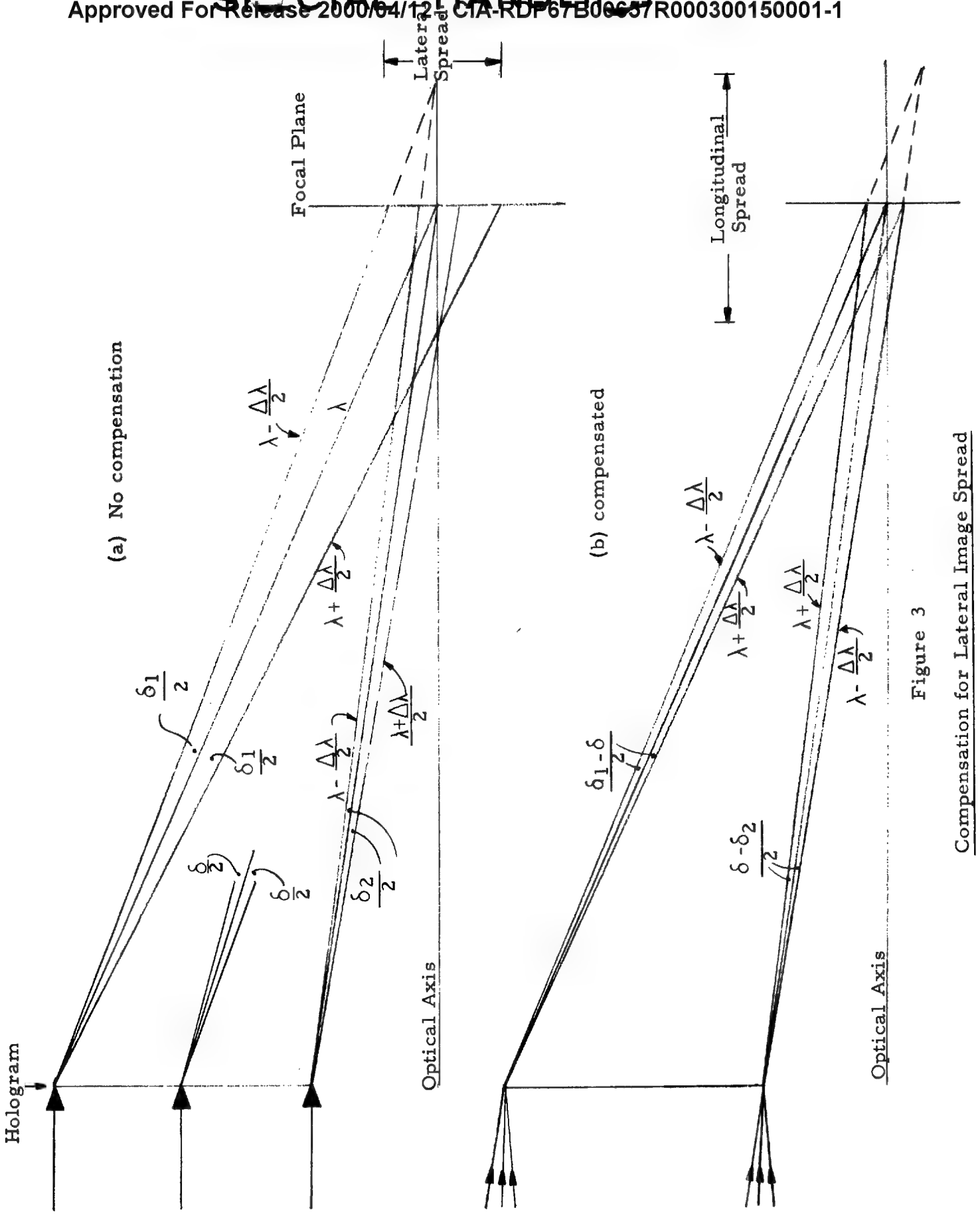

Figure 3
Compensation for Lateral Image Spread

$$\Delta\theta_c = f_c \cdot \Delta\lambda$$

Prism deviation $\theta = \alpha(n - 1)$

where α = prism angle

n = refractive index

Thus $\frac{d\theta}{d\lambda} = \alpha \cdot \frac{dn}{d\lambda}$ the required dispersion $\frac{\theta c}{\Delta\lambda} = f_c$ and $\alpha \cdot \frac{dn}{d\lambda} = f_c$.

In any specific glass the dispersion $\frac{dn}{d\lambda}$ is a function of wavelength. The variation in $\frac{dn}{d\lambda}$ can be reduced to a considerable extent by making a multiple prism using several different glasses.

The actual angular spread at any hologram frequency f_H after prism compensation will be

$$\Delta\theta^1 = \Delta\lambda \left| f_H - f_c \right|$$

$$= \Delta\lambda \left| f_H - \alpha \frac{dn}{d\lambda} \right|$$

The image diameter after compensation $\delta_1^1 = \frac{F\Delta\lambda}{M} \left| f_H - \frac{dn}{d\lambda} \right|$.

If $\frac{dn}{d\lambda}$ is constant with wavelength, then the image diameter will be proportional to $\Delta\lambda$, which is generally proportional to the wavelength λ. Thus using an "ideal" prism, δ_1^1 will vary both with wavelength and hologram frequency as shown in Fig. 4(a) which is based on a bandwidth W of 300 c/inch and offset of 500 c/inch. The uncompensated image size is shown again for reference at Fig. 4(b). With a practical prism, $\frac{dn}{d\lambda}$ will decrease with wavelength.

The effect of this on δ_1^1 is shown in Fig. 4(c) for a single-glass

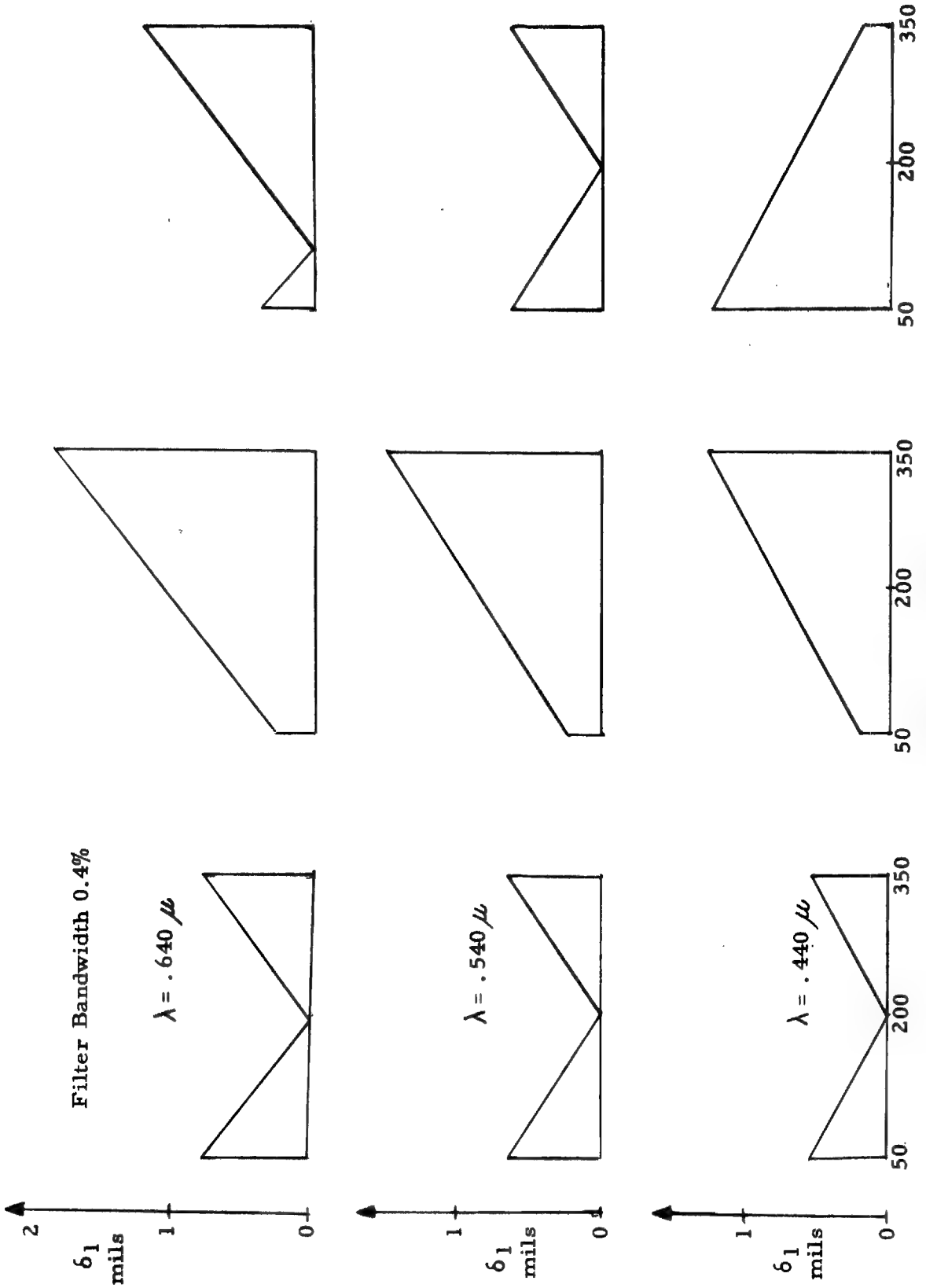

Figure 4

Effect of Compensating Finite Filter Bandwidth

prism of 2.38° angle. The best that can be done here is to arrange the image size to be equal at the two extremes of $\lambda = .44\ \mu$, f = 50 cycles/inch and $\lambda = .64\ \mu$, f = 350 cycles/inch.

As discussed in Section 1.1 the overall resolution δ_T varies with bandwidth and has a minimum value.

It is to be expected that with the inclusion of a compensating prism, the usable hologram bandwidth will be increased with a consequent improvement in δ_T.

2.1 Practical Considerations

The requirements for a prism to minimize the finite waveband are

(1) Constant dispersion of .01 radians per micron over .440 to .650 micron band.

(2) Prism design must allow insertion in the optical system without major changes.

(3) Transmission light loss to be minimal.

(4) The prism must not introduce spherical aberration into the optical system.

After considerable investigation, it was found that these conditions could not simultaneously be met. Some of the problems encountered were:

(1) A 2-element prism of nearly constant dispersion over the required band would be desired for insertion in the optical system just underneath the liquid platen, but such a prism would have a deviation of 20° which cannot be accommodated. A prism in

this position will also cause dispersion of the zero order.

(2) Attempts to eliminate the residual deviation resulted either in causing great changes in dispersion or in the use of impossibly large prism angles. This would lead to a very thick prism composed of a large number of sections cemented together which would take a great deal of space, be heavy, expensive and cause a large light loss.

(3) If the prism were located nearer to the output plane where more space is available, then a greater dispersion would be required and spherical aberration would be introduced because of the converging beam.

As it was not possible to physically accommodate suitable prisms without redesigning the correlator mechanically, the possibility of introducing the required dispersion by means of a diffraction grating was next investigated. The intention was to replace one of the plane mirrors with a blazed reflectance grating. This idea is treated in the next section.

3.0 Correction of Filter Bandwidth by Means of a Reflection Grating

3.1 Deviation Required to Correct Image Spread

The angles of incidence and diffraction in a hologram are related by the following expression:

$$\sin i + \sin \psi = M . \lambda . f$$

where m = order of image

i = incidence angle, to normal

Ψ = diffraction angle, to normal

λ = wavelength of light

f = hologram frequency

In the present case, i and Ψ are small angles and we are concerned only with first order images. Thus we can write:

$$i = \lambda \cdot f \cdot -\Psi$$

To correct lateral image spread, we require Ψ to be constant. Thus, the required condition is

$$\lambda f - i = \text{constant}$$

Differentiating with respect to λ we get

$$\frac{di}{d\lambda} = f$$

In other words, the required rate of correction in radians per inch is equal to the hologram frequency in lines per inch.

A typical hologram contains a range of frequencies, and the correction can only be perfect at one frequency. If we correct the frequency at the center of the hologram, then the low frequency edge is overcorrected and the high frequency edge is undercorrected, by the same amount. The result is to leave a residual longitudinal image spread. In spite of this, an improvement of at least 2:1 in image size is obtained this way. The improvement factor is $\frac{2fH}{fH - fL}$ where

fH = highest hologram frequency

fL = lowest hologram frequency

Thus in a heavily squinted hologram where fL is large, a much greater improvement factor is possible.

3.2 Reflection Grating

If i is the incidence angle and β is the reflection angle measured to the normal of the macro surface of the grating, and if α is the groove angle

Groove angle $\alpha = \frac{\beta - i}{2}$

Total reflection angle $\phi = i + \beta$

In a blazed grating, we require the light to be reflected from the grooves in the same direction that it is diffracted. Thus:

$$a (\sin \beta - \sin i) = M \lambda$$

where a = groove spacing

Angular dispersion $\frac{d\beta}{d\lambda} = \frac{m}{a \cos\beta}$

Combining these equations, we

$$\cot \alpha = \tan \frac{\phi}{2} + \frac{2}{\lambda \cdot \frac{d\beta}{d\lambda}}$$

and

$$a = \frac{m \lambda}{2 \cos \frac{\phi}{2} \cdot \sin \alpha}$$

Thus, given the total reflection angle ϕ, the wavelength λ and the required angular dispersion we can determine the grating frequency and blaze angle.

The best position for a reflection grating appears to be in place of the bottom mirror. This is after the zero stop and so avoids any trouble due

to shifting the zero order image. Also the angular dispersion here is greater, which requires a higher grating frequency making the grating more practical in this case.

The angular dispersion required at any point in the system other than at the hologram itself will now be determined.

Let the hologram focal length be F_o

field lens focal length be F_1

relay lens focal length be F_2

cylinder lens focal length be F_3

spacing of field and relay lens principle planes be A

spacing of relay and cylinder lens principle planes be B

The image formed by the hologram and field lens will be at a distance x_1 given by

$$\frac{F_o F_1}{F_o + F_1}$$

The distance of this image from the relay lens F_2 is

$$x_2 = A = x_1$$

The virtual image formed by the relay lens will be at a distance

$$x_3 = \frac{F_2 x_2}{F_2 - x_2}$$

Finally, this image will be at a distance x_4 from lens F_3 where

$$x_4 = B + x_3$$

Then if θ_o is the angular deviation of the beam at the field lens F_1, the angular deviation of the beam emerging from F_3 will be

$$\theta_3 = \frac{x_3}{x_4} \cdot \frac{x_1}{x_2} \cdot \theta_o$$

If the mirror is situated a distance x_5 from the lens F_3 and the final image plane is a distance x_6 from lens F_3 then the deviation required at the mirror is

$$\theta_4 = \theta_3 \cdot \frac{x_6}{x_6 - x_5}$$

thus

$$\theta_4 = \frac{x_1}{x_2} \cdot \frac{x_3}{x_4} \cdot \frac{x_6}{x_6 - x_5} \cdot \theta_o$$

3.3 Calculations

If the frequency at the hologram center f = 250 cycles per inch, then the required correction at the hologram is

$$\frac{di}{d} = \frac{250}{24,400} \text{ radians/micron}$$

$$= .0098 \text{ radians/micron}$$

We will round this off to .01 radians/micron. The angular deviation required at the lower mirror position will be

$$.01 \cdot \frac{x_1}{x_2} \cdot \frac{x_3}{x_4} \cdot \frac{x_6}{x_6 - x_5} \text{ radians/micron}$$

where x_1 = 20.6 inches
x_2 = 2.97 inches
x_3 = 3.61 inches
x_4 = 12.31 inches
x_5 = 5.5 inches
x_6 = 39 inches

Angular deviation required = $.01 \cdot \frac{20.6}{2.97} \cdot \frac{3.61}{12.31} \cdot \frac{39}{33.5} = .0236$ radians/micron.

The total reflection angle $\Phi = 37^\circ$

$$\frac{\Phi}{2} = 18.5, \quad \tan\frac{\Phi}{2} = .335, \quad \cos\frac{\Phi}{2} = .948$$

$$\lambda = .550 \text{ micron}$$

$$\frac{d\beta}{d\lambda} = .0236 \text{ radians/micron}$$

$$\therefore \cot\alpha = \tan\frac{\Phi}{2} + \frac{2}{\lambda\frac{d\beta}{d\lambda}}$$

$$= .335 + \frac{2}{.55 \times .0236} = 154.3$$

Then groove angle $\alpha = 0.37^\circ$

$$\sin\alpha = .00647$$

$$\text{Groove spacing} = \frac{m}{2\cos\frac{\Phi}{2} \cdot \sin\alpha}$$

$$= \frac{.550}{1.896 \times .00647} \text{ microns}$$

$$= 44.8 \text{ microns}$$

This is equivalent to 22.3 grooves/mm.

3.4 Practical Considerations

The effectiveness of a reflection grating in this application depends on the efficiency of the blazing; with efficient blazing all the incident energy is directed into a single diffraction order. In the present case, diffracted energy of the first order only is required: the presence of appreciable light in the zero and higher order images will cause

overlapping data.

Data from Bausch & Lomb indicated that it was possible to rule gratings in which over 90% of the incident energy was directed into a single order, although they could not guarantee this with a grating of such low frequency. The main problem is in preserving the flatness of the reflecting surfaces of the groove.

Test gratings were ordered from B & L on a best effort basis.

It was found on testing these gratings that only about 50% of the incident energy was actually diffracted into the first order, making the gratings unusable for the intended purpose. This was apparently due to the difficulty of holding optical flatness in the reflecting surfaces of a coarse grating, due to the width of cutting tool required.

4.0 Conclusions

The only feasible method of compensating an optical correlator for finite filter bandwidth appears to be the use of a prism in the collimated beam adjacent to the input film. This would introduce a bend in the optical system, and cause dispersion of the zero order, both of which effects would have to be taken account of in the initial design of the optical system.

Appendix IV

INSTALLATION REQUIREMENTS

This appendix contains a few selected sections from the Operator's Manual. These are reproduced here for the convenience of personnel who may have to provide facilities for the Processor. If possible, recent log books and/or operating personnel should be consulted for further details.

Appendix IV

INSTALLATION REQUIREMENTS

1.0 Introduction

1.1 General

This manual contains operation and maintenance instructions for the Model 9015 Processor manufactured by Itek Corporation. Classified information pertaining to Sections III, IV, and V are contained in Volume two. The Model 9015 Processor (See Fig. 1) is used to enlarge one-half of a $9\frac{1}{2}$ inch wide input film and to expose the enlarged area onto a $9\frac{1}{2}$ inch wide output film.

1.2 Description

1.2.1 Physical

The Model 9015 Processor consists of a carbon arc unit and an optical unit (see Fig. 1). The carbon arc unit contains the carbon arc lamp with its rectifier power supply and water circulator. The optical unit contains the optical system, the input and output film drives, and the film drive controls and power supplies.

1.2.2 Functional

The Model 9015 Processor provides a $9\frac{1}{2}$ inch wide output film showing an image area that is a 2X enlargement of one half of the image area of its $9\frac{1}{2}$ inch input film. During this process, the equipment performs the following functions:

(1) Drives the film at constant speed.

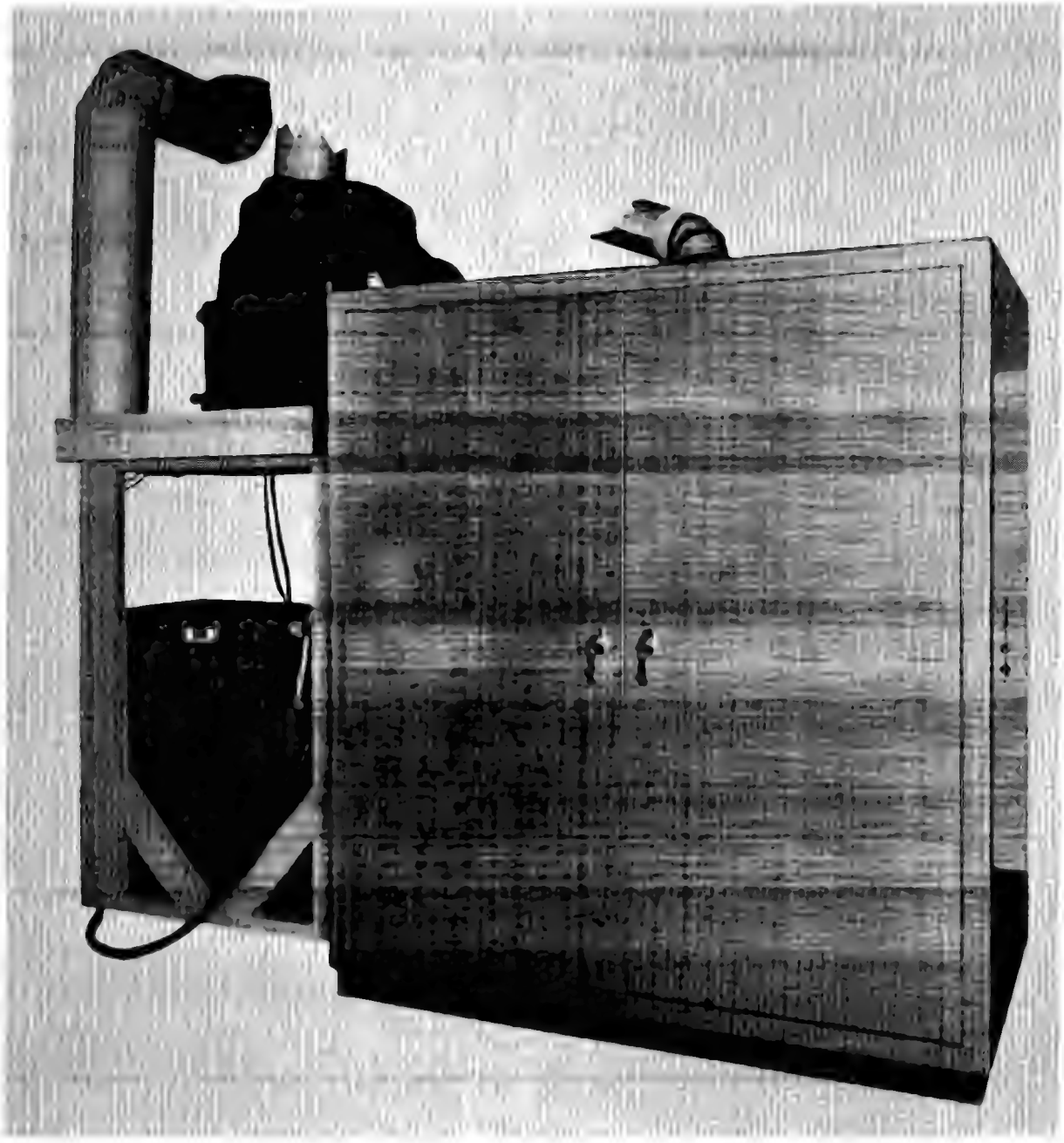

Figure 1

Model 9015 Processor

(2) Maintains the film at the proper tension throughout the operation.

(3) Stops the film drive mechanism upon the occurrence of the following:

a. Failure of certain mechanical components.

b. End of film.

(4) Provides for automatic operation (once the unit is started).

(5) Enlarges one-half the input film and exposes the enlargement on output film having the same width as the input film.

1.3 Equipment Characteristics

The physical and electrical characteristics of the Model 9015 Processor are as follows:

(1) Input power requirements:

a. 120 volts, 15 amperes, 60 cps, 1 phase, 3 wire.

b. 208 volts, 60 amperes, 60 cps, 3 phase, 3 wire.

(2) Temperature limits: 70 $\pm$ 5°F, relative humidity at 40 $\pm$ 10 percent.

(3) Mounting:

a. Arc unit: on frame fitted with jackscrews and casters. Floor moutning provided by lifting the frame and casters off the floor by the jackscrews.

b. Optical unit: self-contained cabinet fitted with

jackscrews and casters. Floor mounting provided by lifting the cabinet and casters off the floor by the jackscrews.

(4) Overall dimensions (arc unit plus optical unit): 100 inches high, 114 inches wide, $48\frac{1}{2}$ inches deep.

(5) Fuse complement:

a. Two type 3AG, SLO-BLO, 0.5 ampere.

b. Two type 3AG, SLO-BLO, 0.6 ampere.

c. One type 3AG, 3 amperes.

d. One type 3AG, 6 amperes.

2.0 Accessory Test Equipment

2.1 General

Table 1 lists the accessory test equipment and special tools used when operating or servicing the Model 9015 Processor.

Table 1
Test Equipment

Name	Manuf. & Model No.	Application
Volt-ohm milliammeter	Simpson Electric Co. Model 260	Voltage measurements and continuity checks
Theodolite (with auto-collimating eyepiece)	Wild, Model T-2	Alignment of optical unit
Mirror (7 inches square)	Libbey Owens Ford Glass Co. (high quality plate glass)	Autocollimation
Centering fixture	Itek Corp. (drawing 9015-0523)	Centering F1 & F2 lenses
Centering fixture	Itek Corp. (drawing 9015-0522)	Centering relay lens
Test film	Itek Corp. (drawing 9015-0521)	Focusing of optical unit
Lamp house draft gage	Strong Electric Corp. (for lamps using 75-100 amperes)	Draft measurements for carbon arc exhaust duct

3.0 Installation

3.1 Site Slection

3.1.1 Power Requirements

The Model 9015 Processor requires the following sources of external power:

(1) 208 volts, 60 amperes, 60 cps, 3 phase, 3 wire terminating in a fuse box with 60-ampere fuses in each line.

(2) 120 volts, 5 amperes, 60 cps, 1 phase, 3 wire terminating in a standard grounding type outlet.

(3) 120 volts, 10 amperes, 60 cps, 1 phase, 3 wire terminating in a standard grounding type outlet.

The power listed in tems (1) and (2) of paragraph 3.1.1 is required by the arc unit that in item (3) by the optical unit.

3.1.2 Temperature and Humidity

The Model 9015 Processor is designed to operate at a temperature of $70 \pm 5^{\circ}F$ and a relative humidity of 40 ± 10 percent.

3.1.3 Intake System Requirement

The arc unit requires an 8-inch diameter intake duct. No blower should be used.

3.1.4 Exhaust System Requirements

The carbon arc lamp of the arc unit requires an 8-inch diameter exhaust duct. The exhaust blower in the lamp hood removes exhaust gases from the arc. An additional blower in the upper stack is required to remove the exhaust gases from the exhaust system. This blower should have an air

velocity of approximately 700 linear feet per minute.

CAUTION

If the upper stack blower is inadequate, the exhaust gases will back up into the Processor area and into the lamp house.

The optical unit requires an exhaust system capable of exhausting 250 cubic feet of air per minute. A 6 inch diameter duct is required for this purpose. A 4 inch diameter duct is also required to exahust the condenser cooling system.

CAUTION

The optical unit exhaust ducts must exhaust independently into the atmosphere. Their outlets must not be located near the intakes of any system, including those of the Model 9015 Processor.

3.1.5 Darkroom

The installation area must include a darkroom for loading and unloading the output magazine.

3.1.6 Dust and Dirt Control

The importance of controlling dust and dirt within the area assigned to the Model 9015 Processor cannot be overemphasized. Accumulation of dust and dirt on the internal lens of the equipment causes not only loss of illumination, but, what is even more important, loss of reproduction resolution due to the scattering of collimated light rays. Although the ideal area, which has a sterile, dust-free atmosphere, is impossible in view of personnel activity and the materials used, areas which approximate the ideal should be seriously considered in preparing to install the equipment.

The main source of dirt is the outside air, which generally contains dirt

in the form of dust or cinders. Common types of open-air contamination and the common methods for the removal of each type are listed in Table 2. Personnel introduce dirt through their activities or through their clothing. Equipment also introduces dirt in the form of metal particles from moving parts, oil deposits from bearings, and dust particles from carbon arcs.

Most dirt can be removed from the air by ordinary commercial air filters. The best of these, however, only cuts down the amount of cleaning required. Some electrostatic filters have proven advantageous in photographic practice. Filters made of bundles or mats of soft crepe or cotton pads give good results and require less maintenance. Since no filter is perfect, some smoke and dirt deposits accumulate on the walls and ducts. These deposits are usually dislodged later by vibration or an accidental blow. Dirt from this source is serious in photographic work. It can be substantially reduced by viscous filters on the ends of long runs of duct work. Ducts should be made of smooth material and constructed so that they can be easily and thoroughly cleaned.

The air movement associated with air conditioning causes more dirt to collect on the films and lenses, thereby increasing the need for air filtration. However, the ducts and fans of existing air conditioning systems can be utilized for systems which filter dust from the laboratory air.

The preparation of the assigned area for dust and dirt control should be supplemented by thorough dirt inspection and cleaning routines.

Table 2

Scale of Atmospheric Impurities

Particle Type	Size Range, microns	Method of Removal
Heavy industrial dust	100 and up	Cyclone separators
General dust	1 - 100	Dynamic precipitators
Fly ash	3 - 70	Water spray; air filters
Fog	1 - 40	Air filters
Pollen	20 - 60	Air filters
Plant spores	10 - 30	Air filters
Bacteria	1 - 15	Air filters
Fumes	0.1 - 1	Air filters and electrical precipitators
Pigments	1 - 7	Electrical precipitators
Smoke	0.001 - 0.3	Electrical precipitators
Tobacco smoke	0.01 - 0.15	Electrical precipitators
Oil smoke	0.03 - 1	Air filters and electrical precipitators

Appendix V

SPARE PARTS

Appendix V

SPARE PARTS

Item	Qty.	Description	Manufacturer	Where Used	Part No.
Fuse	5	AGC 3 Amp	Little Fuse	Main power supply	F203
Fuse	5	AGC 6 Amp	Little Fuse	TV control	F202
Fuse	5	AGC 10 Amp	Little Fuse	TV control	F902
Fuse	5	AGC 4 Amp	Little Fuse	TV control	F901 F903 F904
Fuse	5	AGC Slo Blo .6 Amp	Little Fuse	Loop controller	F302
Fuse	5	AGC Slo Blo .5 Amp	Little Fuse	Loop controller	F301
Circuit Breaker	1	AM-12	Heineman	Power input	CB201
Lamp	2	No. 1820	General Electric Cleveland, Ohio	Panel light	DS405
Lamp	10	T-3¼ NE-51	Dialight Corp. Brooklyn, N. Y.	Panel lights	DS401
Relay	1	MH17D 24VDC 4 PDT	Potter & Brumfield, Princeton, Ind.	Loop controllers	K301 K302 K304
Relay	1	MH17D 115V AC.A	Potter & Brumfield, Princeton, Ind.	Loop controller	K303
Relay	1	PR11D 24V	Potter & Brumfield, Princeton, Ind.	Loop controller	K101

SPECIAL HANDLING

Item	Qty.	Description	Manufacturer	Where Used	Part No.
Light	1	25 watt 120 V frosted	General Electric Cleveland, Ohio	Arc Unit 90310	
Light	2	No. 47 miniature	General Electric Cleveland, Ohio	Arc Unit 19039	
Switch	1	90999	Strong Electric Toledo, Ohio	Arc Unit	
Relay	1	90326	Strong Electric Toledo, Ohio	Arc Unit	
Switch	4	512TS1-3	Microswitch	Control panel	S401 S403 S101 S110 S114
Switch	1	138866A3L	Ucinite	Control panel	S111
Switch	1	138867A3L	Ucinite	Control panel	S112
Switch	5	DT2RV2-A7	Microswitch	Safety circuit	S209 S212 S215 S219
Switch	2	5225	Haydon Switch Waterbury, Conn.	Loop control switches (interchangeable with No. 5227)	(many)
Drive Wheel	1	9015-0689	Itek Corp. Lexington, Mass.	Input film drive	
Drive Wheel	1	9015-0652	Itek Corp. Lexington, Mass.	Output film drive	
Motor	1	N29GMW	Grahm Electric	Main drive motor	B201
Motor	1	B8194E-120m	Bodine Elec. Co. Chicago, Ill.	Condenser cooling	B212
Motor	1	ALPJRE	Electric Indicator Stamford, Conn.	Reel torque motor	B209
Motor	1	NSH-12R	Bodine Elec. Co. Chicago, Ill.	Loop drives #1 & 2	B204 B205

Item	Qty.	Description	Manufacturer	Where Used	Part No.
Motor	1	20-02 - IN T1231B	Inland Motor Northampton, Mass.	Film torque motor	B202 B203
Motor	1	2114C	Inland Motor Northampton, Mass.	Reel torque motor	B210 B211
Motor	1	KC1-23 IN	Bodine Elec. Co. Chicago, Ill.	Loop controller	B206 B207
Rheostat	1	H500-562 shilo	Ohmite Chicago, Ill.	Intensity control	R201 R203
Resistor	1	10W 50 ohm	Ohmite Chicago, Ill.	Intensity control	R204 R202
Capacitor	1	T30ZN 34 - 400 VDC 3.0 mfd	Aerovox	Input supply motor	C202
Capacitor	1	T30ZN 34 - 400 VDC 4.0 mfd	Aerovox	Blower motor	C212
Capacitor	2	VC 1164B	Aerovox	Loop control	C206 C207
Loop controller	1	9015-1038	Itek Corp. Lexington, Mass.	Electronic chassis	
Gear Box	1	9015-1076	Itek Corp. Lexington, Mass.	Main drive	

Appendix VI

DETERMINATION OF THE VELOCITIES OF MOVING TARGETS

Appendix VI

DETERMINATION OF THE VELOCITIES OF MOVING TARGETS

1.0 Introduction

A coherent radar system records the radar return in such a manner that moving targets can be identified. The signal histroy left by a moving target will be slightly different from that for a stationary target. These differences would lead to a slight image blur and/or image displacement in a correlator such as the one used on the IR & D program 5271. However, a correlator of the proper calibration could detect the differences and determine the velocity.

The velocity of the target is the geometrical sum of two perpendicular components: one component parallel to the path of the airplane, and the other component normal to the path. The former would appear as a change in the focal plane, and the latter as a lateral displacement, of the correlated image. Each of these components would be measured separately in the correlator, and each is treated separately below.

2.0 Analysis

The following analysis considers first-order effects only. It is assumed furthermore that the velocity of the target is constant while it is in the antenna beam.

2.1 Parallel Motion

The expression for the focal length of radar data is

$$F_H = \frac{V^2 R_r}{2V_r^2} \cdot \frac{\lambda_r}{\lambda_o},$$

where V = film velocity

V_r = vehicle velocity

R_r = range

λ_r = radar wavelength

λ_o = correlator illumination wavelength.

In the case of a parallel moving target, only V_r, in effect, will change. Let subscript m denote a moving target, and let V_{mx} denote the target velocity component parallel to the vehicle path. Then the focal length of the data relating to the moving target is

$$F_m = F_H \cdot \left(\frac{V_r}{V_r - V_{mx}}\right)^2,$$

where positive V_{mx} is taken to be the same direction as the vehicle's motion.

The change in data focal length is

$$\Delta F = F_m - F_H$$

$$\Delta F = F_H \left[\left(\frac{V_r}{V_r - V_{mx}}\right)^2 - 1\right].$$

Finally, target speed in terms of ΔF is given by

$$V_{mx} = V_r \left(1 \pm \sqrt{\frac{F_H}{\Delta F + F_H}}\right).$$

Since we assume that the target velocity will be less than the vehicle velocity, only the minus sign in the above expression need be used.

It is well to remember that in this expression F_H is the focal length of the data itself; correlator optics have not yet been considered.

2.2 Perpendicular Motion

Analysis of perpendicular motion requires an understanding of the Doppler shift. The Doppler return from a stationary target is shown in Fig. 1.

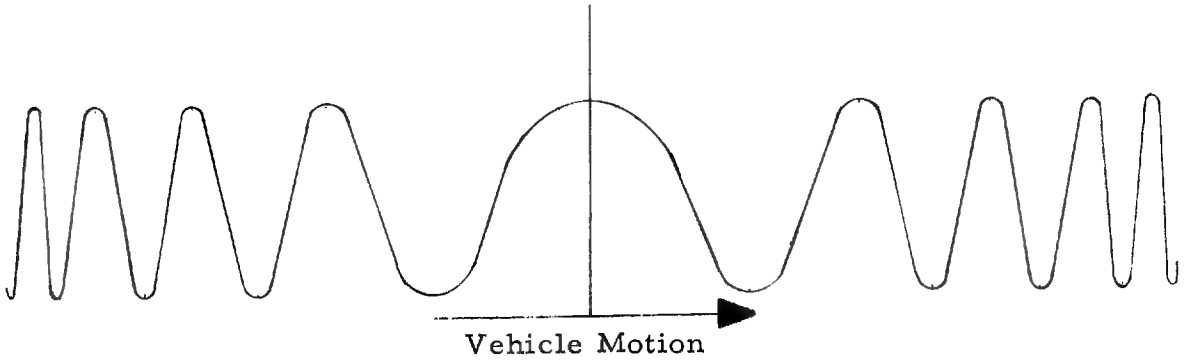

Figure 1

This frequency appears as a modulation of the radar carrier frequency f_r. The carrier is normally heterodyned down to zero so that the modulation ranges from zero cycles out to its high-frequency limit $f_{D\ max}$, as shown in Fig. 2.

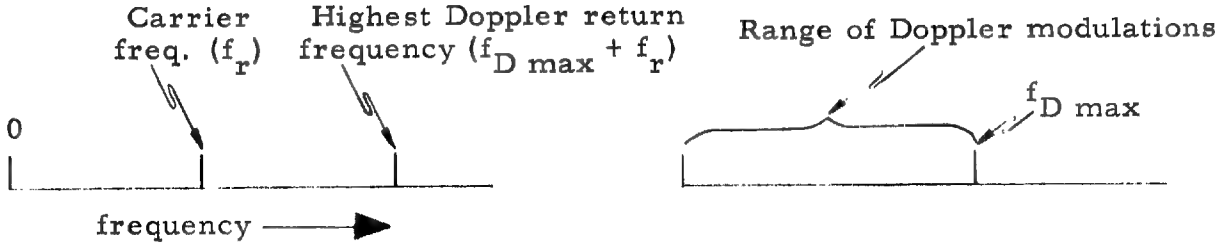

(a) Modulated return (b) Return with carrier removed

Figure 2

Target motion in the normal direction will produce a change in the Doppler spatial frequencies. Suppose a target is moving at a constant velocity V_{my}; the shift in frequency will then be $\frac{2V_{my}}{\lambda_r}$. Let positive V_{my} denote motion away from the vehicle path, and negative V_{my} motion towards it. In Fig. 3 the solid line represents the normal spectrum of the data, and the broken line represents the spectrum of moving-target data which has been shifted by $\frac{2V_{my}}{\lambda_r}$.

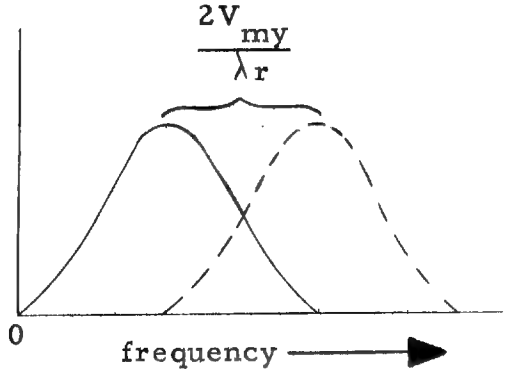

Figure 3

The correlation appears relative to where the zero frequency of the Doppler modulation appears on the data film, for the modulation is a hologram, which acts like a lens: if the optical axis moves, the image moves. Thus a shift in the Dopper return causes an azimuth offset of the correlation. This offset can easily be calculated by reference to Fig. 4.

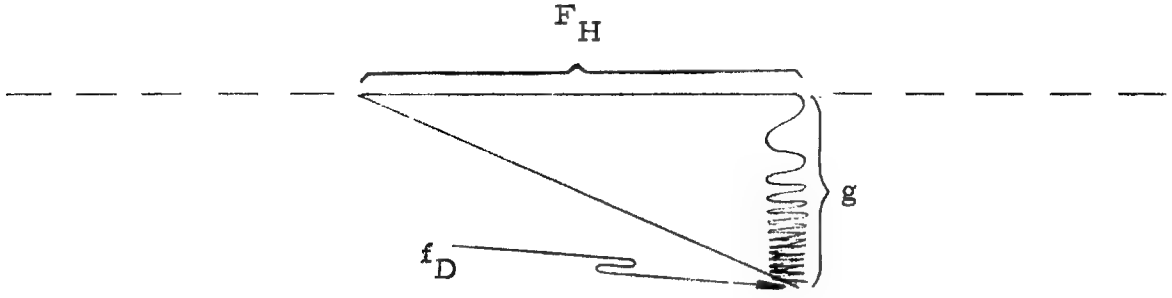

Figure 4

The axis represents zero frequency, and the frequency at any other point on the hologram is denoted by the variable f_D, the Doppler frequency. From previous studies we know that

$$g = F_H \lambda_o f_D,$$

where g is the distance from the axis to the point where the frequency f_D appears, and λ_o is the wavelength of the correlator illumination. The offset can be denoted by Δg, and the Doppler shift by Δf_D. We have then

$$\Delta g = F_H \lambda_o \Delta f_D.$$

We know though that Δf_D is simply $\frac{2V_{my}}{\lambda_r}$, so

$$\Delta g = 2V_{my} F_H \left(\frac{\lambda_o}{\lambda_r}\right).$$

This gives the correlation offset distance at the natural focal length of the data. Finally,

$$V_{my} = \left(\frac{\lambda_r}{2F_H \lambda_o}\right) \Delta g.$$

3.0 Measurement

The following discussions assume a correlator without range compensation. With compensation the need for the range-variable graphs will be obviated.

3.1 Parallel Motion

A change in the data focal-length results in a change in the position of the output plane, which can be readjusted to focus by means of a cylinder

lens. It is difficult to calculate from system parameters the amount of movement required by the cylinder lens; therefore a means has been devised to calibrate the correlator.

Test holograms of known focal length can be inserted in the system, and the position-at-focus of the cylinder lens noted. From these points a curve of data focal-length vs. cylinder lens position can be constructed, and from the curve one can convert a change-in-cylinder-position to a change-in-data-focal-length. Since we have seen that a change in focal length is proportional to velocity, there must also be a curve by which a change in data focal-length can be converted to velocity.

3.2 Perpendicular Motion

In this case the correlator can be calibrated by successively inserting the test holograms and moving each by a known amount. The resultant offset can be noted for each, and a graph constructed. One picks the appropriate value of F_H, then reads the corresponding ratio of $\frac{\Delta t}{\Delta g}$, where Δt is the amount of offset in the correlator output. Since Δt can be measured, Δg can be found and substituted in the equation for V_{my}.

There is, however, a problem involved in finding the offset distance, namely: from where is the correlation offset? Most ground vehicles travel on predetermined paths: automobiles on highways, trains on tracks, etc. One simply decides where the target was probably traveling, and measures the offset distance from that point.

Another class of targets is more difficult: ships at sea, sports cars on sand flats, etc. There are no predetermined detectable paths for these targets, so assuming the target is relatively isolated one can measure its

spectrum and compare it to the spectrum of the complete data. The difference between the two is then the Doppler shift, as was shown in Fig. 3; and the appropriate equation is

$$V_{my} = \left(\frac{\lambda_r}{2}\right) \Delta f_D.$$

This method is, of course, applicable to any type of moving target so long as the target can be effectively separated from its environment in such a manner that Δf_D can be measured.

Appendix VII

APERTURE WEIGHTING

Appendix VII

APERTURE WEIGHTING

1.0 Introduction

The signal-to-noise ratio and diffraction ring ("side lobe") suppression of an aperture-limited system can often be improved by use of aperture weighting. Investigations of the detail correlator were begun about a year ago. The first finding was that photographic film, on which filters are normally made, was insufficiently flat, and impaired the resolution of the relay lens. Obviously optical-quality glass was required for the filter. Another difficulty arose from the granularity of the photographic emulsion, which tended to scatter too much light. Deposited aluminum filters were chosen finally because they offer much better scattering characteristics, although such filters are more difficult to fabricate.

The varying transmission is obtained by depositing the aluminum through a narrow slit which oscillates in front of the surface to be coated. Gradations in density are controlled by the velocity of the slit, since the evaporation rate is constant. A cam of a certain profile is required to drive the slit in the proper manner. The cam operates through a linkage which can be adjusted for any desired bandwidth.

2.0 Determination of Cam Profile

The nomenclature in this section is as follows:

d = rate of evaporation

D = density

V = slit velocity

s = slit width

N = number of revolutions

t = time/revolution

θ = angle of cam revolution

x = distance traveled by the slit

Now we can formulate the basic equations. First,

$$D = dNt \text{ (rate of evaporation x total time)}$$

$$D = dN\left(\frac{2s}{V}\right)$$

$$\frac{1}{V} = \frac{D}{k} \text{ (where } k = 2dNs\text{).}$$

And second,

$$\frac{d\theta}{dt} = \omega \text{ (a constant),}$$

$$\frac{dx}{dt} = v \text{ (a variable).}$$

Substituting and integrating,

$$\frac{d\theta}{dx} = \frac{\omega}{v}$$

$$\theta = \int_0^x \frac{\omega}{v}\, dx$$

$$0 = \frac{\omega}{k} \int_0^x D\, dx.$$

This last equation means that one must construct a graph of the desired density-displacement function and integrate, presumably by direct measurement. For each value of displacement x there will be a unique θ, so the shape of the cam is now completely specified.

3.0 Designing the D-x Curve

The optical system is represented in Fig. 1.

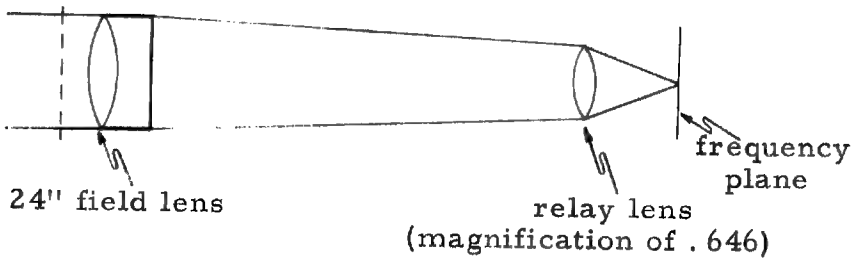

Figure 1

It is known that

$$g = m \lambda f F,$$

as shown in Fig. 2, where f and g are the variables. The frequency plane

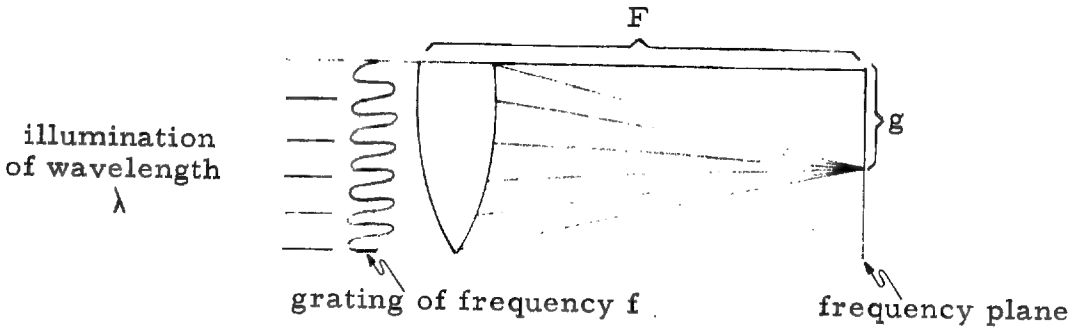

Figure 2

displays the spectrum of the input material.

By calculation, in the optical system of Fig. 1,

$$g = m \lambda f F$$

$$= (.646)\,(2.5 \times 10^{-5})\,(24)\,f$$

$$\frac{g}{f} = 3.88 \times 10^{-4} = .388 \text{ miles per cy./inch}$$

$$\frac{f}{g} = 2.58 \text{ cy./in. per mil}$$

By actual measurement on the system itself,

$$\frac{g}{f} = 3.94 \text{ mils per cy./in.}$$

$$\frac{f}{g} = 2.54 \text{ cy./in. per mil,}$$

which is in excellent agreement with the calculated values.

The spatial frequency spectrum of the input film was measured and found to be as in Fig. 3. It agrees with values that had been calculated

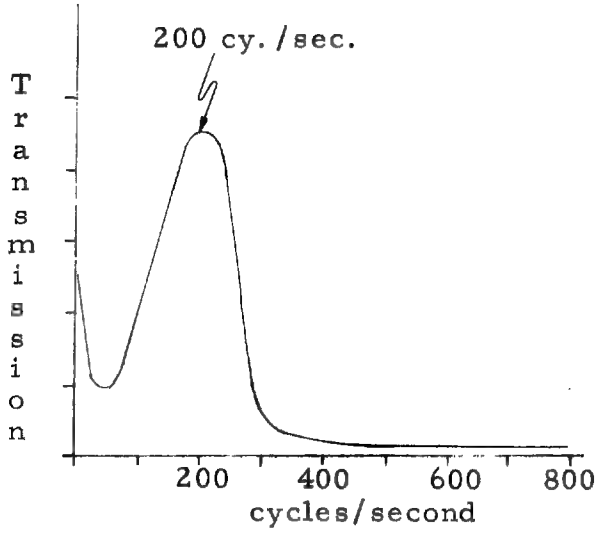

Figure 3

some time ago. The bandwidth at the half transmission points is 125 cy./sec. (The cy./sec. designation incorporated the film speed factor of 1.2 in./sec.)

Now the D-x curve can be drawn, for we know the bandwidth of the data, the location of peak data response, and where this frequency appears on the Fourier plane of the optical system. A model of the curve for 250 cy. bandwidth appears in Fig. 4.

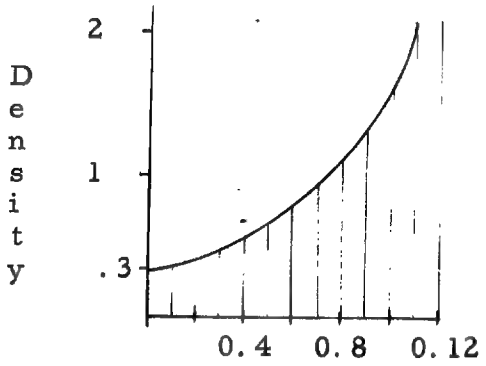

Figure 4

One assumption was made in the construction of this curve. If the center were actually zero density the velocity of the slit would be infinite. This is clearly impossible so a minimum density of 0.3 was chosen, which led to a maximum density of 2.0. The final specifications for the cam are attached.

4.0 Cam Profile Tolerance

The controlling factor on film accuracy is the cam-follower velocity, i.e. the slope of the cam profile. At the filter center let us assume a

maximum allowable tolerance of $\pm 20\%$ of the transmission. The fractional density variation is then $\pm \log_{10} 1.2 = \pm .075$. The center density is 0.3, so the permissable change in density is $\pm \frac{.075}{.3} = \pm .25$. Because density is inversely proportional to velocity the tolerance on velocity is $\pm 25\%$.

The cutting stations on the cam profile are spaced 4 mils in radius. Thus a 25% error in slope corresponds to an error of one mil between cutting points, or an error of 0.5 mil in each cutting point in the worst case.

Appendix VIII

INTERFERENCE PATTERN GENERATOR

Appendix VIII

INTERFERENCE PATTERN GENERATOR

1.0 Summary

This report contains an analysis and design information for an optical device that generates an area interference pattern using a photographic transparency as input. An area containing patterns of any desired length, frequency and focal length can be generated by this method. The problem of obtaining a pattern of varying focal length in one dimension to simulate range has not yet been solved. The method was first proposed by [redacted] in memorandum ED-M-510 dated 12 December 1962.

25X1A

2.0 Basic Principle

2.1 Radar Pattern

The pattern we wish to simulate is that due to the phase shift of a radar signal emitted from a vehicle at A, reflected from a target T and received back at A as shown in Fig. 1. The vehicle velocity is assumed negligible compared with the propagation time of the radar signal.

The phase shift is given by

$$\phi_R = \frac{2AT}{\lambda_R} = \frac{2}{\lambda_R}\sqrt{R_o^2 + x^2}$$

where λ_R = radar wavelength

R_o = offset range

x = distance along vehicle track

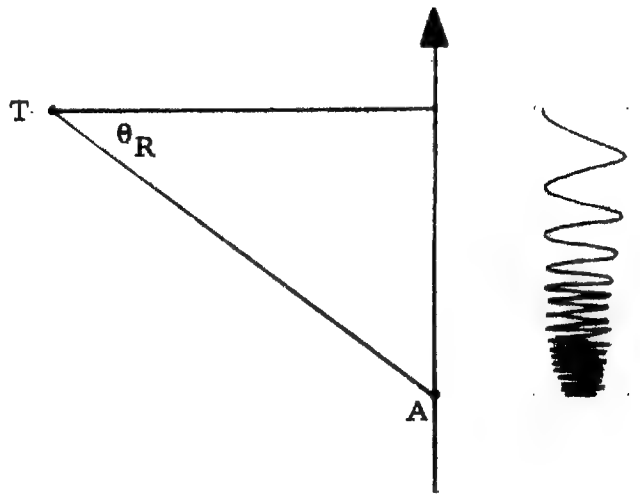

Figure 1

Radar Geometry and Interference Pattern

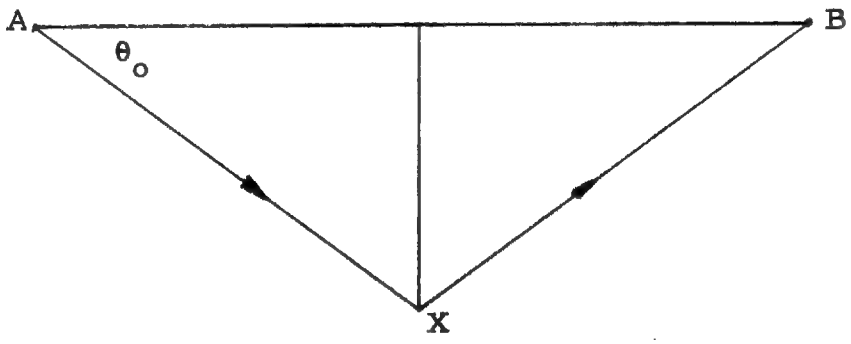

Figure 2

Simulator Geometry

The spatial frequency produced by this phase shift is

$$F_R = \frac{d\phi}{dx} = \frac{2}{\lambda_R} \frac{x}{\sqrt{R_o^2 + x^2}} = \frac{2}{\lambda_R} \sin \theta_R$$

The pattern frequency gradually drops to zero at the point opposite the target as shown in Fig. 1.

2.2 Simulated Patterns

Figure 2 shows the essential geometry of the simulator. Consider a wave emitted from A in the direction AX, and a second wave coherent with the first travelling in the direction XB.

The phase difference between wavefronts at point X is

$$\phi_S = \frac{AX + BX}{\lambda_o}$$

If the point X lies on the axis and AX = BX then

$$\phi_S = \frac{2AX}{\lambda_o} = \frac{2}{\lambda_o} \sqrt{d^2 + x^2}$$

Pattern frequency

$$F_s = \frac{2}{\lambda_o} \frac{x}{\sqrt{d^2 + x^2}} = \frac{2}{\lambda_o} \sin \theta_o$$

Thus a pattern with similar properties to the radar pattern is generated. Note that it is essential for the wavefronts to be travelling in the directions indicated, away from A and toward B, or vice versa. This can be seen from Fig. 3(a) and (b) which show the interference patterns produced by two spherical waves centered on focal points a short distance apart. In Fig. 3(a) both points are radiating coherently to produce an interference pattern at plant P. This is not the pattern required. If the direction of one of the

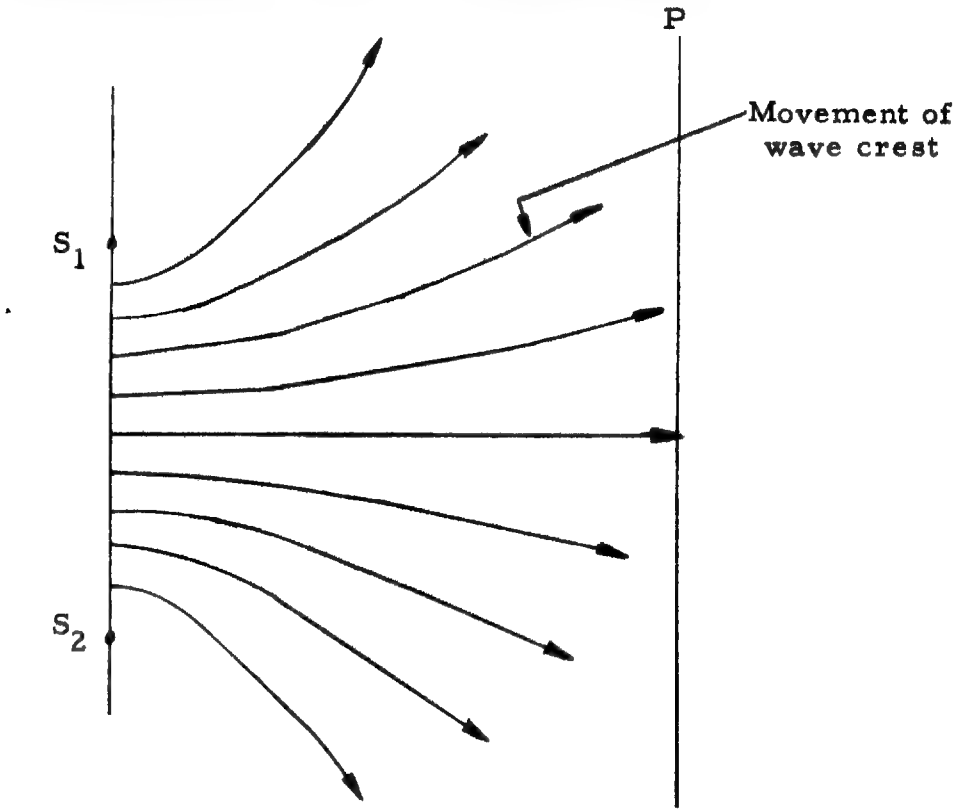

Figure 3(a)

Interference Pattern with Both Sources Radiating

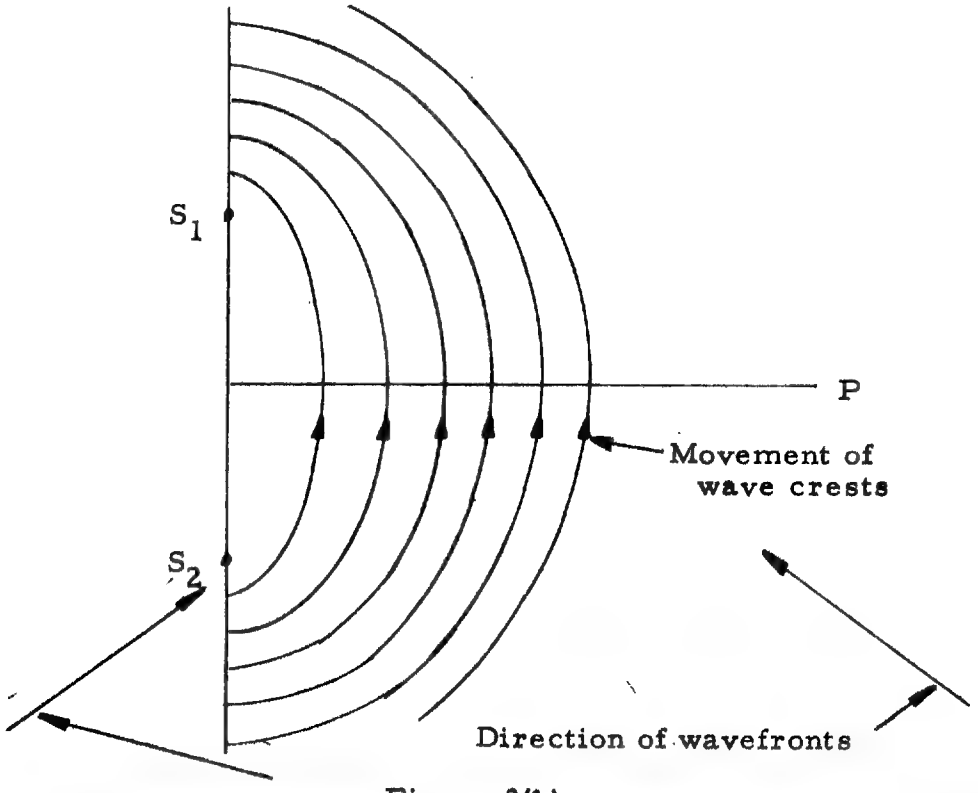

Figure 3(b)

Interference Pattern with Both Sources Radiating

wavefronts is reversed as in Fig. 3(b) the required pattern is produced along the plane P. In practice an opaque film would be placed at P and both waves would impinge from the same side as indicated in the diagram.

2.3 Optical System

The optical system necessary to implement this idea is shown in Fig. 4. The transparency is illuminated with collimated, monochromatic light from source S. In the range dimension the transparency is imaged directly onto the film plane by the spherical lens L1.

In the azimuth dimension, in which the interference pattern is required, the lens L1 would normally image the transparency in the same plane. However, two addition cylindrical lenses L2 (positive) and L3 (negative) split this into two images at points A and B. The two wavefronts produced by these lenses form the desired interference pattern between points C and D as shown.

The lens stop is vital to operation of the system. It is essential that the two wavefronts exactly overlap to produce the pattern. Any spillover will result in the film being fogged.

Exact overlap is achieved when the two sides of the lens have apertures in proportion to their focal lengths, as shown. The zero stop must be of sufficient width to give the desired pattern offset frequency.

Design formulae for the optical system are developed in the next section.

3.0 Analysis of Pattern Simulator

The following analysis is based on a single point T on the transparency. It is equally applicable to an ensemble of points.

Referring to Fig. 5, let the phase angle of the wave reaching A^1 be Φ_o

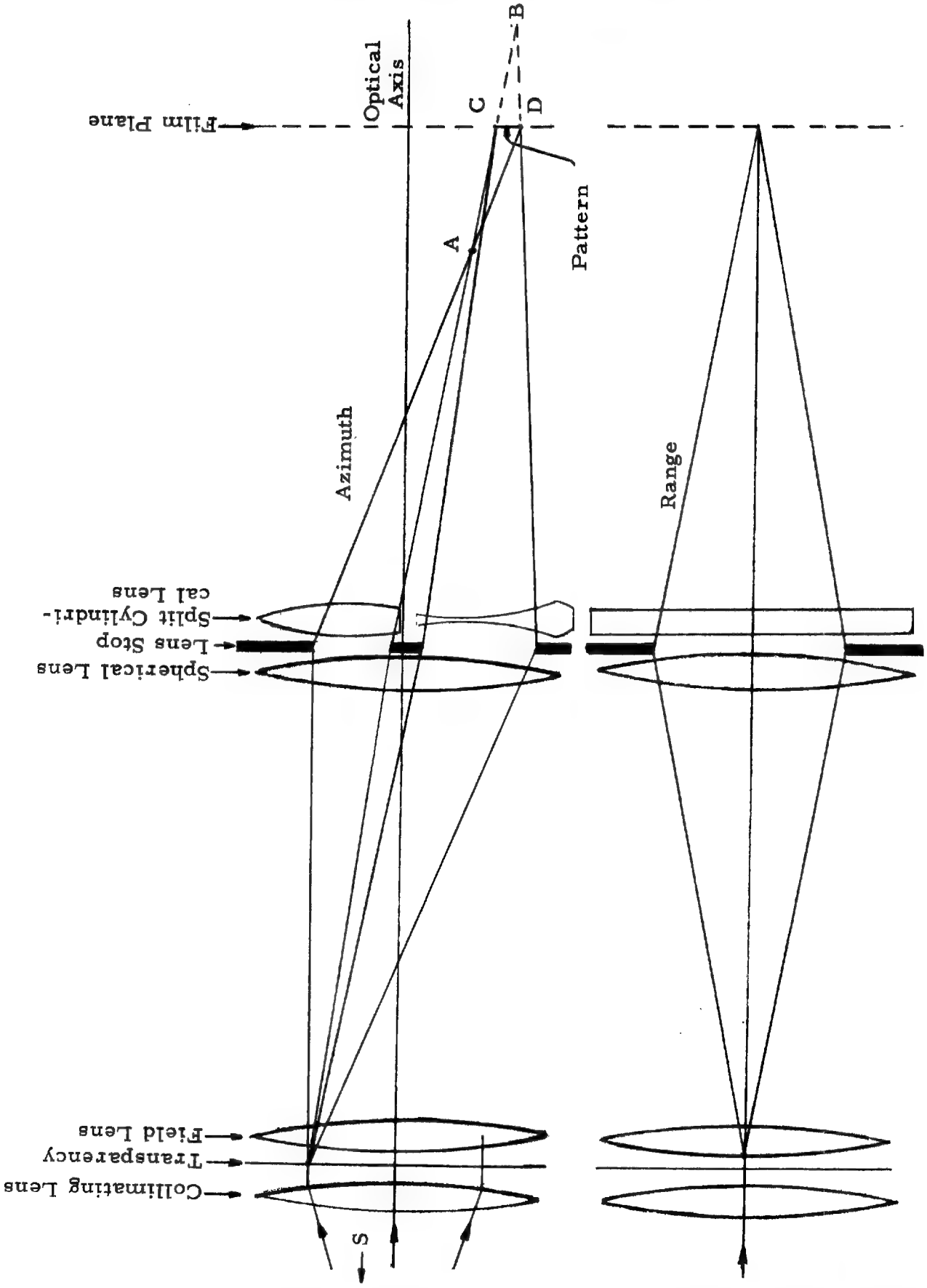

Figure 4 Optical System

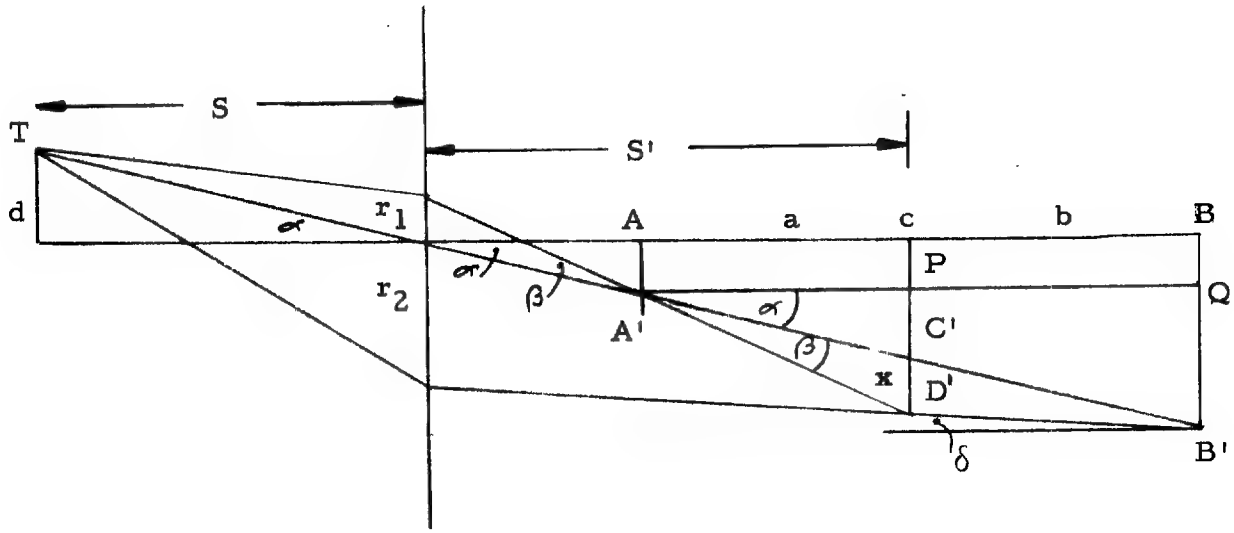

Figure 5

Optical Geometry

and let the phase of the wave reaching B^1 be $\phi_o + \phi_1$. Then phase angle of upper wave at D^1 is

$$\phi_U = \phi_o + \frac{A^1D^1}{\lambda}$$

Phase angle of lower wave at D^1 is

$$\phi_L = \phi_o + \phi_1 - \frac{D^1B^1}{\lambda}$$

Phase difference

$$\Delta\phi = \phi_U - \phi_L = \frac{A^1D^1 + D^1B^1}{\lambda} - \phi_1 \text{ wavelengths.}$$

$$A^1D^1 = \sqrt{a^2 + (PC^1 + x)^2}$$

$$PC^1 = a \tan \alpha$$

$$\therefore A^1D^1 = \sqrt{a^2 + (a \tan\alpha + x)^2}$$

Similarly

$$D^1B^1 = \sqrt{b^2 + (b \tan \alpha - x)^2}$$

Then

$$\Delta\phi = \frac{1}{\lambda}\left[\sqrt{a^2 + (a \tan \alpha + x)^2} + \sqrt{b^2 + (b \tan \alpha - x)^2}\right] - \phi_1$$

If we put a = b the spatial frequency $F_S = \frac{d\Delta\phi}{dx}$

$$\Delta\phi = \frac{1}{\lambda}\left[\frac{x + a \tan \alpha}{\sqrt{a^2 + (x + a \tan\alpha)^2}} + \frac{x - a \tan \alpha}{\sqrt{a^2 + (a \tan \alpha - x)^2}}\right]$$

$$= \frac{1}{\lambda} \sin(\alpha + \beta) + \sin(\beta - \alpha)$$

$$= \frac{2}{\lambda} \sin\beta \cdot \cos\alpha$$

A pattern generated on axis, i.e. when $\alpha = 0$ will be free from distortion. Off axis the frequency error will be some function of α.

$$\frac{\Delta F}{F} = \frac{\text{freq on axis - freq at angle}}{\text{freq on axis}}$$

$$= \frac{\sin\beta - \sin\beta\cos\alpha}{\sin}$$

$$= 1 - \cos\alpha$$

For a frequency error of 0.1%, the field angle α must not exceed 2.5°. This does not present any problem, and means that a flat image (film) plane can be used.

4.0 Lens Focal Length

The lens consists of combination of a spherical lens to focus the image in the range dimension and a split pair of cylindrical lenses, positive and negative to offset the focal points of the sidebands in the azimuth dimension.

If F_o is the focal length of the spherical lens and F_A and F_B the focal length of the auxiliary lenses then the combination focal lengths are given by

$$\frac{1}{F_1} = \frac{1}{F_o} + \frac{1}{F_A}$$

$$\frac{1}{F_2} = \frac{1}{F_o} + \frac{1}{F_B}$$

$$\frac{1}{F_1} = \frac{1}{S} + \frac{1}{S^1 - a} \text{ and } \frac{1}{F_o} = \frac{1}{S} + \frac{1}{S^1}$$

$$\frac{1}{F_A} = \frac{1}{S^1 - a} - \frac{1}{S^1}$$

$$F_A = \frac{S^1(S^1 - a)}{a}$$

$$F_B = \frac{-S^1(S^1 + a)}{a}$$

5.0 Pattern Focal Length

We must now determine the simulator parameters S and a in terms of the radar system constants.

The optical focal length R_o of a pattern given by

$$R_o = \frac{R_1}{2Sx^2} \cdot \frac{\lambda_R}{\lambda_o} \cdot \frac{\cos^3 \theta_2}{\cos^3 \theta_1}$$

where R_1 = radar range

S_x = azimuth scale factor = $\frac{\text{vehicle velocity}}{\text{film velocity}}$

θ_1 = radar squint angle

θ_2 = optical squint angle

This focal length is obtained when the pattern is illuminated by a plane wave of light, or putting it another way, the pattern is similar to that produced by the interference of a plane wave and a spherical wave. The pattern generated by the simulator is due to two spherical waves and in this case it can easily be shown that the focal length is halved. Thus if we put $a = 2R_o$ and $\theta_2 = \alpha$ in the above expression we obtained the required value of a

$$a = \frac{R_1}{Sx^2} \cdot \frac{\lambda_R}{\lambda_o} \cdot \frac{\cos^3 \alpha}{\cos^3 \theta_1}$$

If this value of a is too large for the optical bench, then a smaller value $a^1 = \frac{a}{M^2}$ may be used. In this case the pattern must be subsequently enlarged by the factor M.

Furthermore, as a is directly proportional to R_1, patterns may be simulated at different ranges merely by adjusting the enlargement factor M.

It should be noted however that the stop size must also be adjusted. Lenses do not require changing.

6.0 Minimum Value of S

We have previously determined that the frequency error $\frac{\Delta F}{F} = 1 - \cos \alpha$, i.e.

$$\cos \alpha = 1 - \frac{\Delta F}{F}$$

$$= 1 - q$$

Now from Fig. 5

$$\cos \alpha = \frac{S}{\sqrt{S^2 + d^2}} = 1 - q$$

This gives

$$S = \frac{d(1 - q)}{\sqrt{2q - q^2}}$$

Now q will be very small, so we may write with negligible error

$$S_{min} = \frac{d}{\sqrt{2q}}$$

This gives the minimum value of S to ensure that the pattern frequency error will be less than

$$q = \frac{\Delta F}{F}$$

7.0 Aperture Size (Azimuth)

From Fig. 5 it can be seen that

$$\text{Aperture } V_1 = \frac{S^1 - a}{a} \cdot x$$

$$V_2 = \frac{S^1 + a}{a} \cdot x$$

Where x = pattern length from zero frequency = $L\left(1 + \frac{F_o}{W}\right)$.

From previous analysis we have obtained

$$L = \frac{R}{Sx}(2\beta)\sec^2\theta$$

$$W = \text{doppler bandwidth} = \frac{2Sx}{\lambda R}(2\beta)\cos\theta$$

F_o = offset frequency to lower edge of pattern

Thus x may be determined from the radar parameters. Focal length a and the minimum value of S have already been determined.

Appendix IX

STRAY LIGHT IN THE PROCESSOR

Appendix IX

STRAY LIGHT IN THE PROCESSOR

1.0 Introduction

This is a technical report on an analytical investigation of stray light in the Processor. As a result of this work, the sources of stray light have been identified, methods to reduce the problem have been found and the order of magnitude of the effects are known.

The optical system studied is that in the 9015 Processor and consists of an input slit, two 3-element air spaced collimator lenses, a double glass platen with liquid between, a single lens and small aperture "zero stop" which blocks the direct image of the slit. The remainder of the optical system established certain aperture locations.

The stray light was investigated in detail because only 0.3%* of the light entering the optical system actually reaches the image plane. Thus if as little as 3×10^{-5} of the light is scattered and reached the exit plane, the image will be degraded. Any source of stray light which might contribute 1×10^{-6} stray light was considered.

2.0 Reflections From Lens Surfaces

The optical system from the slit to the zero order stop was ray traced to approximately locate all images formed by one or two reflections. Images formed by four reflections would be much more numerous, but each would be

*Recent tests indicate that this figure may be nearer to 0.003% or even less.

further attenuated by a factor of 20,000 and thus were not considered. There are 17 air-glass surfaces and 2 liquid-glass surfaces in the optical system. These give rise to 153 reflection images. Many of the images from parallel or nearly parallel surfaces were identical, and were combined to make a total of 117 computations. The location, magnification, and strength of each image was determined. This information was then used to calculate the amount of light which would pass through the zero stop and exit slit. The amount of light was calculated as a ratio to the total light entering the entrance slit.

The results can be summarized as follows:

		Stray Light
A.	images located more than 5 inches from the zero stop (129 images)	14.6×10^{-6}
B.	images located less than 5 inches below the zero stop (2 images)	20.0×10^{-6}
C.	images located less than 5 inches above the zero stop or at the zero stop, with zero stop set at 60 cycles per inch*	61.0×10^{-6}
	Total passed by zero stop	95.6×10^{-6}

The exit slit further reduces the amount of light passed. It reduces the effective areas for quantities A and B by a factor of four. It blocks completely the images listed under C. (Assuming all parts are aligned on axis.) The reduced values are:

A	3.7×10^{-6}
B	5.0×10^{-6}
C	0
Total stray light striking film	8.6×10^{-6}

*With the zero stop set to near 0 cps this contribution is 316×10^{-6}.

This light will nearly all fall in the center $2\frac{1}{2}$ inches of the exit platen. Thus it will tend to have a non uniform contribution of about 30×10^{-6} over the center 2 inches and nearly zero elsewhere.

These images can be seen visually by looking into the optical system from the exit slit position. It was not possible to verify the actual figures because of the presence of other stray light sources.

2.1 Illumination from Slit Jaws

After the first reflection from each surface, some light returns to the slit and illuminates the jaws. This light is reflected with a measured diffuse reflection of R = 35% and is re-imaged by the optical system into the zero stop and onto the exit slit. The illumination is calculated in the same fashion as in the above section, except that we now have only 18 images. The slit illumination is $10,000 \times 10^{-6}$. Since the slit reflection is diffuse, only 5% is collected by a $4\frac{1}{2} \times 3''$ platen aperture, to give a total of 170×10^{-6} through the zero stop and 45×10^{-5} through the exit slit. These figures can probably be cut by a factor of 5 or 10 by painting the slit jaws with a gloss black to reduce the apparent reflection.

The light reflected from the zero stop jaws is similar except a diffuse reflectance considerably below 1% is designed into the system. If we assume an R of 1%, then from 4.6×10^{-6} to 15.6×10^{-6} will pass the stop (depending on an alignment) and 1.1×10^{-6} will pass the exit slit.

3.0 Scattering Sources in the Optics

Scattering arises from a number of sources, namely

(1) the glass

(2) scratches on the glass

(3) dust on the glass

(4) hazy films on the glass

(5) scattering on the mirror

The data presented here is taken from a recent article on Coronagraphs*. It was found that scattering due to the glass with very few bubbles in BSC-2 and BK-7 is 1.2×10^{-6} and 2.5×10^{-6}. The geometry of our system is such that we would expect to pick up about 4 times as much light as is accepted in the Coronagraph discussed in the reference, so we can expect about 10×10^{-6} contribution from the glass.

In the reference, they found that "faint scratches" contributed 1 to 2×10^{-6} per scratch. This is a difficult figure to work with, but it indicates that a few dozen scratches could easily predominate the stray light problem.

Dust on the glass: Ideally there should be no dust or lint on any of the optical surfaces. In practice, however, there will be some dust. The amount of light contributed by dust can be determined from scattering theory. It was found that the stray light through the exit slit would be

Size of Particle	Contribution Per Particle through zero stop	through exit slit
5	$.0003 \times 10^{-6}$	$.00007 \times 10^{-6}$
50	$.14 \times 10^{-6}$	$.035 \times 10^{-6}$
10 μ diam. x $\frac{1}{8}$ inch thread (parallel to slit)	1×10^{-6}	$.25 \times 10^{-6}$

The dust population under operating conditions is difficult to estimate. If we assume, on each exposed surface, a population of

	On Film
50 5 μ particles	$.0035 \times 10^{-6}$
5 50 μ particles	$.165 \times 10^{-6}$
1 $\frac{1}{4}$" long 10 μ thread at 45°	$.37 \times 10^{-6}$

*Newkirk and Bohlin, "Reduction of Scattered Light in the Coronagraph." Applied Optics, v. 2, n2, p. 121, February 1963.

There are 7 air glass surfaces. These would then give a total contribution of about 4×10^{-6} to the film.

Hazy film on the glass: A film on the optical surfaces caused by smoke (cigarette or carbon arc) will cause scattered light. The contribution would be very difficult to measure directly, but could be measured at large angles (5 or 30°) where other scattering effects are not a problem. Recourse would then be made to particle size and scattering theory to obtain estimates at the correct angle. This has not been done because the experiments and calculations would require considerable time and experience has indicated that haze can be successfully eliminated by adequate cleaning procedures.

Scattering on the mirror: Small angle scattering on the mirror is very difficult to determine. Very little information has been published, apparently because most people seriously concerned with scattered light avoid the use of mirrors in their optical systems*. Attempts to measure the scattered light from a good mirror only pointed out the difficulty and hence the cost and time required to obtain reliable data. However, this work, coupled with visual observations, did lead to the conclusion that the mirror does cause a serious amount of stray light. On this basis the mirror has been made to the best quality standards. One source of stray light, that passing through the mirror surface and reflecting from the back, has been eliminated by painting the back black.

4.0 Diffraction

Some of the zero order light is spread out of the geometrical slit image by diffraction at the edges of the beam aperture, in this case the platen. For

*Designs with no upper mirror were considered for the Processor, but were found impractical.

a platen width of 3.5 inches, the diffraction pattern at the zero stop has its first nul at a distance of .006 inches from the axis, this corresponds to a spatial frequency of 12 cycles per inch.

For a zero stop passband of 60 to 600 cycles per inch, the accepted diffraction pattern is beyond the fifth "ring" or sidelobe, about 140×10^{-6} of the light will pass through this opening. The exit slit will accept one fifth of this light. However, in the present system the input platen is re-imaged by the relay lens and cylinder lens in a plane nearly coincident with the lower mirror. Over 95% of the diffracted light is reconcentrated into an image of the platen edges at this plane. A black aperture mask has been made to cover this mirror and stop this image. By this method the diffracted light contribution has been reduced to 1×10^{-6} or less.

Appendix X

CYLINDER LENS EFFECTS

Appendix X

CYLINDER LENS EFFECTS

1.0 Introduction

This technical note records some preliminary work done to study some of the effects of cylinder lenses. It assumes that the optical lenses are "ideal" in a paraxial sense, then computes certain effects which occur at finite apertures and angles.

1.1 Effects Due to Slant Angle ϕ

A cylinder lens suffers from two gross problems due to the inclination ϕ of a fan of rays above the optical axis.*

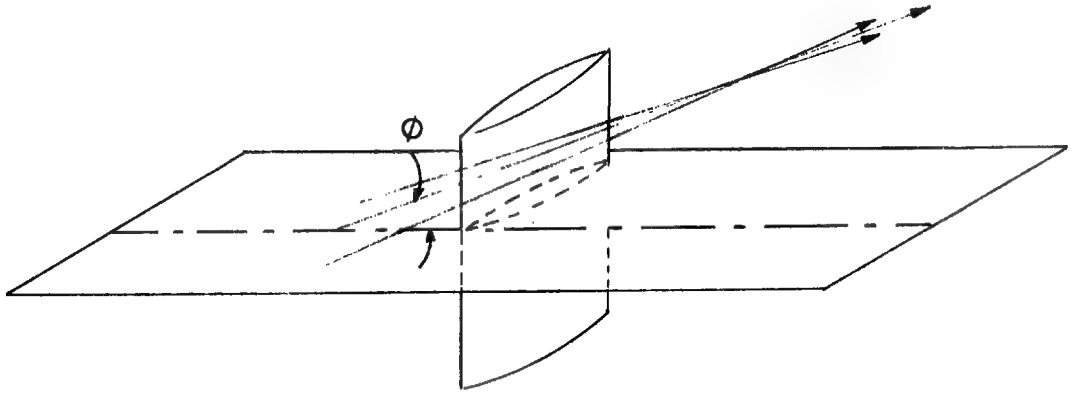

Figure 1

*There are certainly other "aberrations", but it is believed that the two described are the major effects.

One effect will be termed the parallel plate displacement effect and creates a deviation out of the plane of the original fan of rays. The second effect is a change of effective focal length due to the tilt angle. This focal length change can appear as field curvature and/or as image blur, depending on the overall optical system.

1.1.1 Parallel Plate Displacement (ϕ)

The parallel plate displacement assumes that a ray going through the cylinder lens will be displaced a distance d in the plane in which the cylinder lens has no power. This can be calculated by considering a section parallel to the w axis

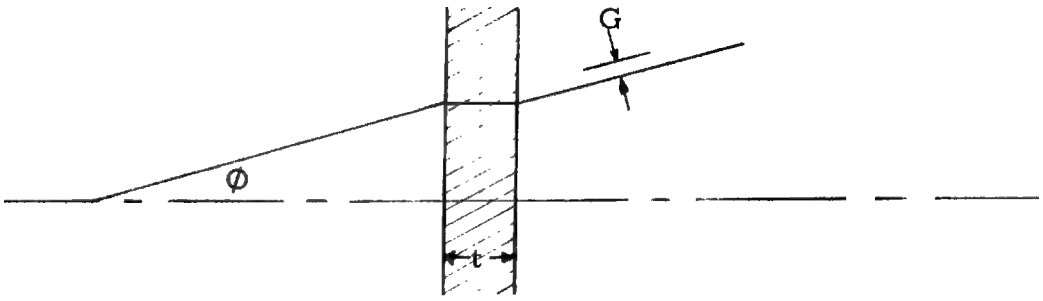

Figure 2

From standard parallel plate theory

$$G = t_c \sin \phi \left(1 - \frac{1}{n} \frac{\cos \phi}{\cos \phi'}\right)$$

or, for small ϕ

$$G = t_c \sin \phi \left(\frac{n-1}{n}\right) *$$

The variation in t can be determined by assuming a plano-convex lens.

* at $\phi = 5^o$, the error is $\frac{\Delta G}{G} = .003$; at 10^o $\frac{\Delta G}{G} = .02$.

For a lens of focal length F, the radius R is

$$R = (n-1)F$$

At an aperture v the sag Δt is

$$\Delta t = \frac{v^2}{2R}$$

$$= \frac{v^2}{2F(n-1)}$$

so that

$$G_v = t_v \sin \phi \left(\frac{n-1}{n}\right)$$

$$= (t_c - t) \sin \phi \left(\frac{n-1}{n}\right)$$

We are interested in the variation of displacement from the central range (i.e. we assume that the overall optical system is corrected for a parallel plate of thickness t_c)

$$g = G_c - G_v$$

$$= t_c \sin \phi \ \frac{n-1}{n} - (t_c - \Delta t) \sin \phi \ \frac{n-1}{n}$$

$$= \frac{v^2}{2F} \ \frac{\sin \phi}{n-1} \ \frac{n-1}{n}$$

$$g = \frac{v^2 \sin \phi}{2nF}$$

The $\frac{\sin \phi}{n}$ is the angle of the ray inside the lens, but the present form is usually easier to use.

1.1.2 Focal Length Change

The change in focal length can be approximated by calculating the decrease in R at slant angles.*

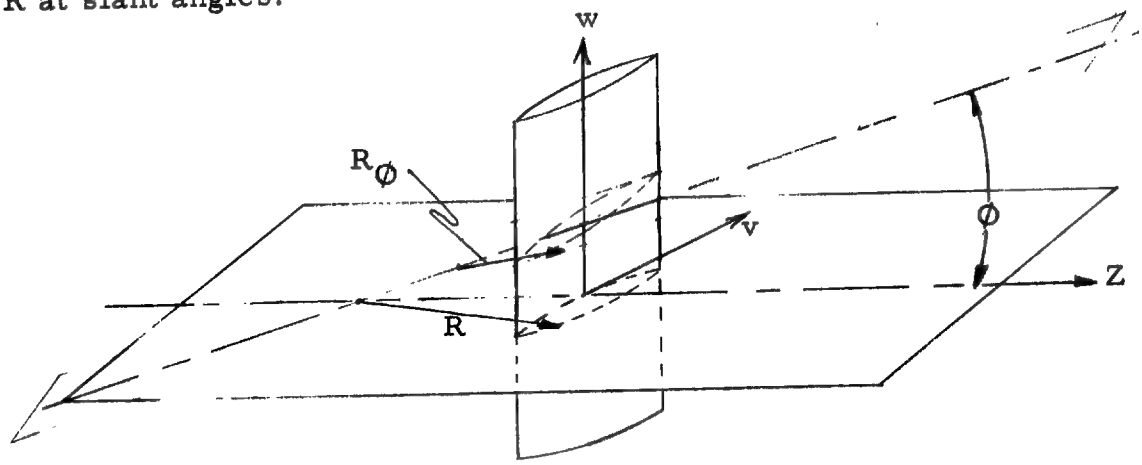

Figure 3

The sag S has now increased by cos ϕ while the aperture is constant. The new radius is

$$R_\phi = \frac{v^2 \cos \phi}{2}$$

$$= R_o \cos \phi$$

Thus the focal length in the tilted plane has also increased

$$F'_\phi = F_o \cos \phi$$

As usually defined, the focal length is measured along the optical axis, so

$$F_\phi = F'_\phi \cos \phi$$

$$F_\phi = F_o \cos^2 \phi$$

$$= F_o (1 - \sin^2 \phi)$$

*The approximate "correctness" of this approach was verified experimentally by checking the $F'_\phi = F_o \cos \phi$ relationship.

thus there is a change of focus

$$\Delta F_{\phi} = - F_{o} \sin^2 \phi$$

1.2 Effects Due to Cylinder Lens Rotation

1.2.1 The Optical System (spherical and cylinder lens coincident)

The physical system is shown in Fig. 4, where the "object" is a pair of slits, one horizontal (along the x axis) and one vertical (parallel to the y axis). They will be identified by the symbols ⊥ and ||. These slits are separated by a distance d along the optical axis (z axis).

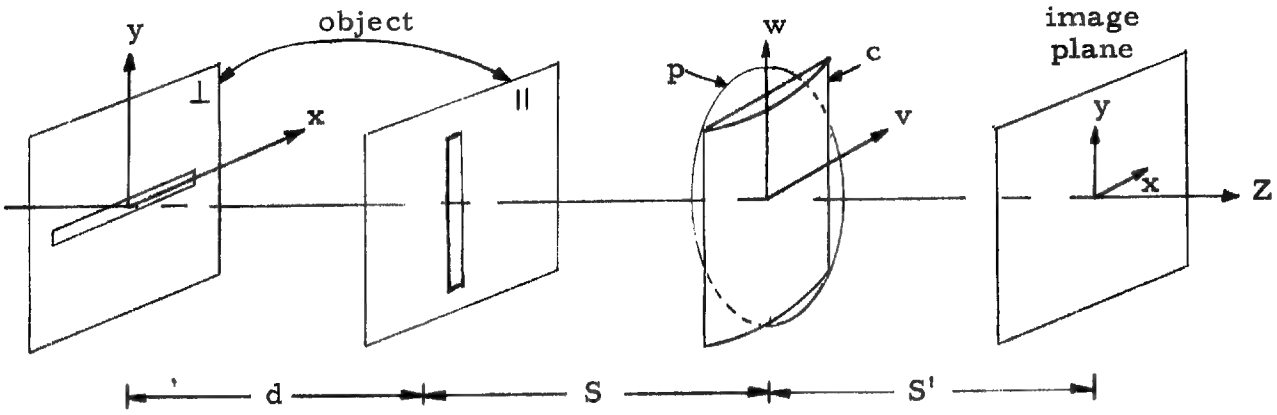

Figure 4

In the figure S and d are negative.

The slits are assumed to have an infinitesimal width. The half lengths L_x and L_y for slits ⊥ and || respectively.

A sperhical lens P is located on the optical axis and images the slit ⊥ into the image plane as shown. A cylinder lens C is placed with its cylinder axis in the w direction (parallel to the y axis and hence to the || slit) and adds sufficient power to the sphere to image the || slit into the image

plane. For simplicity, we assume the lenses to be thin lenses with no spherical or other aberration and assume the lenses to be coincident. The focal length of the spherical lens will be

$$\frac{1}{F_P} = \frac{1}{S'} - \frac{1}{S+d}$$

$$F_P = \frac{(S+d)\,S'}{(S+d) - S'}$$

using the convention of all + distances running to the right.

The focal length of the cylinder can be found by

$$\frac{1}{F_{pc}} = \frac{1}{F_p} + \frac{1}{F_c} = \frac{1}{S'} - \frac{1}{S}$$

$$\frac{1}{F_c} = \frac{1}{S'} - \frac{1}{S} - \frac{1}{F_p}$$

$$= \frac{1}{S'} - \frac{1}{S} - \frac{1}{S'} - \frac{1}{S-d}$$

$$= -\frac{1}{S} + \frac{1}{S+d}$$

$$= \frac{S-S-d}{S(S+d)}$$

$$F_c = -\frac{S}{d}(S+d)$$

The aperture at the lens will be described by the rectangular coordinates v and w.

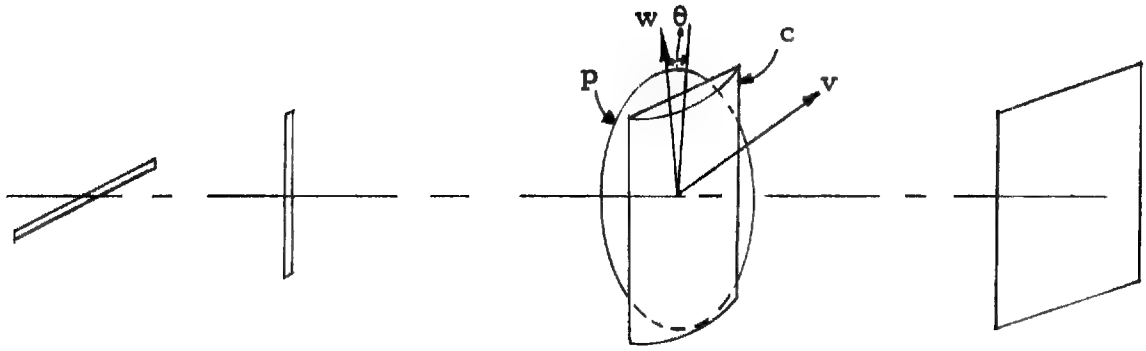

Figure 5

1.2.2 Cylinder Lens Focal Length Change

The focal length of the cylinder lens in the v and w directions.

$$F_v = \frac{F_c}{\cos^2 \theta} *$$

$$F_w = \frac{F_c}{\sin^2 \theta}$$

The new image distance will be

$$\frac{1}{S_{||}} = \frac{1}{F_v} + \frac{1}{F_p} + \frac{1}{S}$$

and

$$\frac{1}{S_{\perp}'} = \frac{1}{F_w} + \frac{1}{F_p} + \frac{1}{S+d}$$

The focal shifts are given by

$$\Delta S_{||}' = S_{||}' - S'$$

$$\Delta S_{\perp}' = S_{\perp}' - S'$$

*This is quoted in Martin "Technical Optics," Vol I., p. 303

For the image $\perp$ we have

$$\frac{1}{S_\perp} = \frac{1}{F_w} + \frac{1}{F_p} + \frac{1}{S+d}$$

$$= \frac{1}{F_w} + \frac{1}{S'}$$

$$\Delta S_\perp = \frac{F_w S'}{F_w + S'}$$

$$\Delta S_\perp = \frac{F_w S'}{F_w + S'} - S'$$

$$= \frac{F_w S' - F_w S' - S'^2}{F_w + S'}$$

$$= \frac{S'^2}{F_w + S'}$$

$$= -\frac{S'}{F_w} \quad \text{if} \quad F_w \gg S'$$

$$\therefore \Delta S_\perp = -\frac{S'^2}{F_c} \sin^2 \theta$$

In the $\parallel$ direction

$$\frac{1}{S'_n} = \frac{1}{\Delta F_v} + \frac{1}{F_c} + \frac{1}{F_p} + \frac{1}{S}$$

where a change in the cylinder lens focal length ΔF_v is defined by

$$\frac{1}{\Delta F_v} = \frac{1}{F_v} - \frac{1}{F_c}$$

The value of ΔF_v is

$$\frac{1}{\Delta F_v} = \frac{\cos^2 \theta}{F_c} - \frac{1}{F_c}^2$$

$$\frac{1}{\Delta F_v} = -\frac{\frac{S^2}{n}\theta}{F_c}$$

i.e.,

$$\Delta F_v = -F_w$$

or

$$F_v + F_w = F_c \text{ for all angles,}$$

and interesting fact implied in Martin's book.

Thus,

$$\frac{1}{S'_{\parallel}} = \frac{1}{F_w} + \frac{1}{S'}$$

$$S'_{\parallel} = \frac{F_w S'}{F_w - S'}$$

$$\Delta S'_{\parallel} = \frac{FS'}{F_w - S} - S'$$

$$= \frac{FS' - F_w S + S'^2}{F_w - S'}$$

$$= \frac{S'^2}{F_w + S'}$$

$$\therefore \Delta S'_{\parallel} = \frac{S'^2}{F_c} \sin^2 \theta$$

using the same approximation as above. This focal shift occurs for a paraxial bundle of rays.

1.2.3 Effects of Lens Displacement

For a bundle of rays which pass through the lens at w, there is a

displacement of the bundle due to the displacement of the optical center of the lens b_w as shown in Fig. 6.

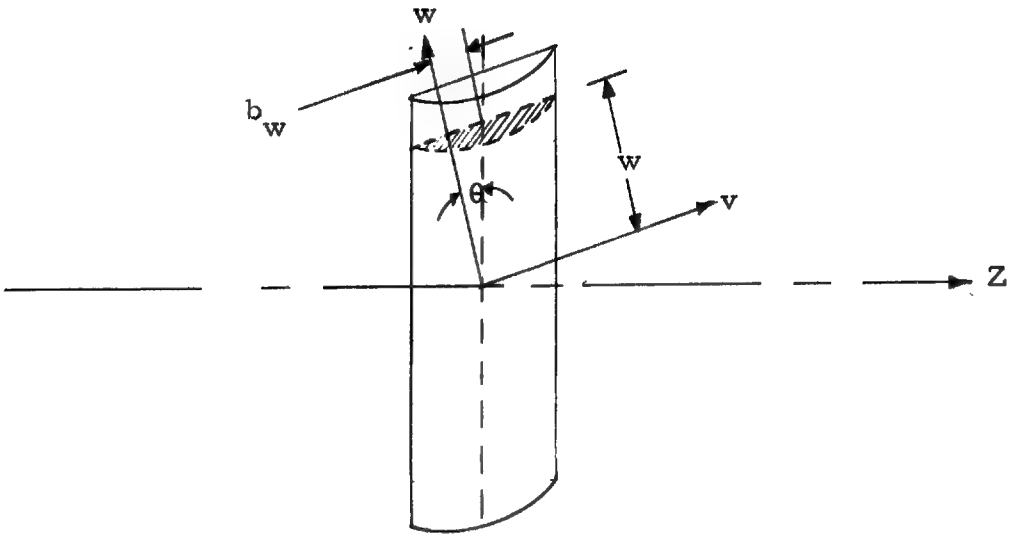

Figure 6

The geometry gives the amount of displacement as

$$bw - w \sin \theta$$

This acts upon the virtual image (formed by the spherical lens) at a distance S_1'.

$$\frac{1}{S_1'} = \frac{1}{F_p} + \frac{1}{S}$$

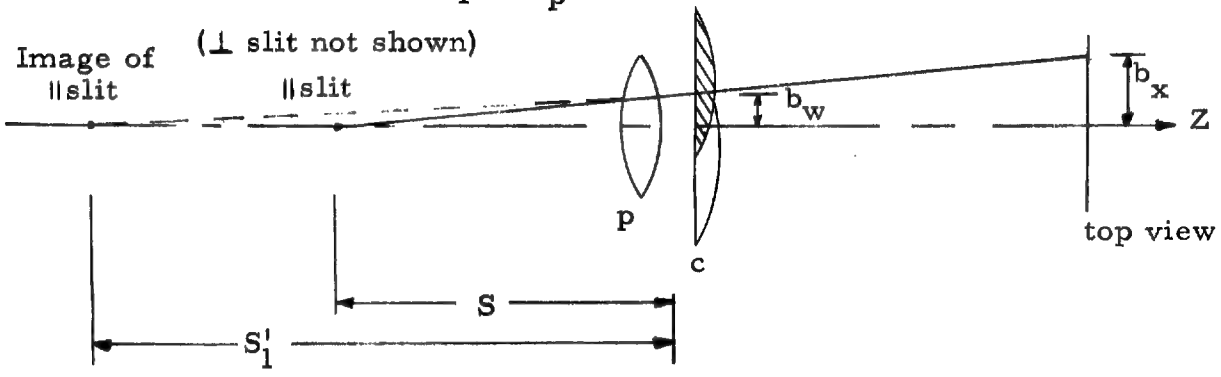

Figure 7

The image displacement is found from similar triangles

$$b_x = b_w \frac{S_1' - S'}{S_1'} \quad *$$

$$b_x = w \frac{S_1' - S'}{S_1'} \sin \theta$$

Using the relationship

$$\frac{1}{S'} = \frac{1}{S_1'} + \frac{1}{F_c}$$

we obtain

$$b_x = \frac{w\, S' \sin \theta}{F_c}$$

A ray which passes through the cylinder lens at a distance v from the w axis will also suffer a displacement. This can be considered to be due to the fact that the center of the lens section is at the point where the cylinder axis crosses the v line. This approach is included as Section 2.0 of this appendix.

The calculations for b_y consider the section of the lens to be a wedge. The wedge angle can be calculated simply by assuming that the cylinder is plano, and thus the radius across a v section before rotation is

$$R = (n-1)\ F_c$$

The radius along the w section after rotation is

$$R_\theta = \frac{R}{\sin^2 \theta}$$

The wedge angle can be found from the geometry in Fig. 8.

*S and S_1' shown are negative.

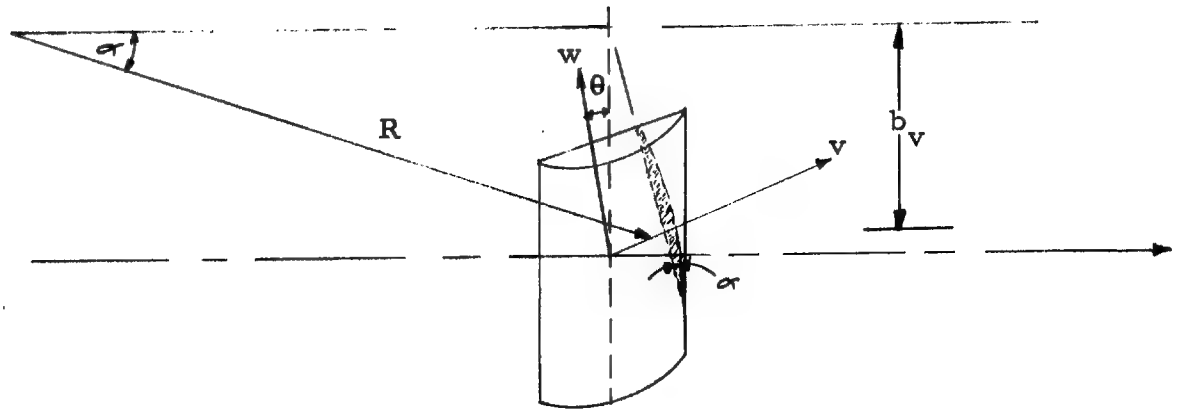

Figure 8

$$\sin\alpha = \frac{b_v}{R} \qquad b_v = \frac{v}{b_v = \sin\theta} \qquad R = \frac{(n-1)F}{\sin^2\theta}$$

$$\sin\alpha = \frac{v \sin^2\theta}{\sin\theta(n-1)F_c}$$

For rays which pass above or below the VZ plane, the height should be subtracted from V. For small θ, $b_v >> w$, and this correction will be ignored.

The deviation of the ray is given by

$$\sin\delta = (n-1)\sin\delta$$

$$= \frac{v \sin\theta}{F_c}$$

The deviation b_y is

$$b_y = S' \sin\delta$$

$$= \frac{S' v \sin\theta}{F_c}$$

This gives the same answer as Section 2.0, but it is clearer as to the mechanism of the deviation.

1.2.4 An Analysis of the Effects

The effects of rotation θ will usually interact with the effects of slant angle ϕ, so the two will be combined.

From Section 1.1 we have

$$\Delta F_{c\phi} = - F_c \sin^2 \phi$$

and

$$g = \frac{v^2 \sin \phi}{2n F_c}$$

For the system under description,

$$\sin \phi = - \frac{n}{S'}$$

$$\Delta F_c = \frac{F_c w^2}{S'^2}$$

This change in focal length gives rise to a focal shift of (see Section 3.0):

$$\Delta S'_{II} = \frac{K S'^2}{F_c}$$

$$K = \frac{\Delta F}{F}$$

$$= - \frac{w^2}{S'^2}$$

$$\Delta S'_{II} = - \frac{w^2}{F_c}$$

The g factor is a ray shift in the y direction and is

$$g_y = \frac{v^2 w}{2n f_c S'}$$

The shift in image position will cause a shift in the ray intersection.

$$h_x = \frac{v}{S'} \Delta s_{\parallel}$$

$$h_y = \frac{w}{S'} \Delta s_{\perp}$$

Thus the ray shift is

$$\Delta H_x = \frac{vS'}{F_c} \sin^2 \theta + \frac{wS' \sin \theta}{F_c} - \frac{v}{S'} \frac{w^2}{F_c}$$

$$\Delta H_y = - \frac{wS'}{F_c} \sin^2 \theta + \frac{vS' \sin \theta}{F_c} - \frac{v^2 w}{2n F_c S'}$$

The first term arises from a focal shift due to rotation, the second term arises from a lens center shift (i.e., wedge) effect, and the last terms occur as deviations due to the slant angle of rays out of the X2 plane.

The equations can be simplified and cast into other forms to better show the effects. For example, the common factor $\frac{S'^2}{F_c}$ can be taken out of each term, and the aperture values v and w can be replaced by their corresponding slant angles ϕ_v and ϕ_w.

$$\tan \phi_v = \frac{v}{S'} \qquad \tan \phi_w = \frac{w}{S'}$$

$$\phi_v \approx \frac{v}{S'} \qquad \phi_w \approx \frac{w}{S'}$$

In addition, for small values of θ, $\sin \theta - \theta$, and the $\sin^2 \theta$ term can be

dropped. This gives

$$\Delta H_x = \frac{S'^2}{F_c} \Phi_w (\theta - \Phi_v \Phi_w)$$

$$\Delta H_y = \frac{S'}{F_c} \Phi_v \left(\theta - \frac{\Phi_v \Phi_w}{2n}\right)$$

The relationship to the S_1 S' and d can be seen if F_c is eliminated giving

$$\Delta H_x = \frac{S'^2 d}{-S(S+d)} \Phi_w (\theta - \Phi_v \Phi_w)$$

and similarly for ΔH_y.

Various definitions of the basic parameters could be made relating focal length, distances, and magnifications. One such makes use of the magnification and an "astigmatic ratio",

$$m_{||} = \frac{S'}{S}$$

$$A = \frac{d}{S+d}$$

giving

$$\Delta H_x = m_{||} \; A \; S' \Phi_w (\theta - \Phi_v \Phi_w)$$

$$\Delta H_y = m_{||} \; A \; S' \Phi_v \left(\theta - \frac{\Phi_v \Phi_w}{2n}\right)$$

Some observations are:

If the effects of θ are small,

$$\Delta H_x = - m_{||} \; A \; S' \Phi_w^2 \Phi_v$$

$$\Delta H_y = - \frac{m_{||} A S'}{3} \Phi_w \Phi_v^2$$

A symmetrical (on axis) image would be obtained if

$$\Phi_v = 3\Phi_w$$

ΔH varies as the cube of the aperture. As a result, the image is composed of a hard core with large flare (see spot diagram).

If the Φ is reasonably small, then θ will be the controlling factor.

$$\Delta H_x = m_{||} \; A \; S' \; \Phi_w \; \theta$$

$$\Delta H_y = m_{||} \; A \; S' \; \Phi_v \; \theta$$

In this case, the image will be a uniform smear with an outline related to the outline of the aperture "mirrored" around the line x = y.

It will now be instructive to compute and plot the spot diagram for a specific system:

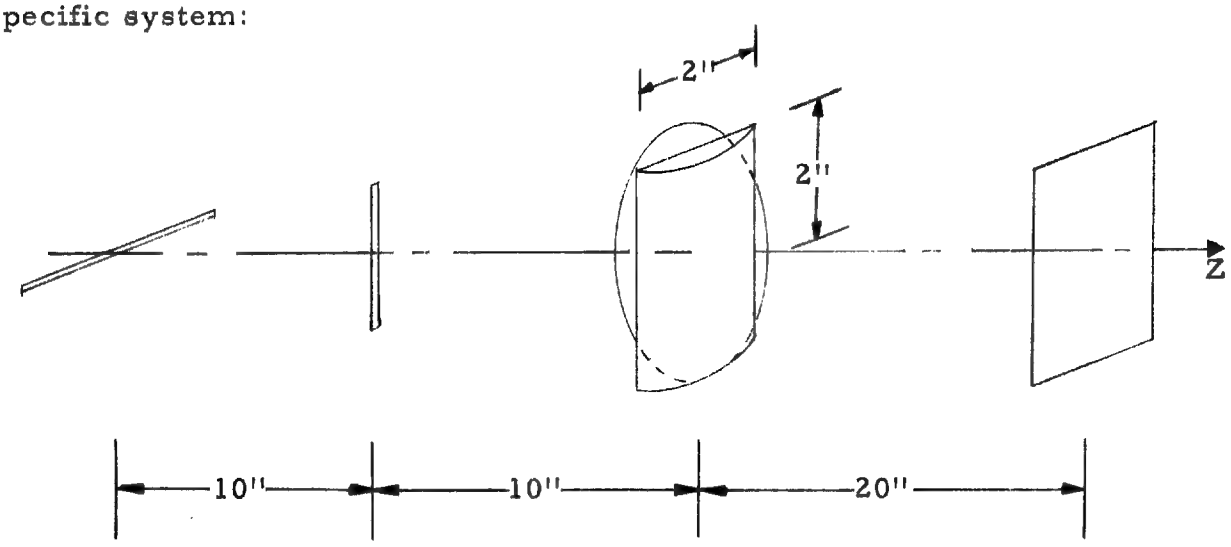

Figure 9

$$S = -1^{o}\ d = -1^{o}\ S = 20\ m \quad = 2\ A = \tfrac{1}{2}$$

$$F_p = 10\ F_c = 20\ v_A = w_m = 2\ \Phi_{vm} = \Phi_{vm} = 1\ n = 1.5$$

$$\Delta H_x = 2 \times \tfrac{1}{2} \times 20\ \Phi_w\ (\theta - \Phi_v\ \Phi_w)$$

$$\Delta H_x = 20\ \Phi_w\ (\theta - \Phi_v\ \Phi_w)$$

$$\Delta H_y = 20\ \Phi_v\ \ \theta - \frac{\Phi_v\ \Phi_w}{3}$$

for $\theta = 0$

$$\Delta H_x = -20\ \Phi_v\ \Phi_w$$

$$\Delta H_y = -6.6\ \Phi_v\ \Phi_w$$

These values have been computed and plotted for increments of .01 for 3 values of θ. A change of scale factor makes the diagrams suitable for certain other values as shown.

A scale change would also suffice for other values of S', m, and A.

The case for very large θ has not been plotted. It would be simply a square assembly of evenly spaced ray intersections.

1.2.5 Further Work to be Done

Some further considerations which are not included at this time are:

(1) effects off axis

(2) the variation of the image with refocusing

(3) further development of useful parameters

(4) the effects of separating the spherical and cylinder systems

(5) a consideration of systems with additional lenses

(6) the precise calculations of typical systems to check on other aberrations so as to determine the useful range of the above relatively simple calculations

(7) the effects of non-othogonal objects.

2.0 Alternative Calculation of Displacement b_y

In the figure the location of the intersection of the center of the lens and the distance v of the ray from the w axis is located.

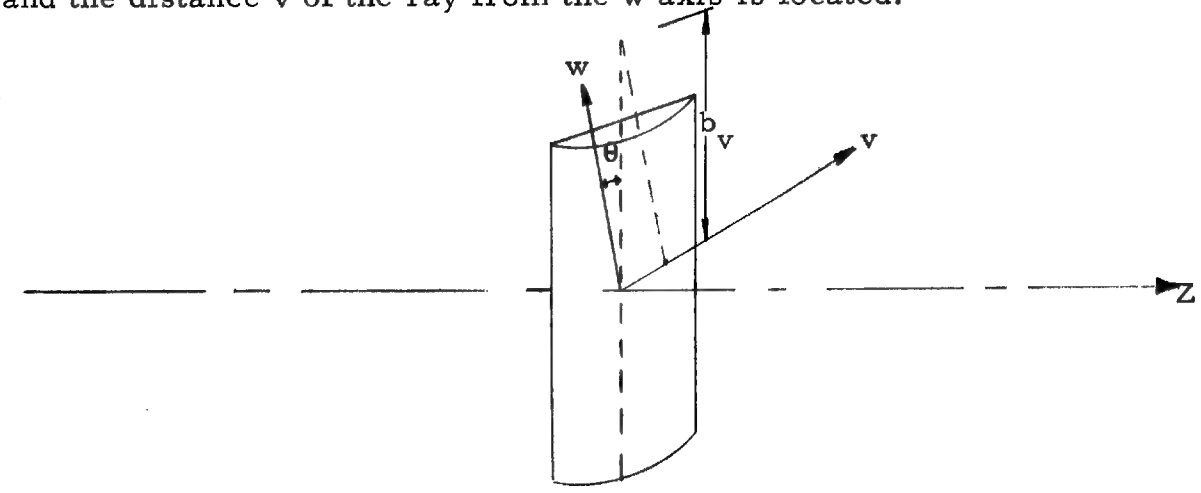

Figure 10

the distance b_v is given by $b_v = \frac{v}{\sin \theta}$.

In this case the image formed by the spherical lens is at the image plane.

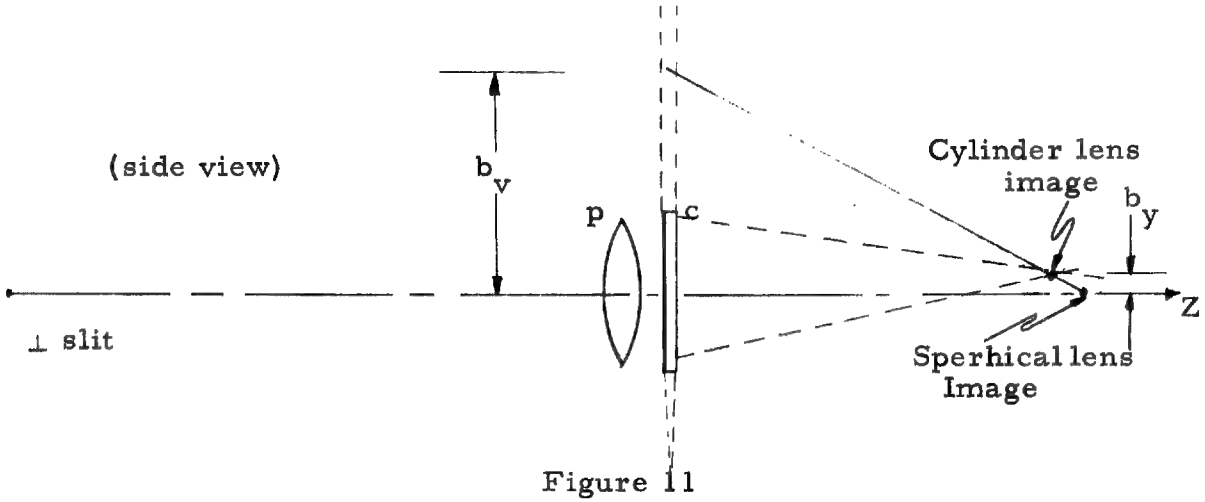

Figure 11

the value for b_y is

$$b_y = \frac{b_v}{S'} \Delta S_{||}'$$

$$= \frac{v}{S' \sin \theta} \frac{S'^2 \sin^2 \theta}{F_c}$$

$$b_y = \frac{v S' \sin \theta}{F_c}$$

Note that the cone of light is coming from the lens, not along the fictitious ray shown.

3.0 Image Shift Due to Lens Focal Length Change

For the original condition

$$\frac{1}{S'} = \frac{1}{F} + \frac{1}{S}$$

$$S' = \frac{F_S}{S+F}$$

with an increased focal length

$$F_n = F (1+K)$$

$$\frac{1}{S_n'} = \frac{1}{F_n} + \frac{1}{S}$$

$$S_n' = \frac{F_n S}{F_n + S}$$

the shift is

$$\Delta S' = S_n' - S'$$

$$= \frac{F_n S}{F_n + S} \quad \frac{F_S}{F+S}$$

$$= \frac{FF_nS + F_nS^2 - FF_nS - F_S^2}{(F_n+S)(F+S)}$$

$$= \frac{S^2(F_n - F)}{(\quad)(\quad)}$$

or

$$\Delta S = \frac{S^2(F+FK-F)}{(F_n+S)(F+S)}$$

$$= \frac{S^2 FK}{(F+KF+S)(F+S)}$$

If we assume

$$KF \ll F + S$$

(i.e., that the image is not near infinity) this simplifies to

$$\Delta S = \frac{S^2 KK}{(F+S)^2}$$

$$= \frac{S^2 FK S^2}{F^2 S^2}$$

$$\Delta S = \frac{K}{F} S'^2$$

This can be put in another form by substituting for F

$$S = \frac{KS'^2 (S-S')}{SS'}$$

$$= KS' \left(1 - \frac{S'}{S}\right)$$

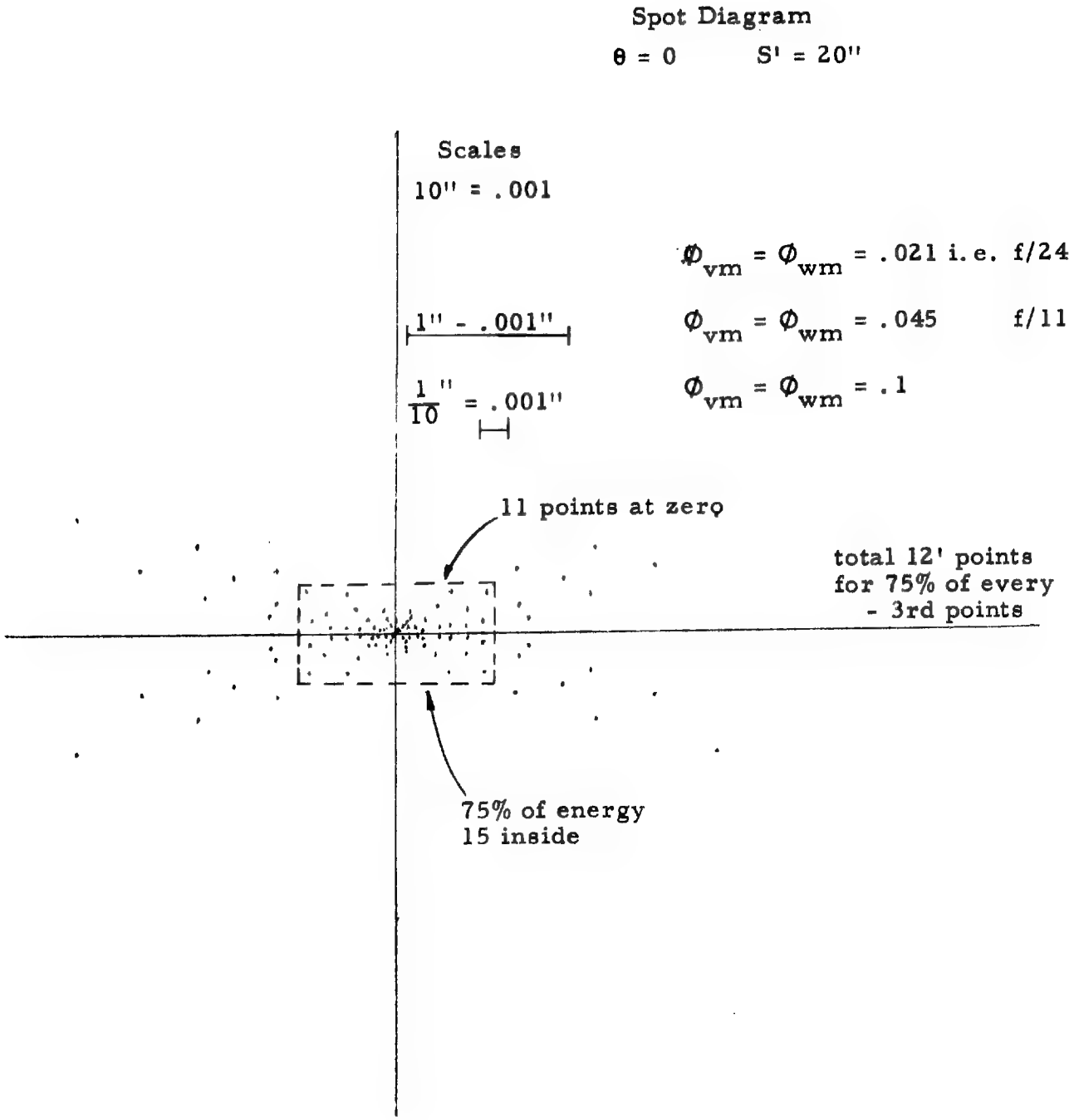

Figure 12

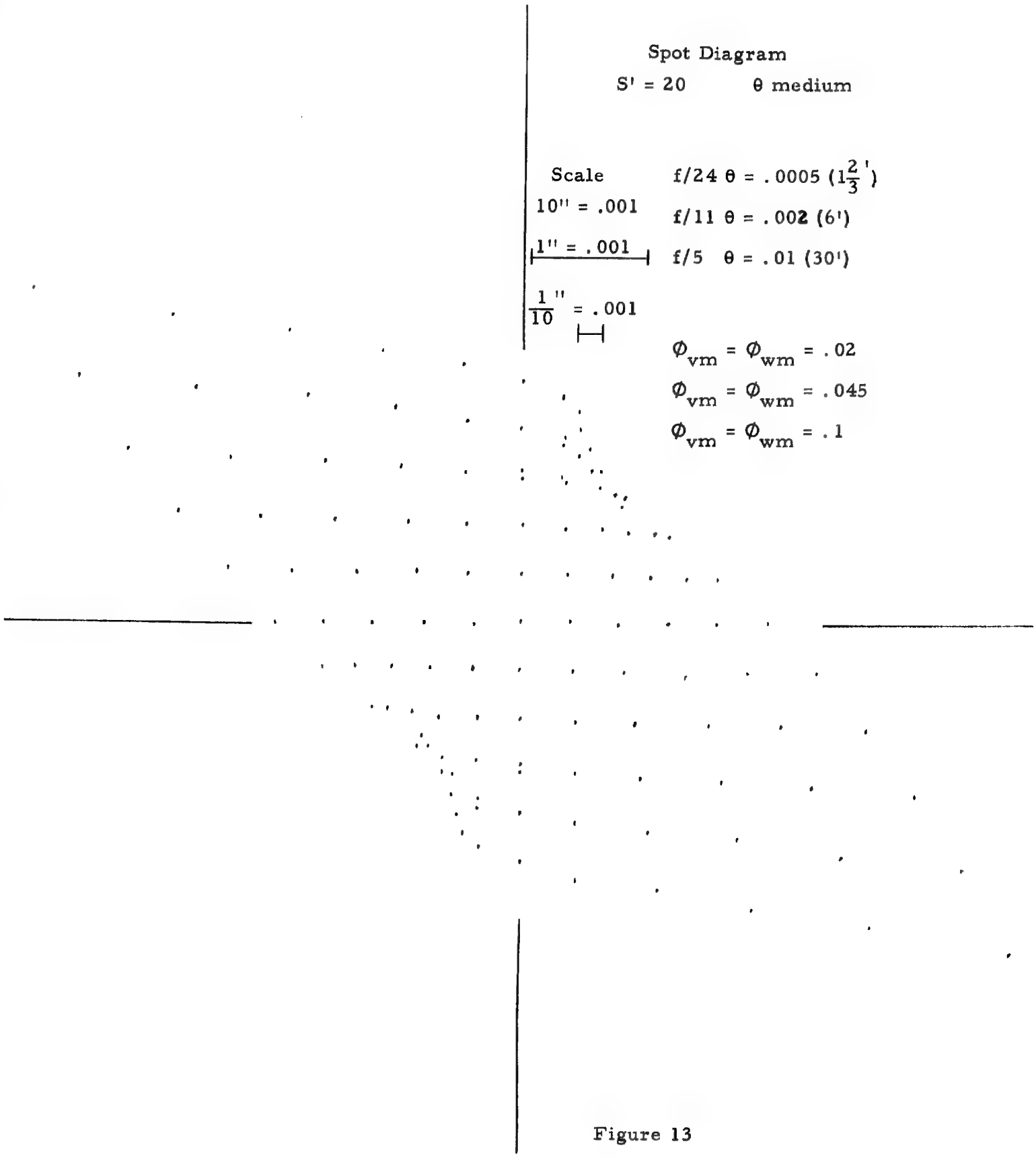

Figure 13

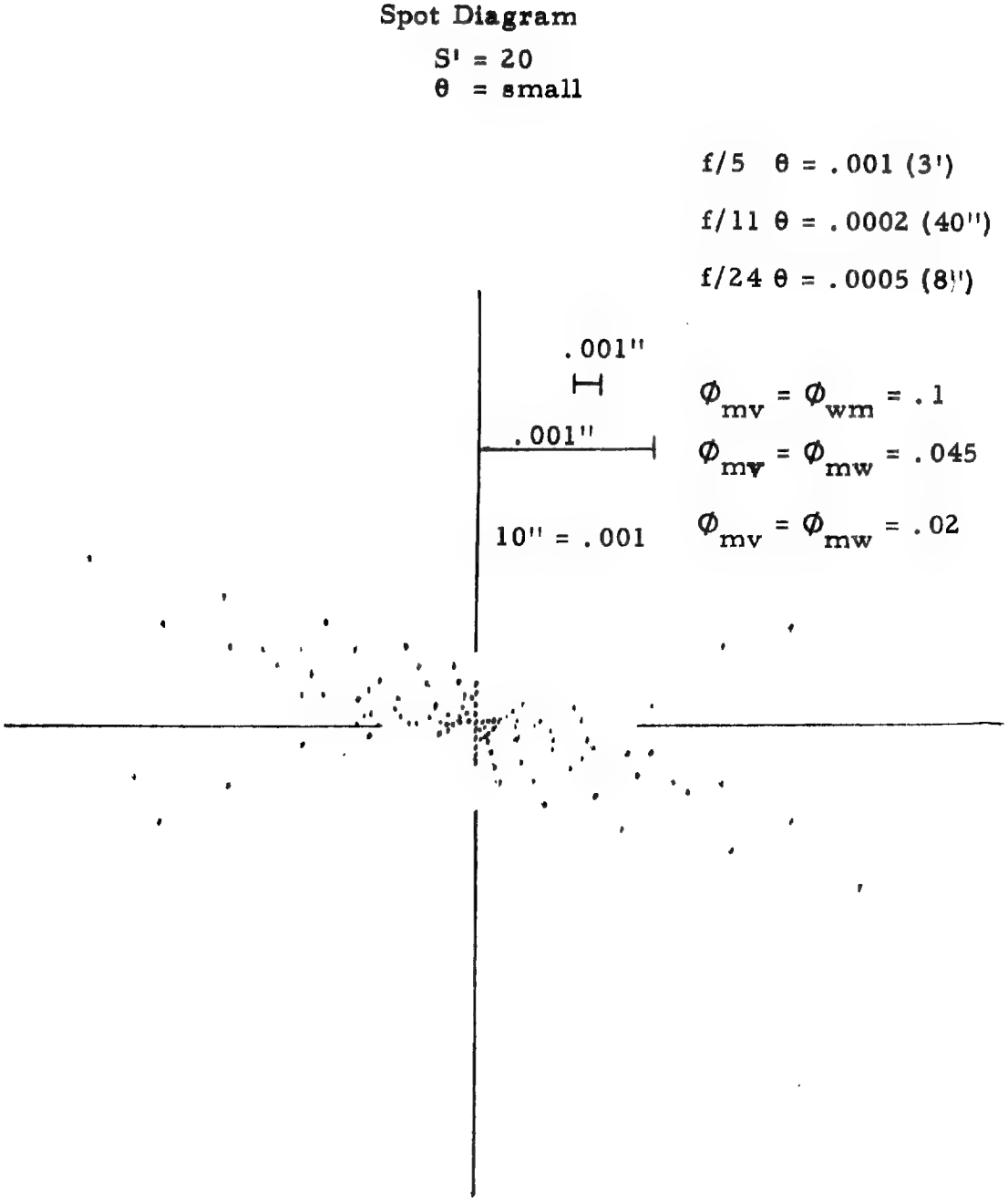

Figure 14

Appendix XI

FLIGHT TEST REPORT FORMS

Appendix XI

FLIGHT TEST REPORT FORMS

The Westinghouse flight test form is shown in Fig. 1. This form is filled in at Westinghouse and sent along with the film to the processing site. No company names or identifying nomenclature is included for security reasons. The key is included after the form as Figs. 2.

The form shown in Fig. 3 contains the specific settings of the Processor. It superseded notebook entries and an earlier form. It is filled out and distributed each time a change is made or the alignment is re-checked.

The third form (see Fig. 4) records most of the sensitometric and processor adjustment data in use at the present time. This form is originated at the Itek field site and duplicates are sent to Westinghouse and Lexington.

The "Special Handling" is not included on the actual forms used.

FLIGHT NO. _____
DATE _____
PILOT _____
OBSERVER _____

Section I

A.
B.
C.
D.
E.
F.
G.
H.
I.
J.
K.
L.
M.
N.

Section II

	Run 1	Run 2	Run 3	Run 4	Run 5
1.					
2.					
3.					
4.					
5.					
6.					
7.					
8.					
9.					
10.					
11.					
12.					
13.					

Section III

Figure 1

SPECIAL HANDLING

Flight No. :_____
Date:_____
Pilot:_____
Observer:_____

Section I: System Preflight Configuration

A.	Average Power Out of Ring	(watts)
B.	Pulse Width	(n sec)
C.	Noise Figure	(db)
D.	Light Level Meter	(units)
E.	Light Level Pot Setting	(units)
F.	Tracking Offset Frequency	(cps)
G.	Tracking Gate Position	(u sec)
H.	AGC	(volts)
I.	IF Limiting	
J.	Lens Opening	(f stop)
K.	Video Noise Level	(volts p/p)
L.		
M.		
N.		

Section II:

	Run 1	Run 2	Run 3	Run 4	Run 5
1. Altitude 1000					
2. Ground Speed					
3. Vortac Radial (IP)					
4. Distance on Vortac Rad. (IP)					
5. Run Heading					
6. Run Duration					
7. Average Drift Angle					
*8. Autopilot Modes					
**9. System Mode					
10. Desired Offset					
11. Observed Offset					
***12. Video Levels p/p					
13. Average Pod Pos.					

Section III:

1. Particular system changes which do not necessarily occur on every flight.
2. Particular flight conditions which would affect results.
3. Particular weather conditions which would affect results.
4. Any other noteworthy comments.

*Autopilot Modes

AH = Altitude Hold
HH = Heading Hold
NA = Not Used

**System Modes

100 Accelerometer Network in
020 Doppler Frequency Tracker in
003 Antenna Rate Gyro in
040 Vertical Gyro Stabilized

***Video Levels

1. Saturation
2. Strong
3. Average
4. Poor
5. None

Figure 2

Input	Film Date		Input Duplicate								
Original	Film type Emulsion #		Duplicate	Film Emulsion #							
Density	Ground Run Data Water Base + Fog Gamma		Density	Ground Run Data Water Base + Fog Gamma							
Noise	Cycles/inch Cycle/sec										
Resolution	Range Azimuth										

COMMENTS:

Range	Mark	Width
1	7	
2	8	3--4
3	9	
4	10	9-10
5	11	
6	12	

Output	Film Date												
Original & Duplicate	Film type Emulsion #												
Density	Ground Run Data Water Base + Fog Gamma												
Slit	Opening												
Zero stop	Low Freq. High Freq.												
Filter	Filter Position												
Filter Corr.	Film Filter												
Exposure	Speed												
Drive	Ratio												
Resolution	Range Azimuth												

COMMENTS:

Figure 3

SPECIAL HANDLING

Film Date Notebook					
Variable	Component No of chgs Interval				
Changes	Number Date Component				
Light source					
Condensor					
Slit	Opening Rotation				
Top mirror	Slide Forward tilt Side tilt				
Collimator	Lens Focus Dial				
Platen					
Field Lens	Lens Focus Dial				
Relay Lens	Lens Focus Dial				
Zero stop	Squint Focus High freq Micrometer Low freq Micrometer Band pass				
Fixed Cylinder	Lens Focus Dial Rotation				
COMMENTS:					

Bottom Mirror	Slide Forward tilt Dial Side tilt				
Interchangeable Cylinder	Lens Slot Focus Dial Side Dial Rotation				
TV mirror	Slit				
Filter	Shutter Output Red End Wavelength Blue End Wavelength Position				
Output slit	Lower Upper				
Exposure	Coarse dial Fine wheel Reducer				
Drive ratio	Small wheel Dial Tension Ratio				
Film	Type Emulsion				
Camera	Dial Film Exposure				
Check list	Data arm Platen screws Fluid levels Magazine Blowers				
Brightness	Platen				

Figure 4

Appendix XII

EFFECT OF FILM EXPOSURE ON RECORDER/CORRELATOR PERFORMANCE

Appendix XII

EFFECT OF FILM EXPOSURE ON RECORDER/CORRELATOR PERFORMANCE

1.0 Introduction

From the input signal into the recording unit to the forming of an image in the correlator, there are nine (9) basic electronic, optical and photographic parameters which affect the system performance.* These parameters are:

(1) Relation between input voltage and output brightness on the CRT.

(2) Bias setting on the CRT.

(3) Signal amplitude voltage.

(4) Systematic electrical and photographic noise.

(5) Average density of recorded transparency.

(6) Photographic contrast (gamma).

(7) Callier Q-factor of films used.

(8) Photographic parameters of films used; negative and positives.

(9) Placement of exposure; toe or linear portion.

Maximizing the intensity of the image and/or minimizing the generation of harmonics or similar energy-wasting effects serves as the fundamental criterion for parametric optimization. The effect these parameters have on

*The problems of mechanical vibrations and/or optical misalignment in either recorder or correlator are not considered here.

the final result, the image strength stemming from a given input signal varies not only in degree, but in kind. The best approach to defining their inter-relationship is to consider their effect on a typical input signal.

1.1 Input Signal

The input signal is a voltage variation describing a hologram whose mathematical description is written

$$V(s) = 1 - m_o \cos(ax^2)$$

where the modulation is assumed constant at all useful values of x (or at least drops off slowly with increasing x, as the pattern converges). This voltage is converted to brightness on the CRT face. It has been established that a power-law generally relates these variables, and can be described generally as

$$I(x) = C_o + C_1 V^b(x)$$

Then the intensity available to place on a recording film is

$$I(x) = C_o + C_1 \left[1 - m_o \cos(ax^2)\right]^b$$

The constants C_o and C_1 are absolute terms upon which the choice of film type (in terms of exposure speed) and signal bias setting must be made. It is possible to have a signal amplitude large enough to drive the tube below cutoff, at a given bias setting. This prevents realization of the full signal in subsequent processes. While the periodic characteristics are sufficient to form an image at the correct focal length, the intensity will have diminished. Then, even for weak signals and low bias settings, it will be

possible to focus an image whose location is correct, but whose strength is far below its optimum. It is, therefore, important that the bias setting be high enough to prevent such signal cutoff, unless it is actually desired that large signals undergo such discrimination.

1.2 Photographic Constants

The brightness variation on the tube-face is converted to a density variation in a photographic emulsion through exposure and subsequent chemical processing. The typical object under consideration here is a continuous-tone zone-plate. Since this will be illuminated coherently, and immersed in a fluid gate, its transmission distribution will be the significant quantity. Further, its amplitude transmission characteristics will determine the focusing properties peculiar to such zone-plates. The three practical ways of transferring the CRT brightness variation into a photographic transparency will be discussed, together with an analysis of the images they produce.

1.3 Recording on the Linear Portion of the Characteristic Curve

When the linear portion of an emulsion's characteristic curve is used, the intensity resulting from the variation on the CRT is converted to a distribution of transmission which can be written

$$T(x) = T_o \left[1 - m_1 \cos(ax^2)\right]^{-b\gamma}$$

where the original modulation has been modified to m_1 by the frequency of the emulsion and recorder optics. This value decreases as the pattern converges, but is shown here as a constant for purposes of simplification. When placed in the correlator, the amplitude transmission is given by the square root of the above, and is written.

$$\sqrt{T(x)} = \sqrt{T_o} \cdot \left[1 - m_1 \cos(ax^2)\right]^{-\frac{1}{2} b\gamma}$$

Now, this is non-linear as it stands and in order to effect its evaluation; it must be expanded. Through use of the Binomial Expansion or through a Fourier Series representation, the amplitude transmission distribution can be written

$$\sqrt{T(x)} = \sqrt{T_o} \sum_{p=0}^{P} A_p \cos(pax^2)$$

$$= \sqrt{T_o} \left[A_o + A_1 \cos(ax^2) + A_2 \cos(2ax^2) + \ldots \right.$$

$$\left. \ldots + A_p (pax^2)\right]$$

The A's are functions of modulation m_1, gamma γ, and the CRT factor b.

The above distribution may be rewritten in a normalized form as

$$T(x) = A_o \sqrt{T_o} \left[1 + \frac{A_1}{A_o} \cos(ax^2) + \frac{A_2}{A_o} \cos(2ax^2) + \frac{A_3}{A_o} \cos(3ax^2) + \frac{A_4}{A_o} \cos(4ax^2) + \ldots \right.$$

$$\left. \ldots + \frac{A_p}{A_o} \cos(pax^2)\right]$$

By comparing it with the original signal, this can be seen to be a set of zone-plates of increasing convergence and diminishing strength, since

$$\lim_{p \to \infty} \frac{A_p}{A_o} \to 0$$

The focal length of these harmonic images, for that is what these harmonic zone-plates form, is simply

$$\sqrt{T(x)} = \sqrt{T_o} \cdot \left[1 - m_1 \cos(ax^2)\right]^{-\frac{1}{2}b\gamma}$$

Now, this is non-linear as it stands and in order to effect its evaluation; it must be expanded. Through use of the Binomial Expansion or through a Fourier Series representation, the amplitude transmission distribution can be written

$$\sqrt{T(x)} = \sqrt{T_o} \sum_{p=0}^{P} A_p \cos(pax^2)$$

$$= \sqrt{T_o} \left[A_o + A_1 \cos(ax^2) + A_2 \cos(2ax^2) + \ldots \right.$$

$$\left. \ldots + A_p (pax^2)\right]$$

The A's are functions of modulation m_1, gamma γ, and the CRT factor b.

The above distribution may be rewritten in a normalized form as

$$T(x) = A_o \sqrt{T_o} \left[1 + \frac{A_1}{A_o} \cos(ax^2) + \frac{A_2}{A_o} \cos(2ax^2) + \frac{A_3}{A_o} \cos(3ax^2) + \frac{A_4}{A_o} \cos(4ax^2) + \ldots \right.$$

$$\left. \ldots + \frac{A_p}{A_o} \cos(pax^2)\right]$$

By comparing it with the original signal, this can be seen to be a set of zone-plates of increasing convergence and diminishing strength, since

$$\lim_{p \to \infty} \frac{A_p}{A_o} \to 0$$

The focal length of these harmonic images, for that is what these harmonic zone-plates form, is simply

$$f_p = \pi/pa\lambda$$

Thus, for each harmonic there exists an image. The intensity of these images will be proportional to the square of the coefficient of the corresponding cosine-term. When modulation m_1 is not too large, there will be only a few of these images. However, no choice of gamma can eliminate them; and the higher the modulation (which is a measure of input signal amplitude) the more energy is taken out of the correct image and placed in the spurious ones.

Experiments were carried out in which these predictions were verified. The multiplicity of the images was well established, usually there being at least three which could be observed visually. For convenience, the "virtual" images were examined and are the images referred to in this paper.

1.3 Toe Recording

In a specific region of the toe, amplitude transmission is linear with respect to incident exposure. Through use of the toe, it is possible to maintain generally low densities (which is highly desirable) and to minimize the harmonic content. The region is not particularly wide in range (usually about 3:1 in exposure under optimum conditions), and its reproducibility characteristics are poor. The toe also produces harmonic images, as the following analysis will show.

In the region of the toe where transmission and exposure are linear (above fog level and into the beginning of the linear portion), the density variation can be written.

$$D(x) = D_o + C\,E(x),$$

where D_o = minimum density (not necessarily fog level)

C = constant of proportionality

$E(x)$ = exposure

Since, by definition,

$$D = -\log T,$$

$$\log\left[\frac{T(x)}{T_o}\right] = -C\,E(x)$$

$$= \left[-C\,1 - m_1\cos(ax^2)\right]^b$$

Then

$$\frac{T(x)}{T_o} = 10^{-C\left[1 - m_1\cos(ax^2)\right]^b}$$

Taking the square roote of both sides (equivalent physically to illumination in the coherent mode of the correlator and immersion in a fluid gate),

$$\frac{T(x)}{T_o} = 10^{-\frac{1}{2}C\left[1 - m_1\cos(ax^2)\right]^b}$$

Since the exponent is small in this region, the above equation can be expanded in a power series, only the first two terms of which have significant value. Thus,

$$\frac{T(x)}{T_o} = 1 - \tfrac{1}{2}C\,\ln(10)\left[1 - m_1\cos(ax^2)\right]^b$$

Finally, the amplitude transmission distribution becomes

$$T(x) = T_o\left\{1 - 1.151\,C\left[1 - m_1\cos(ax^2)\right]^b\right\}$$

Depending on the value of b, the toe therefore produces a finite number

of images as may be deduced through arguments previously presented for the linear case. When b = 2, a double frequency component is added, and there are images at focal positions of $\pi/a\lambda$ and $\pi/2a\lambda$. There are no other images.

It can be seen that no choice of photographic gamma can possibly eliminate the spurious images. The CRT characteristics are usually quadratic, and in all instances observed experimentally, the toe recordings of zone-plates has produced just these two images.

1.4 The Image of a Duplicate

Assume an exposure of the type previously discussed, and placed on the linear portion of the emulsion's characteristic curve. After processing, this is contact-printed onto the linear portion of a positive-type material and processed. The gammas of the processes are designated, γn and γp, respectively. The resultant amplitude transmission distribution of the positive, or duplicate, in the correlator can be shown to be

$$T(x) = \sqrt{T_o}\ \left[1 - m_2 \cos(ax^2)\right]^{\frac{1}{2}b\ \gamma n\ \gamma p}$$

where m_2 is the modulation of the original input signal by both emulsions.

For a special case, this amplitude transmission can bear a linear relationship to the input signal voltage of the recorder. When b = 2,* the distribution becomes a perfect zone-plate when

$$\gamma n\ \ \gamma p = 1$$

Here there are no spurious images, and all the energy goes into only the

*This has been found to hold quite closely experimentally.

one at

$$f = \pi / a \lambda$$

assuming no other image degradations. For all other cases, harmonics will be present, and spurious virtual images formed at fractional multiples of the basic pattern focal length.

It should be noted that this gamma-product of unity is not quite as simple to obtain as it appears. The optical system operates in a coherent mode, and the effect of density is basically specular. Thus specular densities must be used to define gamma, and when so determined will be considerably higher than those measured with the standard diffuse-measuring instruments.

The ratio of specular to diffuse density, the Callier Q-factor or Callier coefficient, has been the subject of study since 1909. It has been found to vary with gamma and density, as well as film type. Because the specular gammas are higher, a specular gamma-product of unity requires both emulsions to be processed to extremely low diffuse gammas. This results in film speed losses.

To illustrate the problem quantitatively, the film-type generally used of the original (negative) record is Plus-X Aerographic, having an approximate Q-factor of 1.5 under the usual development conditions, on the linear portion of the curve. The film-type used for duplicating has Q-factor of approximately 1.3 (but whose diffuse gamma is quite difficult to get below 1.5). Then, a diffuse gamma-product of unit for these two films has a specular gamma-product of 1.95, nearly twice as large as desired.

Extensive sensitometric studies in relation to this problem must be carried out before the unity gamma-product relationship can bear fruit.

Because the duplicate process can eliminate harmonic images, an effort should be made to attain this condition and assess the strength of the resultant image. However, with the cited Q-factors, the gamma-product of approximately 2 will produce only one spurious image. This is certainly no worse than that produced by the toe under similar circumstances. With the materials presently in use, it was found to be impossible to achieve even a gamma-product of 2 experimentally.

1.5 Discrete Electrical Noise

When specific electrical noise frequencies are present in the recorder signal, they serve to diminish the image intensity by creating ghost images in a plane perpendicular to the main optical axis. This noise is placed on the film as sine-waves, which become carriers through intermodulation with the zone-plate signal. Under coherent illumination, they form separate images (in the same plane) but are displaced from the correct one by distances proportional to the frequencies of the noise carriers. This is best illustrated photographically.

Figure 1(a) is the photograph of the coherent power spectrum of a zone-plate containing three specific noise frequencies. Part of the object was blocked-out, for this picture, to better exhibit the noise in the spectrum. The three intensity peaks on either side of the center correspond to 120, 240, and 400 cycles/second respectively.* Figure 1(b) is a photograph of the virtual image (squinted, to remove extraneous light) showing the spurious images. The spacing between these images is readily seen to be proportional to the spacings of the noise peaks in the power spectrum photograph. These spurious

*It is difficult to say whether the 240 cycle/sec. frequency existed in the recorder or is a harmonic of the 120 cycle/sec. signal as a result of the non-linearity of the photographic process.

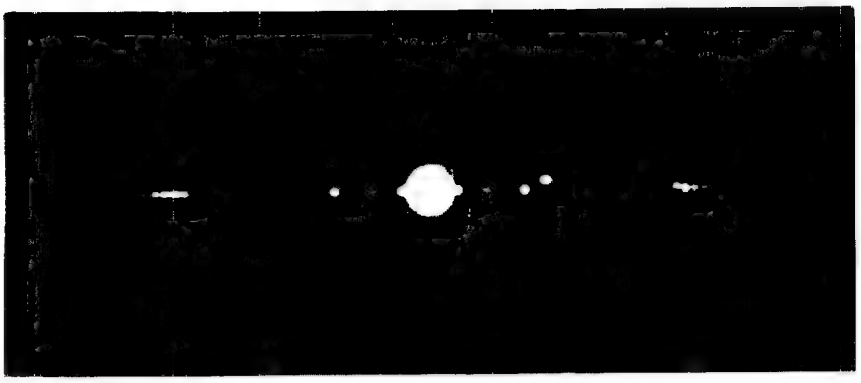

(a) 5X enlargement of the coherent power spectrum of a zone plate containing three discrete electrical noise frequencies.

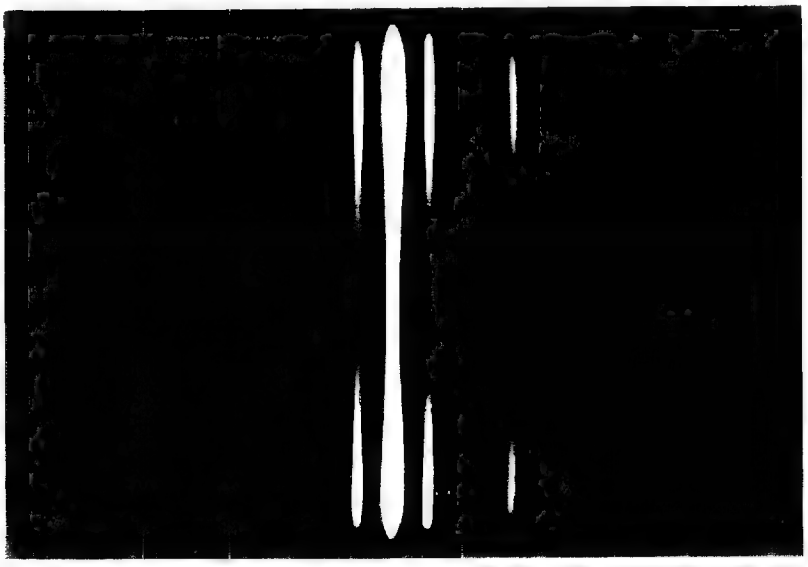

(b) 5X enlargement of the squinted virtual image.

Figure 1

Photographic evident relating discrete electrical noise frequencies and spurious virtual images.

images also accompany the harmonic virtual images produced through the non-linearities of the photographic process previously discussed. The net effect is to extract light from the desired virtual image and create new ones which can add ambiguities to the information being passed to the image plane of the correlator.

1.6 Average Density

Experiments have shown that for a one-step process, the brightest image results from the least dense object, at the same comparative signal strength, toe and linear portion alike considered.* On this basis alone, preference can be given to toe recording. On a similar basis, for the same average density, the highest signal strength produces the brightest image, as could naturally be expected.

1.7 Toe, Linear, Duplicate Recording

The density differences were calculated out of the experimental data, and the image intensities normalized to the highest signal strength at a given bias setting. The normalized intensities for a typical emulsion developer combination are plotted in Fig. 2. It can be seen that, aside from the density variation noted above, toe and linear behavior is fundamentally different. Figure 3 contrasts typically general characteristics for toe, linear and duplicate behavior. The toe tends to favor small signals, the linear portion larger signals. Since small signals predominate in the recorder, this is an additional reason for preferring the least dense object-type found on the toe.

On the other hand, when the linear portion of the curve was used for both processes, the duplicate produced a stronger virtual image at a comparable

*This does not include the case where the bias setting is low enough to afford signal cutoff.

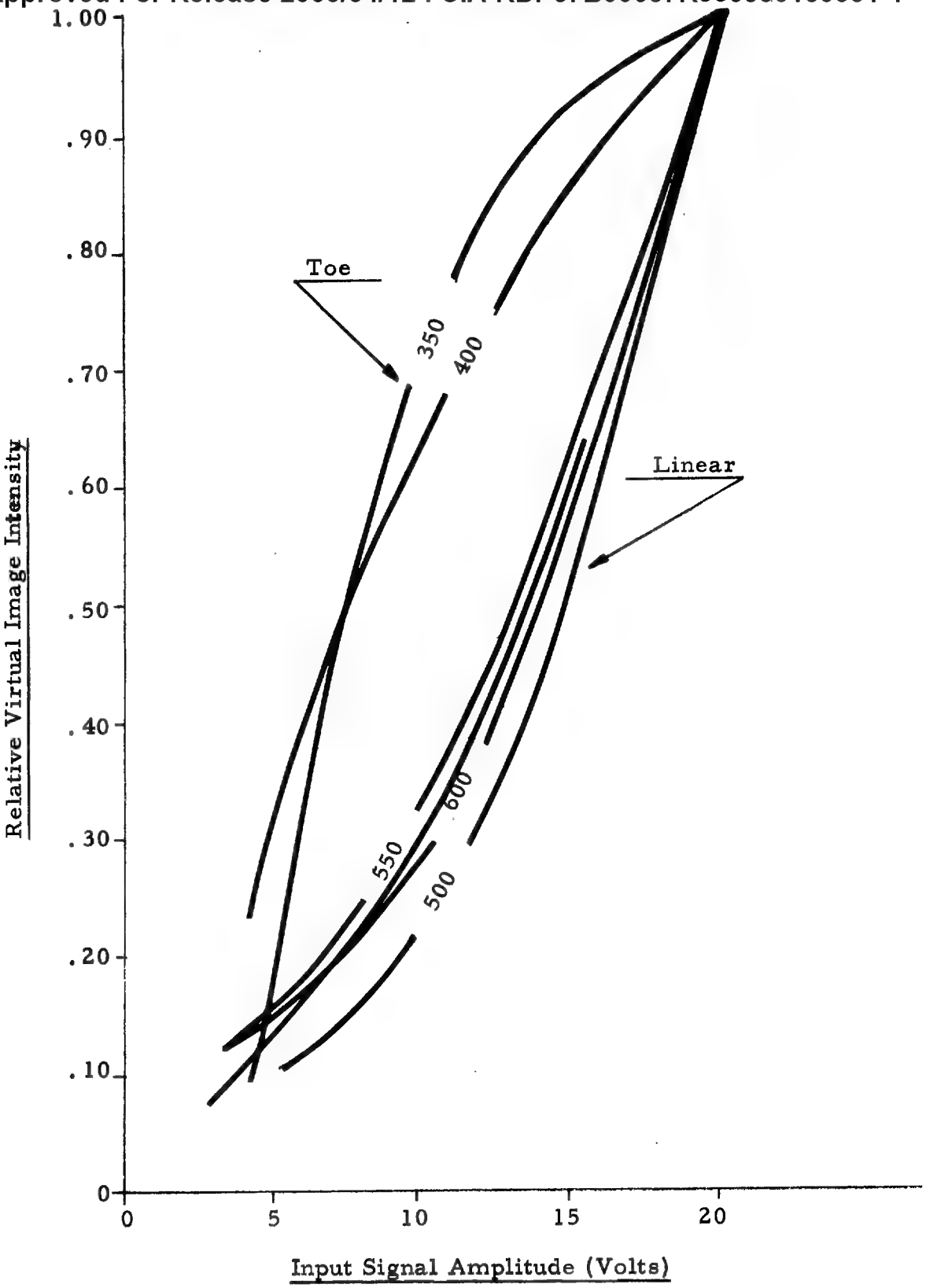

Figure 2

Plot of Relative Virtual Image Intensity as a function of Input Signal Amplitude, for various bias levels, of an equivalent density basis. The bias settings are shown on their corresponding curves. The emulsion used was Plus-X Pan and was processed to diffuse a gamma of 1.20 in D-76.

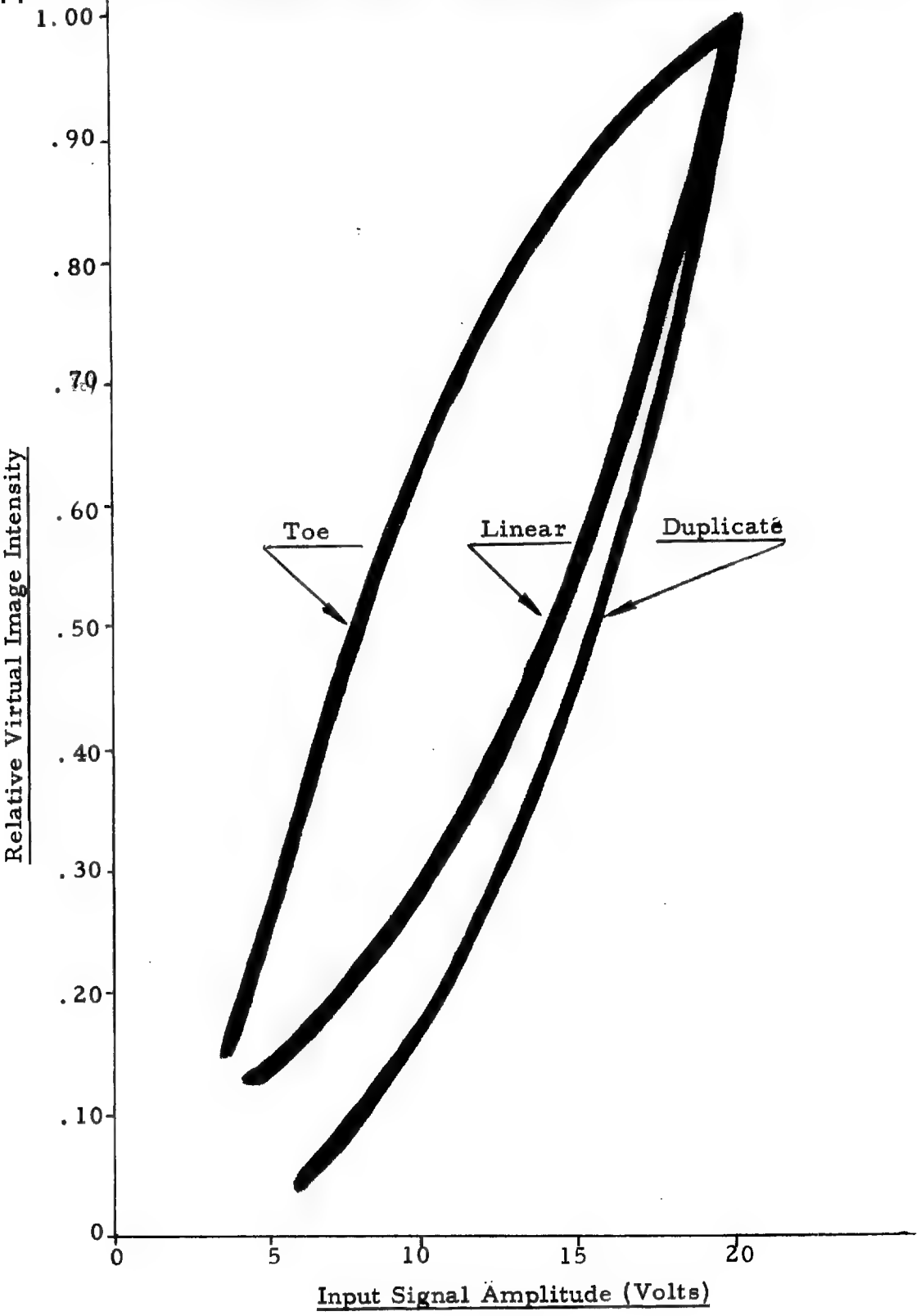

Figure 3

Typical plot of general characteristics resulting from using the toe, linear characteristics, or duplicate process for recording. These curves apply to specific gammas, but will not change significantly for others, using the same type of emulsions.

density. The major advantage in duplicate recording is the elimination of harmonic images when the gamma-product condition is met. Since duplicates are generally made on emulsion types which have a relatively short toe (and the linear portion thereby starting at a low density value), a properly exposed and processed duplicate can challenge the toe's image brightness. The duplicate behavior, as for the one-step process on the linear portion of the characteristic curve, favors the larger signals: in fact, it tends to discriminate against the very small signals, as may be seen in the figures. The major disadvantage of duplicate recording is the time involved and quality control necessary to maintain the proper development and exposure conditions.

Considerably more experimental work must be carried out, particularly in critical sensitometric studies, before the duplicate process can replace toe-recording (if, indeed, it can), unless the small signal discrimination characteristic is desired. The duplicate process offers much in the way of harmoinc suppression, and its usefulness should not be traded away solely on the basis of its generally reduced image intensities.

2.0 General Summary

Most of the systematic parameters have been studied. These parameters affect the "macroscopic" performance of the system, as opposed to those which affect the limiting signal/noise such as continuous electrical and photographic grain noise. Probably the most significant result of these studies is the manner in which deficiencies in the optical, photographic, and electrical systems tend to sort themselves out in the correlator. The photographic nonlinearities generate spurious virtual images along the optical axis. Discrete electrical noise creates suprious virtual images perpendicular to the optical

axis, as "ghosts". The net effect is to take useful light from the desired image and add ambiguities which can affect other range-information light in the correlation process.

Under the present circumstances, since the duplicate sensitometry is quantitatively uncertain, it is expedient to remain on the toe of the emulsion's characteristic curve for recorder exposure. This is further justified by the fact that general toe behavior favors small signals, a condition which can be expected to appertain in practice.

For an approach to the continuous noise (electrical and photographic), the following references should be consulted:

(1) Leith, E., "Photographic Film as an Element of a Coherent Optical System", P S & E, 6, March - April 1962.

(2) Doerner, E. C., "Wiener Spectrum Analysis of Photographic Granularity", JOSA, 52, June 1962, 669-672.

(3) Thiry, H., "Power Spectrum of Granularity as Determined by Diffraction", Journal of Photo - graphic Science, 11, March/April 1963, p. 69-77.

Appendix XIII

COHERENT SLR RECORDER-CORRELATOR SYSTEM

This Appendix is a number of technical sections taken from Proposal #3536 made to Westinghouse in late 1964. It was requested for inclusion in a larger proposal for an advanced system. This material is presented here as a description of current thinking for a new optical system.

Appendix XIII

COHERENT SLR RECORDER-CORRELATOR SYSTEM

1.0 Summary

The design and fabrication of a recorder-correlator system compatible with the specified performance requirements presents no new problems. We propose to use the same system for both the long range and short range modes.

1.1 Recorder

The recorder will be capable of recording a line scan containing over 15,000 resolution elements in range. The sweep speed will be selectable for either long or short range operation. The film speed will also be selectable for different ranges and servo controlled to vehicle velocity within these settings.

The correlator will process the data film at an overall speed equal to or greater than the acquisition rate in a maximum of four and usually two passes (depending upon a detail computer analysis of the off-axis performance of the optical system, and of the ratio of far range to near range on a single recording).

The proposed recorder employing a pair of fiber optic faceplate CRT's is an extension of a recorder that we have previously produced. In addition, we have also performed laboratory tests on those aspects of this proposed design which represent changes with respect to recorders previously built. The configuration shown for the proposed recorder is intended to illustrate

a possible form. The exact form factor to be adhered to is not known to us. We anticipate little difficulty with reasonable form changes. A radical size reduction will involve the development of improved recording techniques such as direct electron-beam-recording. We are very interested in pursuing such improvements, but they represent a technique not yet reduced to practice and not included in this proposal.

1.2 Correlator

The proposed correlator represents the configuration which we believe, from our experience with larger aperture precision optics in coherent light processors and with precision film transports, will meet the requirements with the greatest reliability, consistency and stability. At the same time the correlator configuration is such as to allow the modifications and improvements that are certain to develop over the time period envisioned for this program.

The proposed correlator is a monochromatic type with tilted cylinders for focal length compensation and configured to provide constant azimuth magnification for all range elements within the field of view. With interchangeable lens elements short or long range data may be processed. The proposed light source is a 100 mw helium-neon continuous laser. A shorter wavelength light would be preferred for better film sensitivity and if such a source becomes available it would be considered.

We have included in our proposal, in addition to the large continuous film correlator, a small detail correlator. Our experience has demonstrated that the examination of a small section of radar data film on an optical bench will always reveal more information than can be recorded on a single

pass with a large aperture moving film system. The large unit must be set for nominal focal length and exposure, and thus cannot completely cover a possible dynamic range of 10^5 in target reflection as is obtained between background and strong target nor can it bring moving targets into focus. Cost wise the detail unit is a minor item, but we believe it to be essential for maximum utilization of the recorded data.

1.3 Test Equipment

We have proposed that a test equipment cart be provided with facilities to provide electrical inputs to the recorder to allow ground operation, calibration and checkout. For the correlator we will provide artificial input films adequate to permit alignment and focusing for all operational modes.

1.4 Program

In addition to the specific equipments to be provided we have proposed an initial design phase in which the necessary liaison between various suppliers will be established and the system decisions made. The details of the recorder-correlator system will be designed and an initial system performance analysis will be performed. This performance analysis will be used as the basis for a continuing program of performance analysis and prediction to be carried on through the design, fabrication and testing of the prototypes.

1.5 Theory

In the body of the proposal we have included explanations of various optical correlator schematics as well as experimental and laboratory data on recorder performance to support our proposed configurations.

2.0 Technical Discussion

Since Itek initiated work on high resolution radar recorders and recorder data analysis through the study, design and test phases, a considerable body of practical and theoretical knowledge of the performance of SLR has been acquired and a capable group of people who hold and can practice this knowledge has been assembled.

There is no doubt that a system with an overall resolution less than 10 feet in both range and azimuth can be built and operated.

Insofar as the correlator is concerned resolution measured in feet on the ground has no meaning; the only pertinent requirements are,

(1) how small is a resolution element on the film,

(2) how many resolution elements are there across the film, and

(3) what is the focal length ratio to be accommodated?

In the recorder the ground resolution in feet determines the upper limit of the video frequency to be recorded in the range direction, and this determines the dwell time of the CRT electron beam on a resolution element. Given further, a fixed number of resolution elements across the face of the CRT, the range dimension that can be covered by a single CRT trace is determined as well as the sweep speed or exposure time. From the above it is obvious that insofar as the recorder and the correlator are concerned, it is not so much the size of a ground resolution element that limits the performance as it is the number of resolution elements.

Our experience and calculations indicate the separate major system components should have a resolution element size of about half or less than

the desired system element size. This argues for a resolution of 5 feet or less, for each component, and we feel that a reasonable and attainable goal is 4 feet for the components in order to obtain a system resolution of less than 10 feet.

2.1 Recorder

The best available cathode-ray-tubes have a spot size of 0.0005" and will deliver 8,500 resolution elements, or spots, in a single $4\frac{1}{4}$ inch trace onto the recording film thru a fiber optic faceplate. This is vanishing resolution, and represents a factor of two improvement over the performance of a lens recorder. It is not practical with these tubes to use multiple traces and to separate them with additional fibers or lenses; the resolution cannot be maintained. If two CRT's are used then the range that can be accommodated is:

$$\frac{2 \times 8,500 \text{ spots} \times 4 \text{ feet}}{6,000 \text{ feet/mile}} = 11.3 \text{ nautical miles}$$

A wider range swath could be accommodated with a proportional loss in resolution. Of course, additional recorders can be used to increase the range width and maintain resolution.

2.2 Correlator

A correlator to process the data delivered by the above described recorder will require two passes of the data, one for each of the $4\frac{1}{4}$ inch recording traces. Each pass will, therefore, be required to accommodate 8,500 range elements, and if a range magnification of two is used, each output will be on 9.5 inch film with a useful recording width of about 8.5 inches, or about 1,000 resolution elements per inch which is 40 per millimeter.

This does not represent exceptional performance for conventional optical devices in which the field is symmetrically treated, but our experience has shown that this is very good performance in an astigmatic system employing cylinders if a relatively wide and flat image plane is desired.

In order to maintain the above resolution, the position of the film must be held to very close tolerances as it is transported across the aperture. A resolution of 1 mil at the output indicates one half mil at the input. In order to maintain the desired resolution the input film should not move laterally by more than about $\frac{1}{4}$ mil. Furthermore, the direction or skew of the film, or more correctly, the skew of the data must be such that the data patterns are parallel to the azimuth direction of the correlator optics to a small fraction of a degree. For instance, if a data pattern 1 inch long is to be collapsed along itself without increasing its range dimension by more than $\frac{1}{4}$ mil, then the angular tolerance is 0.25/1000 = 0.00025 radians or less than 1 minute of arc.

Since the tolerances on film dimensions are much greater than this, and the recorder is not likely to maintain skew and sweep position to these tolerances, it is necessary that the alignment servo in the correlator operate upon the data itself rather than the film. In order to affect this it will be necessary that the recorder record a reference mark that can be used for this purpose.

2.2.1 Optics

A laser is the only light source available that will provide the required monochromacity at an intensity level consistent with a reasonably high output speed.

In order to use monochromatic light in a correlator the optical system

must be designed to provide for pattern focal length correction and to insure uniform magnification. There are two basic techniques to accomplish this and they are described below in a simplified form. In addition, it will be necessary to use either two dimensional or one dimensional correlation and this is also discussed below.

2.2.2 Conical Lens Schematic

Figure 1 is a sketch to illustrate the principle that enables a conical lens to be used to correct focal length, but not produce varying magnification. The arrangement shown with a large number of astigmatic elements is not the most practical one, but it best illustrates the separate optical functions required. The central feature is that the conical lens is placed in the plane containing the azimuthal image of the light source (the azimuth frequency plane). It could be placed in an image of this plane. As is seen from the upper diagram, light rays through the optical center of any signal pattern, such as P_1, P_2, on the input film pass through point 0, the image of the source which is also the center of L_4 the conical lens. These rays pass on undeflected to the output plane where they intersect the plane at P_1' and P_2' representing the images of P_1 and P_2 as formed by the conical lens. The separation between P_1' and P_2' is determined by the separation between the patterns on the input film, and as the input film is translated in azimuth the output images will follow the ends of their respective optical center rays as these rays pivot about point 0.

Lens L_2 images the range dimension onto the conical lens to insure that only the proper lens power is brought to bear on the various signal patterns. Lens L_5 then reimages the range dimension onto the output plane.

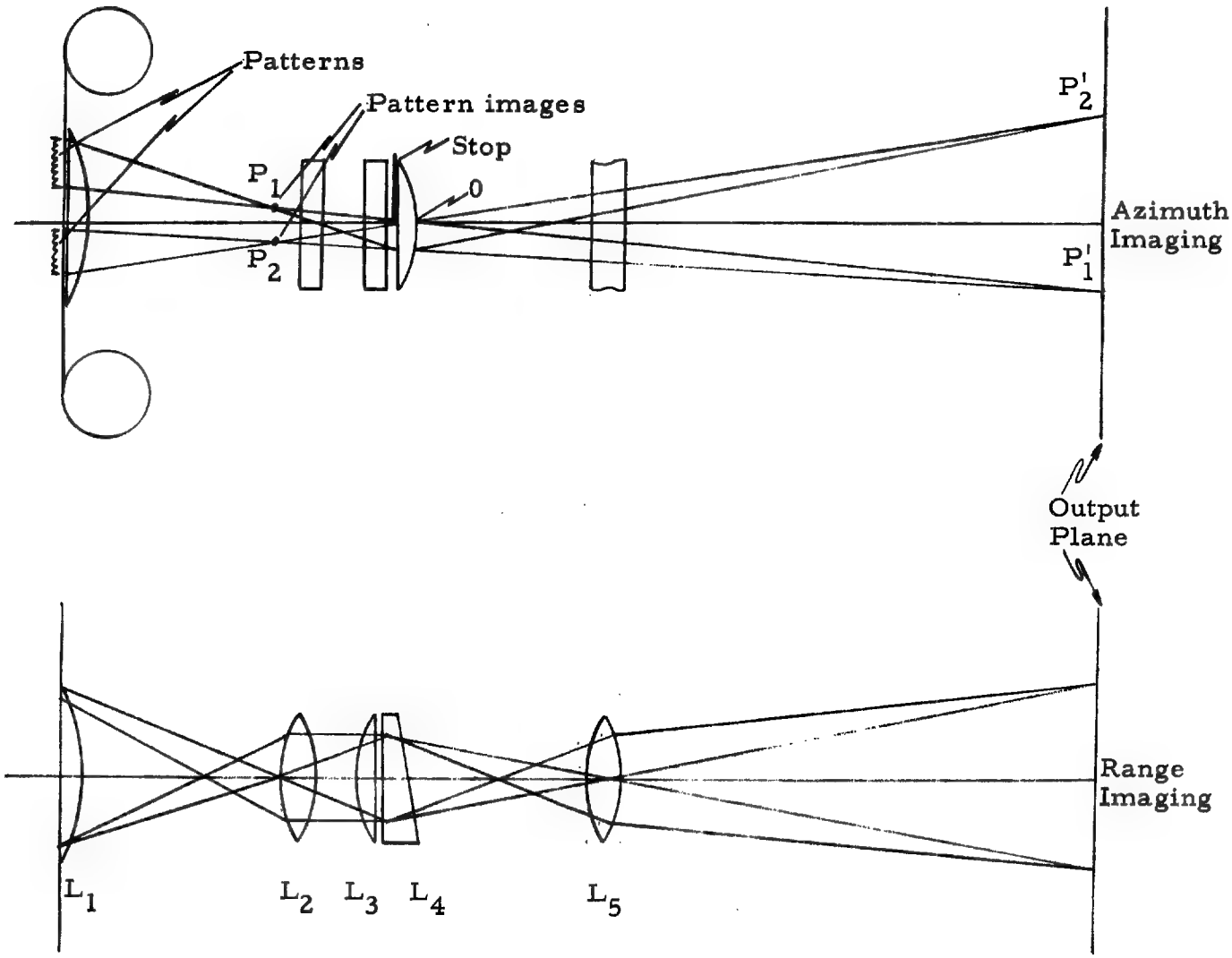

Figure 1

Conical Lens System

There are a large number of possible variations to this basic schematic, but in each one the conical lens is placed in a plane containing an image of the light source in azimuth and an image of the input film in range.

2.2.3 Cylindrical Lens Schematic

Because of the astigmatic imaging requirements, a conical lens correlator must also use cylindrical lenses, and as a rule cylindrical lenses are easier to fabricate and test than conical lenses. Furthermore, a conical lens once fabricated does not permit much latitude of adjustment. For these reasons it is very desirable to examine the possibilities of using tilted cylinders to accommodate the varying pattern focal lengths. Tilted cylindrical systems have been used for similar uses in oblique cameras and these techniques with modifications can be used here.

Figure 2 is an illustration of a possible correlator using cylindrical lenses. The upper view shows the range imaging action in which lens L_2 images the range dimension directly onto the output plane. The cylindrical lenses L_3, L_4 and L_5 have no effect in this dimension except that due to glass thickness. Also shown in the upper diagram is the line AB representing a line image as might be formed by a series of target patterns on the input film the centers of which are all at the same azimuth, but at different ranges. Because of the varying focal lengths of such patterns the line is tipped.

The relay lens L_2 plus the cylinder L_3 reimage this line AB on the line A'B'. The lens L_4, a negative cylinder, is inserted parallel to A'B' at a distance equal to its focal length. Thus, the light rays proceeding to the line A'B' are collimated and proceed as parallel bundles to lens L_5, a

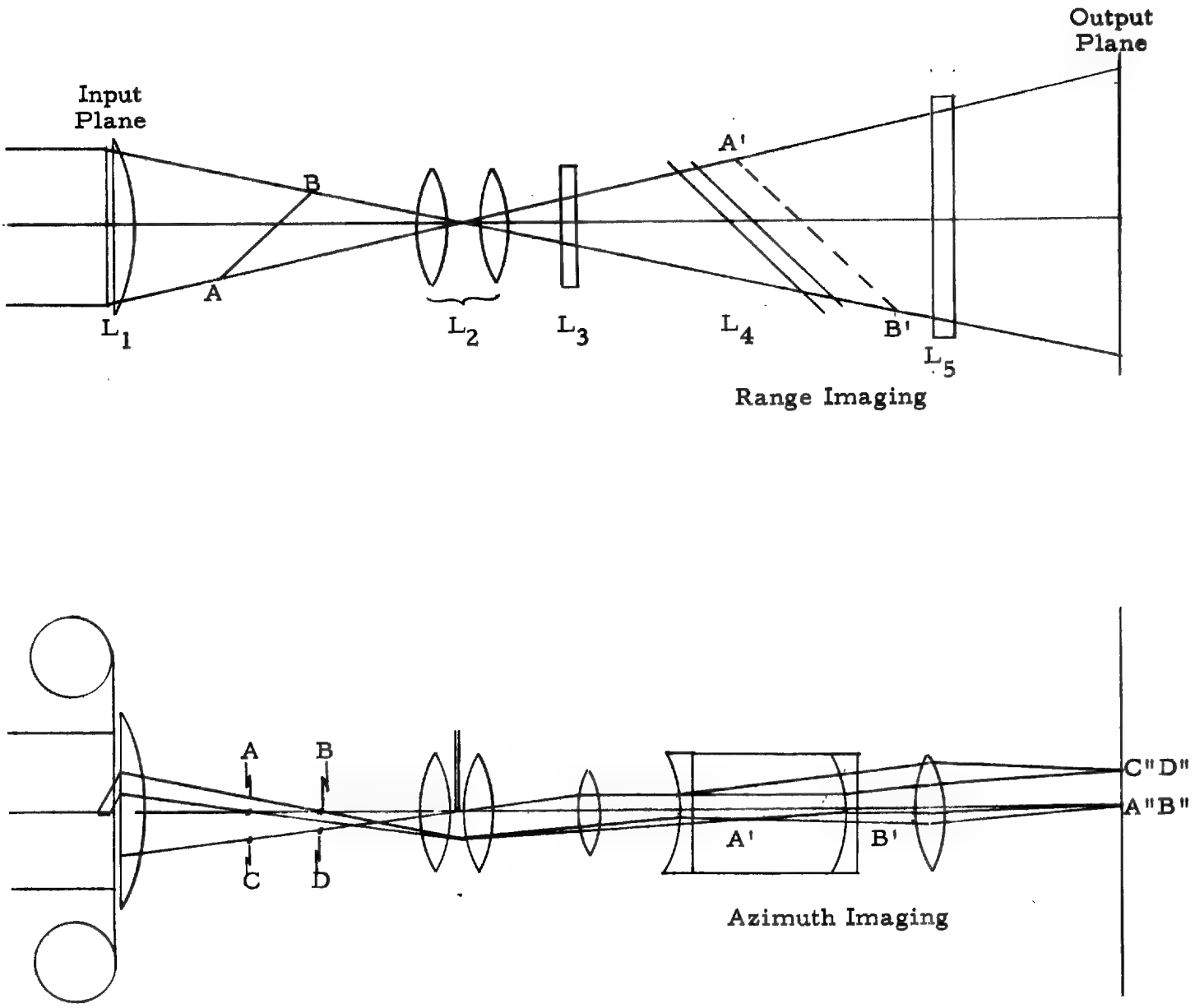

Figure 2

Tilted Cylinder System

positive cylinder, which converges the collimated rays to points at a distance equal to its focal length. Lens L_5 is placed, therefore, at its focal length from the output plane, and its focal length is chosen so as to provide the proper overall azimuth magnification.

One further requirement must be met concerning uniform output image motion as the input film is translated, and this is the reason for lens L_3. As shown in the lower diagram of Fig. 2, the projection of the line AB is shown to lie along the optical axis of the system, and light from the centers of the data film patterns proceeds undeviated along the optical axis to the output plane. As the input film is translated downward then the line AB will take a new position say CD, but, as always, the rays thru the pattern centers must pass thru the light source image between the elements of L_2. The lens L_3 is placed so that its focus is at the plane of this source image thus it collimates all rays from data pattern centers so that they become parallel to the system optical axis. No matter what part of lens L_4, these rays pass thru they are deflected so that rays from the same azimuth section of the input film (i.e. from C and D) emerge at the same angle. Being at the same angle, the lens L_5 will direct them to the same azimuth on the output plane. In this way relative image motion at the output plane is eliminated.

Although the system of Fig. 2 is only one of many possible configurations, it appears to have a number of attractive features concerning the flexibility of adjustment and accommodation. The principle limitation pertains to how much tilt can be accommodated within the resolution limits, and how wide an angle of rays in range can be accommodated from the same point. The tilt limitation will determine the maximum ratio of near and far ranges for a

single correlation, and the angle limitation will determine the range resolution. The practical limits on these parameters have not yet been determined. Since cylindrical (and conical) lenses have a limited field of view, the useful width in azimuth of the output image will be much smaller than in range, but this is not a serious restriction.

2.2.4 Chirp Requirement

In order to obtain higher range resolution with the radar and maintain or increase the radar average power, it will be necessary to provide signal integration or correlation in the range dimension as well as in the azimuth dimension. This requirement is dictated by the peak power limitations of the radar transmitter.

In principle, the range correlation could be accomplished electronically, but this could be a problem at the video frequencies required. Furthermore, there are very definite advantages to doing the correlation optically in both dimensions. If both dimensions are treated optically, then it is only necessary to squint in one of these dimensions.

The accommodation of two dimensional correlation requires that the light be spatially coherent in both range and azimuth; this requirement almost demands a laser light source because of the low light level with other point sources. Because of the high degree of temporal and spatial coherency of a laser source, the system becomes very sensitive to dust, dirt and stray light. Additional detail on the characteristics and treatment of two dimensional target patterns, or holograms, is presented in Appendix XIV.

2.3 Two Dimensional Correlator Schematics

If relatively short focal length patterns are to be produced in the range

dimension, and the squint is still to be in the azimuth dimension, the correlators of Figs. 1 and 2 will still provide the desired functions. The effect of range patterns will be to move the input range plane to a new apparent position. In other words, the input plane of Figs. 1 and 2 would be displaced from the actual film by the range pattern focal length. Whether this displacement is to the left or right will depend upon whether real or virtual images are to be used, and whether the two dimensional data patterns are elliptical or hyperbolic.

3.0 Proposed Correlator

We propose to design and build a correlator with the following characteristics:

INPUT:

9.5" roll film with two data swaths each $4\frac{1}{4}$" wide.

One data swath to be correlated on one pass through the correlator.

OUTPUT:

9.5" roll film on which one input swath will be recorded as an 8.5" map.

RESOLUTION:

Range: 40 1/mm limiting on film referred to output (4 ft. half cycle on 10 mile swath).

Azimuth: 40 1/mm limiting on film referred to output (4 ft. half cycle on 10 mile swath).

LIGHT SOURCE:

Laser, Helium Neon, $\approx$100 mw (Blue or Green if available).

CORRELATION SPEED:

1" per second (output film) or faster.

AUTOMATIC INPUT DATA ALIGNMENT:

Reference line on input data film will be automatically aligned to fiducial marks on input platen to $\pm$ 0.00025".

TYPE OF CORRELATION:

1 or 2 dimensional, Hyperbolic or Elliptical

Focal length of patterns:

Azimuth: 80" to 200" depending upon range selection

Range: 0 to 2" adjustable

Azimuth Stretchout: $\approx$ 8:1 capable of utilizing full pattern length.

TV MONITOR:

A closed loop TV camera and monitor system will provide the operator with a view of the output image during operation.

MAGNIFICATION:

Range Dimension 1:2 input to output.

Azimuth Dimension input to output to produce square map.

RANGE SELECTION:

Interchangeable lenses will be provided for switching operation between long range and near range operations.

As presently conceived the improved correlator will be mounted on a bench like structure with the input film platen horizontal to facilitate liquid gate design. The output film will be mounted vertically, at the end of the bench permitting most of the optical elements to be mounted along a horizontal optical axis, permitting maximum adjustment flexibility. Figure 3 is a preliminary sketch of the proposed correlator.

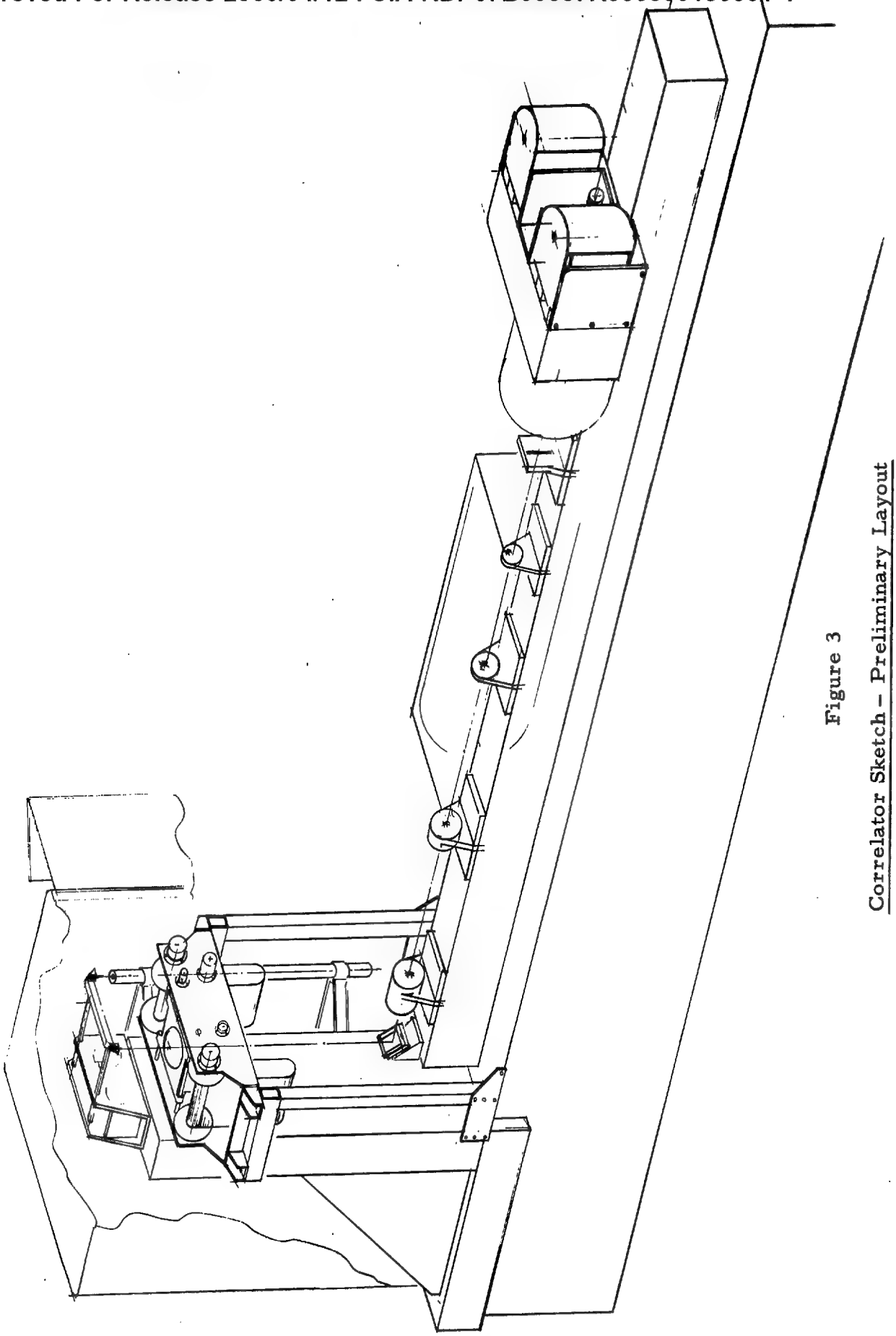

Figure 3
Correlator Sketch – Preliminary Layout

3.1 Design

As indicated in Section 2.0 of this Appendix, there are several possible optical designs, and the first task to be completed is the selection of the optimum design. The two principle layouts that must be analyzed are shown in Fig. 4. The optical design will include analyzing both of these designs on a digital computer with detail specifications on each glass surface. The computer and the computer programs necessary for this effort are both available, the bulk of the work will be specifying glass type and surface and interpreting the results.

The design of the film transport system represents the next most significant aspect of the design. The ratio of input film speed to output film speed must exactly match the azimuth magnification ratio and this must be adjustable smoothly over a small range to allow for sensor velocity variations. Furthermore, the tilt or skew of the input film must be continuously controlled by automatic alignment of a reference line on the data film. This allows the tilt correction to be independent of film dimensions, of slight shifts in recorder sweep position, and it simplifies the tolerance required on the recorder transport. The drive ratio will be controlled by means of the depression of a steel puck into the rubber rim of a driven wheel. This system we have used successfully on previous instruments. The tilt control will be by means of two line-following photocell units connected to two jack screws, one pair on each side of the input aperture. As a part of the design phase a breadboard of the drive system will be constructed.

3.2 Detail Correlator

For the reasons and purposes outlined below we strongly recommend and

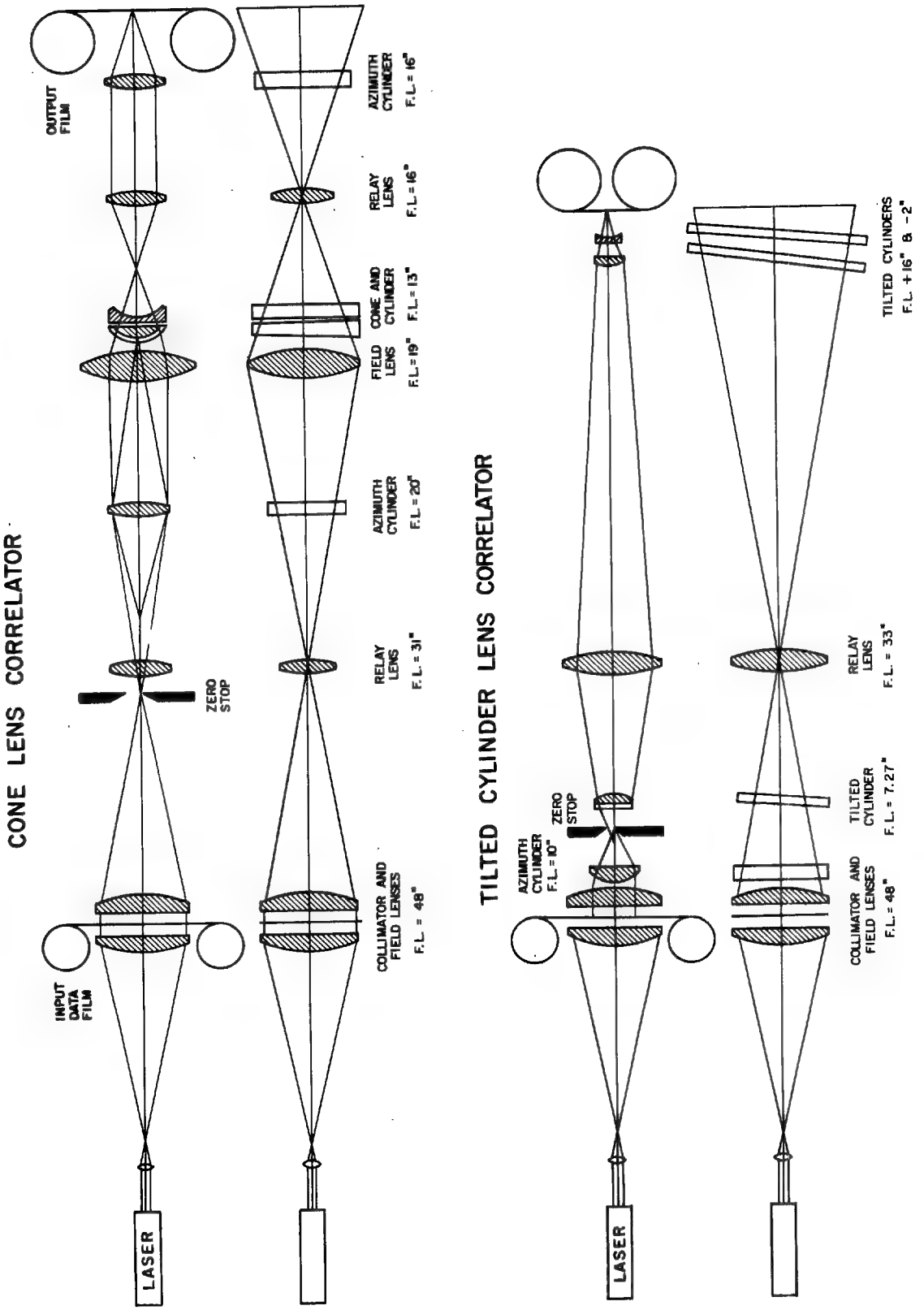

Figure 4

Monochromatic Correlator Optical Layout

have included a detail correlator in the proposed program.

In a large correlator treating the entire range swath on continuous roll film certain complications arise and compromises must be made;

(1) The image is recorded on moving film and this can cause image smear if the magnification-to-velocity ratio is not exact.

(2) The output film exposure is adjusted to give the proper overall exposure, but this results in an over exposure of the very strong reflectors or inadequate exposure of the weakly reflecting areas. The dynamic range of radar reflectors is about 100 times as great as in conventional photography because of its specular nature and the considerable difference in reflection coefficients.

(3) The focal length of the interference patterns vary with range and any distortions due to recorder CRT sweeps, lenses or filters, require that focal length correction adjustments to compromises.

(4) Perturbations of the vehicle or film motion will cause the optimum adjustments for focus, tilt, spatial frequency band, and noise rejection to change for different parts of the recording.

(5) Moving targets appear out of focus.

The above difficulties make it desirable to have available an instrument which will permit the detailed examination of a small region of interest on the

original record. By sacrificing the large and continuous field of view one would be able to adjust all parameters while viewing the correlator output of a small area.

The optical diagram of the unit is shown in Fig. 5, not to scale, and the arrangement of elements for the table correlator is shown in Fig. 6.

3.3 Mode of Operation

The operation of the unit is as follows: the decollimator, or field lens, brings the collimated light to a point focus at the frequency plane at the same time diffracted light from target patterns such as A and B are converged to points A' and B' in the azimuth plane. This action demagnifies the azimuth direction by an amount equal to $M = 1 - \frac{n}{f_F + h}$ where h is the focal length of the target patterns and f_F is the focal length of the field lens. Since the raw data film has an azimuth stretch this demagnification is desirable. The cylinder lens is placed so that its power is in the azimuth direction and at a distance such that the points A' and B' are inside its focus. The cylinder lens is adjusted so that virtual magnified images of A' and B' appear back on the film plane, or on the plane of the range images in the case of 2-D correlation. This is the same action as takes place with a common hand held magnifying glass. The purpose is not to magnify, but to place the azimuth image in the same plane as the range images, i.e. the data film. Now the relay lens is used in a conventional way to image the range plane onto the output plane.

This arrangement permits the relay lens to operate with only one set of conjugates and makes the adjustment of the cylinder lens independent of the relay lens. Furthermore, with the available off-shelf components this optical configuration appears to produce the least distortion across the field.

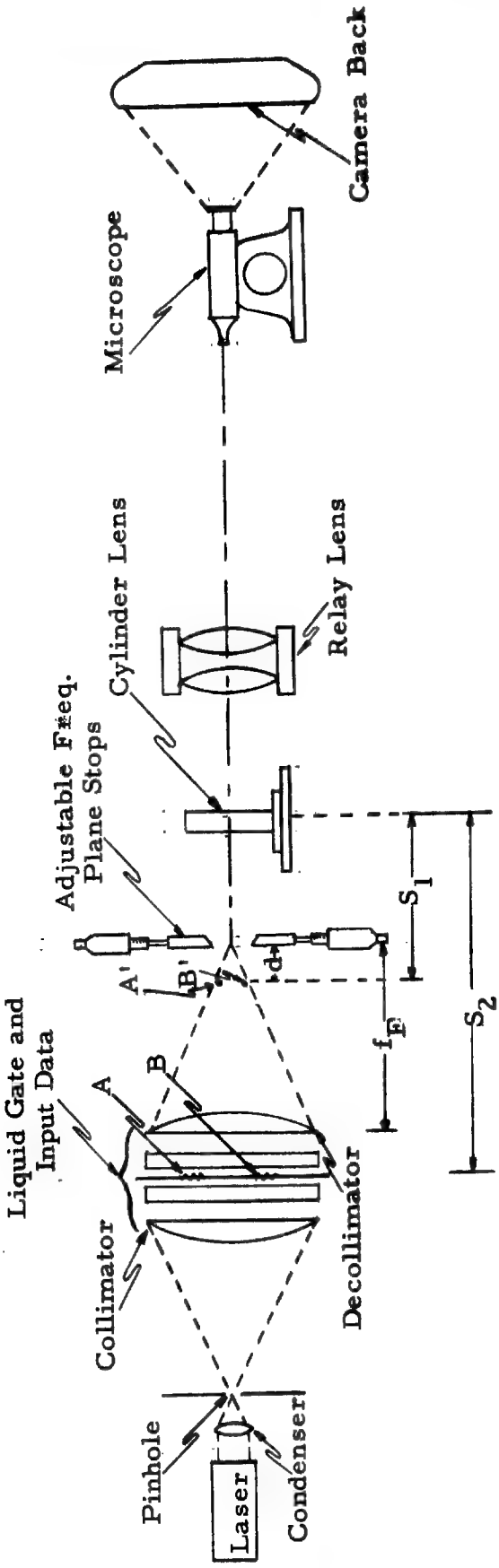

Figure 5. Optical Sketch of Detail Correlator

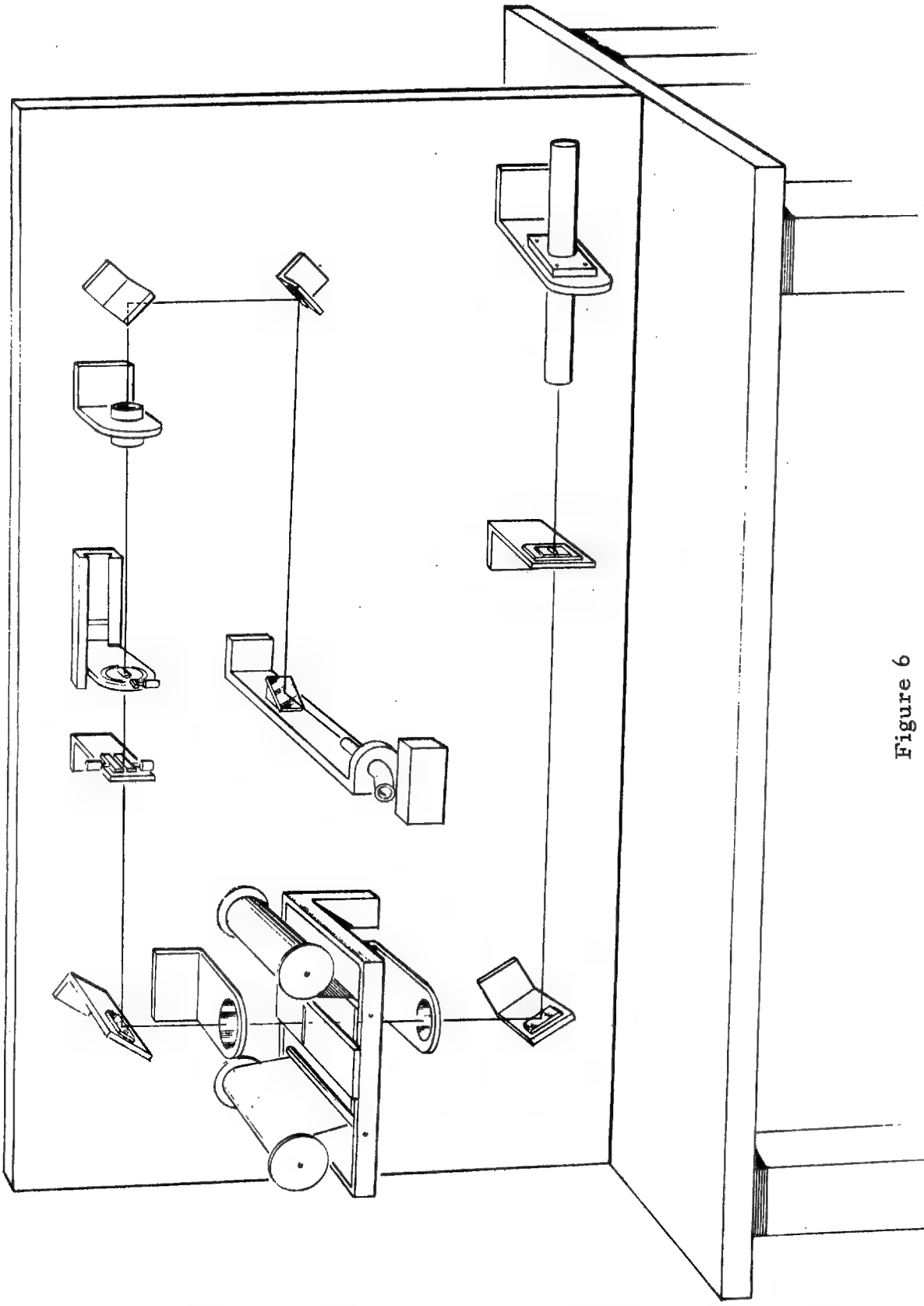

Figure 6

Proposed Detail Correlator Layout

There is one drawback, however, and that is that the scale of the output will be stretched in azimuth with respect to range by about 2:1, using available lenses. This is because of the magnification provided by the cylinder.

In any case, unless multiple lenses are provided the scale cannot be square over the entire range.

The unit would not provide any provision for rectification of distortion of the output. The azimuth scale of the output would vary with the range being observed and with the type of input material. It will, however, provide a degree of detail extraction quite impractical to obtain with a large correlator especially detail on extremely bright targets and on calibration of moving targets.

4.0 Ground Support Equipment

4.1 Recorder

Equipment necessary for the flight line or hanger level checkout and calibration of the recorder will be provided. This equipment will supply power and the necessary trigger and test signal inputs to the recorder unit. This support equipment will also contain the components necessary to meaure the various recorder test points.

Inasmuch as the recorder and its test gear must operate in close conjunction with the radar the details of the equipment design and layout must await close coordination between the radar and recorder groups.

4.2 Correlator

Other than a few artificial target samples on film, no special support equipment is now envisioned as required to checkout the correlator. It is assumed that complete photographic processing and film handling equipments will be provided through other channels.

Appendix XIV

TWO DIMENSIONAL HOLOGRAMS

Appendix XIV

TWO DIMENSIONAL HOLOGRAMS

This memorandum summarizes the main features of two dimensional holograms and discusses system improvements and trade-offs that are possible in coherent radar systems using optical correlation.

1.0 Generation

A two dimensional hologram is generated by recording a signal varying in frequency in both azimuth and range directions. The azimuth signal is produced in the usual way by the doppler frequency returns from the target. The range signal is produced by transmitting a long pulse during which the frequency is continuously changed, usually but not necessarily, in a linear manner.

It is well known that the range resolution of a radar depends on the frequency bandwidth of the transmitted pulse. High resolution is normally achieved by transmitting a short pulse. The bandwidth of a pulse of length t seconds (of constant frequency) is approximately $\frac{1}{t}$ cycles per second, thus the smaller t the greater the bandwidth and the greater the resolution.

Another method of increasing the bandwidth is to transmit a comparatively long pulse in which the frequency is swept from f_1 to f_2 as shown in Fig. 1. This is known as a "chirp" radar. By suitable processing, the long received pulse can be collapsed into a much shorter pulse of length

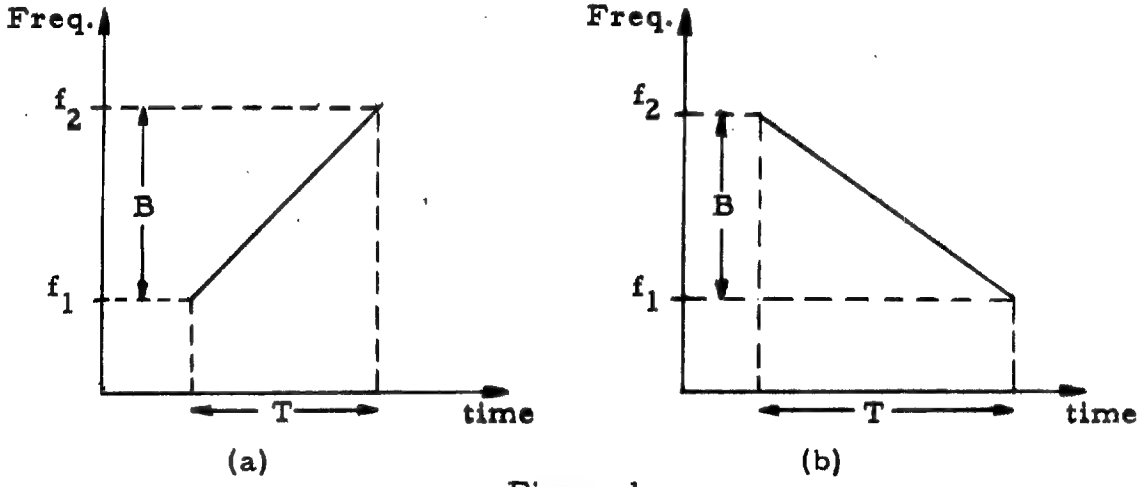

Figure 1

Chirp Frequency Sweeps

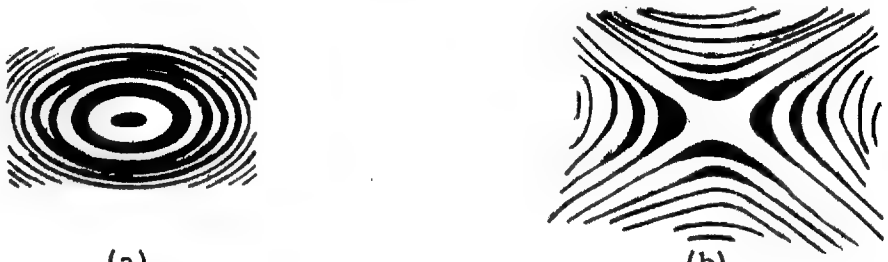

Figure 2

Zone Plates

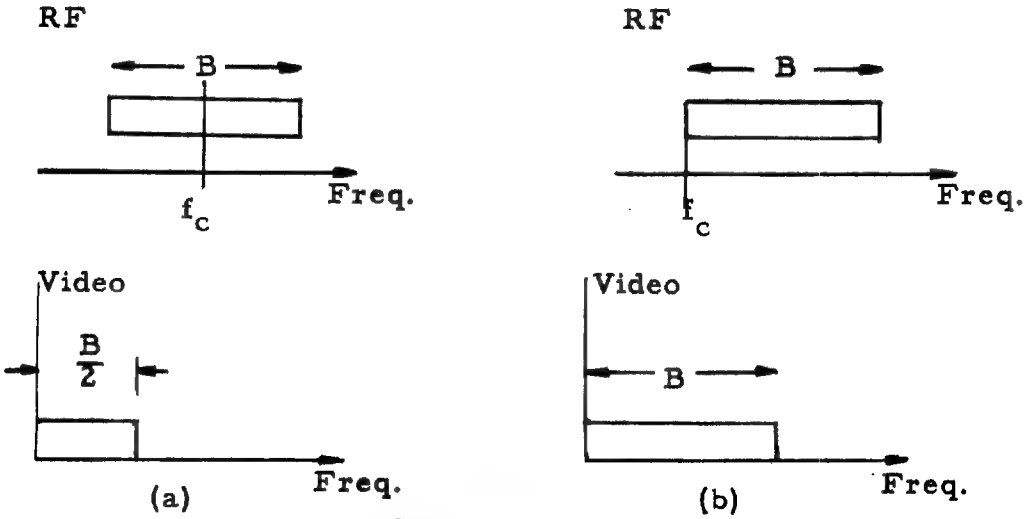

Figure 3

Demodulation

$t \approx \frac{1}{B}$ where B is the long pulse bandwidth. One advantage of this method is that the radiated pulse power from a peak power limited transmitter can be greatly increased, thereby improving the range without sacrificing resolution. Alternatively, the chirp system can be used to improve resolution at existing ranges.

These advantages are gained by any type of chirp signal processing; most chirp radars use electronic networks for collapsing the received pulse. However, when optical correlation is used an additional advantage accrues, namely that either the pulse spectrum or the doppler spectrum may be "folded", thus halving the bandwidth.

Referring to Fig. 1, the transmitted pulse of length T may be swept upwards in frequency from f_1 to f_2 as at (a) or downwards from f_2 to f_1 as shown at (b).

The doppler frequencies may also vary in either direction depending on whether the side looking antenna is squinted forward or backward.

When both frequencies vary in the same direction an elliptical pattern is recorded as shown in Fig. 2(a). While if the frequencies vary in opposite directions a hyperbolic pattern is recorded as in Fig. 2(b).

2.0 Demodulation

The received range pulse of bandwidth B may be demodulated either by placing the reference frequency in the center of the spectrum as in Fig. 3(a) or at the end of the spectrum as in Fig. 3(b). The resulting video spectrum is shown in each case. Placing the reference frequency in the center, folds the spectrum and halves the required video response.

The resulting holograms are shown for the elliptical mode in Fig. 4(a)

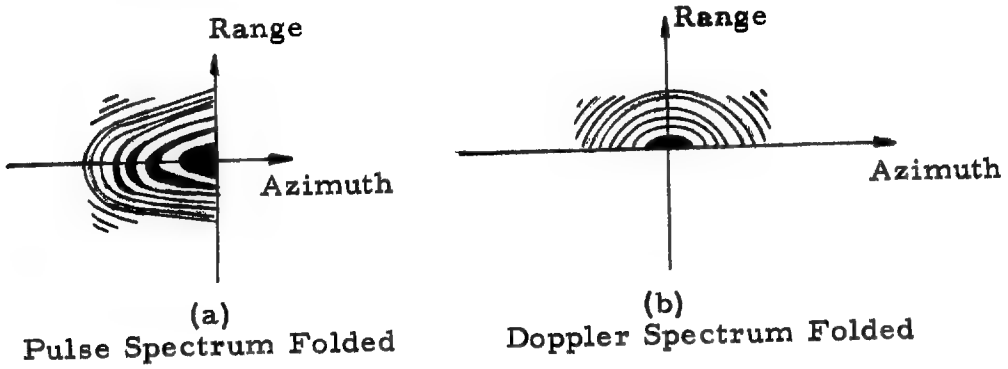

Figure 4

Folded Holograms

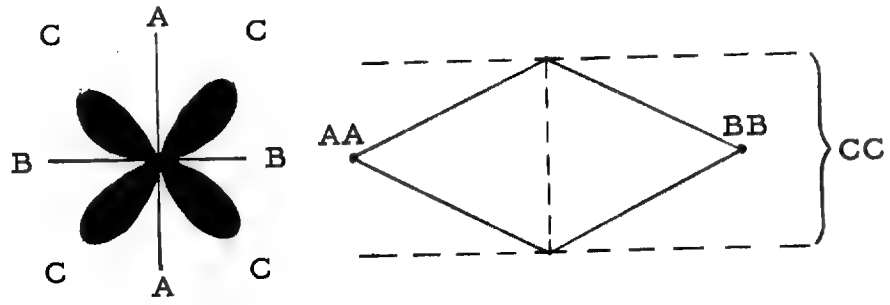

Figure 5

Image Formed by Hyperbolic Hologram

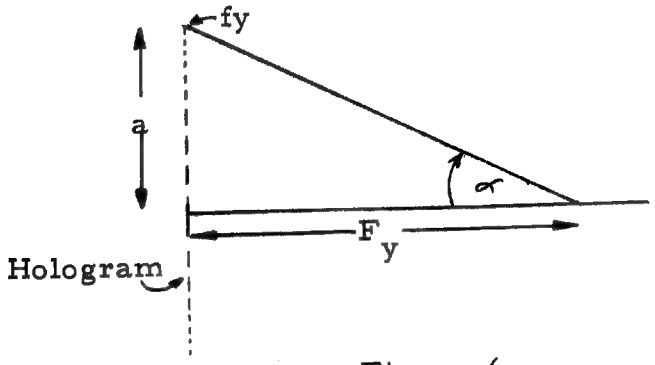

Figure 6

Focal Length Hologram

and (b). Folding the pulse spectrum gives the hologram of Fig. 4(a) in which the azimuth pattern is squinted. The features of this mode are:

(1) Video bandwidth is halved for the same range resolution.

(2) The highest range frequency to be written on film by the recorder is halved, i.e. recorder range resolution is effectively doubled.

Folding the doppler spectrum gives the hologram of Fig. 4(b). Features of this mode are:

(1) No azimuth squint is necessary.

(2) Doppler bandwidth is halved, so film speed may be reduced.

(3) Pulse repetition frequency may be halved, thus reducing range ambiguity problem.

3.0 Optical Correlation

The equations of the recorded patterns in polar form are

$$r^2 = \frac{a^2 b^2}{a^2 \sin^2\theta \pm b^2 \cos^2\theta}$$

A positive sign in the denominator is associated with an elliptical pattern, and a negative sign with a hyperbolic pattern.

The focal length of a zone plate pattern is given by $F = \frac{r}{\lambda \cdot f}$ where f is the radial spatial frequency at a distance r from the center. The focal length varies as the square of the linear dimension, thus we can write the focal length at any angle θ

$$F_\theta = Ar^2 = \frac{A a^2 b^2}{a^2 \sin^2\theta \pm b^2 \cos^2\theta}$$

If the focal lengths of the patterns along the x and y axes are Fx and Fy respectively, then by setting $\theta = 0$ and $\frac{\pi}{2}$ we get

$$Fx = \pm Aa^2$$

$$Fy = Ab^2$$

$$\frac{Fx.Fy}{A} = \pm Aa^2b^2$$

Thus,
$$F_\theta = \pm \frac{Fx.Fy}{Fx.\sin^2\theta \pm Fy\cos^2\theta}$$

In the case of an elliptical pattern, the focal length varies smoothly from Fx to Fy as θ increases from 0 to $\frac{\pi}{2}$.

However, in the case of a hyperbolic pattern it can be seen that the denominator must be zero at some angle θ_o, thus giving an infinite focal length at this angle. The image formed by a hyperbolic zone plate in a collimated beam would resemble Fig. 5. This can be corrected by the use of a cylinder lens.

The focal length of a cylinder lens at angle θ is

$$F_\theta(cyl) = \frac{Fc}{\cos^2\theta}$$

We require the combined focal length of the hyperbolic hologram and cylinder lens to equal that of an elliptical hologram at all orientations.

Thus

$$\frac{1}{F_\theta(\text{Hyp})} + \frac{1}{F_\theta(\text{Cyl})} = \frac{1}{F_\theta(\text{Ell})}$$

i.e.

$$\frac{Fx \sin^2\theta - Fy \cos^2\theta}{Fx.Fy} + \frac{\cos^2\theta}{Fc} = \frac{Fx \sin^2\theta + Fy \cos^2\theta}{Fx.Fy}$$

This gives $2Fc\,Fy = Fx.Fy$

or $Fc = \frac{Fx}{2}$

Thus a cylinder lens of focal length $\frac{Fx}{2}$ will correct a hyperbolic zone plate of any ratio Fx/Fy.

As optical correlators are in general astigmatic, the requirement of an additional cylindrical function does not necessarily imply an extra physical lens. It does mean, however, that elliptical and hyperbolic patterns require optical systems of different focal lengths.

4.0 Basic System Parameters

4.1 Long Pulse System

In a long pulse system, the chirped pulse bandwidth is determined largely by the frequency sweep and not by the pulse width. A system of this type has a large pulse compression ratio, in the order of 100 or more.

Let transmitted pulse length	= T seconds
Pulse bandwidth	= B cycles/sec.
Compression ratio, K	= TB
Velocity of propagation	= C inches/sec.
Range scale factor $\frac{\text{Ground Swath}}{\text{Film Width}}$	= Sy

Video bandwidth = W cycles/sec.

Then, length of range pulse in space = CT inches

Range pulse length on film, 2a = $\frac{C.T}{S_y}$ inches

Maximum hologram frequency f_y = $\frac{2W.S_y}{C}$

When the pulse spectrum is folded, W = $\frac{B}{2}$.

The ground resolution in range, as determined by effective pulse width, will be approximately

$$D \approx \frac{C}{2B}$$

The hologram focal length F in the range dimension can be determined from the diffraction formula (see Fig. 6)

$$\sin \alpha = \lambda o . fy \approx \frac{a}{F}$$

Thus

$$F = \frac{a}{\lambda o . fy}$$

The ratio $\frac{a}{fy} = \frac{a.c}{2B.Sy}$ does not vary with range squint.

Thus $F = \frac{a.c}{2.\lambda oB.Sy}$

If the pulse compression ratio K = TB, then substituting for a we get

$$F = \frac{KC^2}{4\lambda oB^2 Sy^2}$$

These relationships are shown graphically in Fig. 7. Starting on the left hand graph the required range resolution determines the approximate

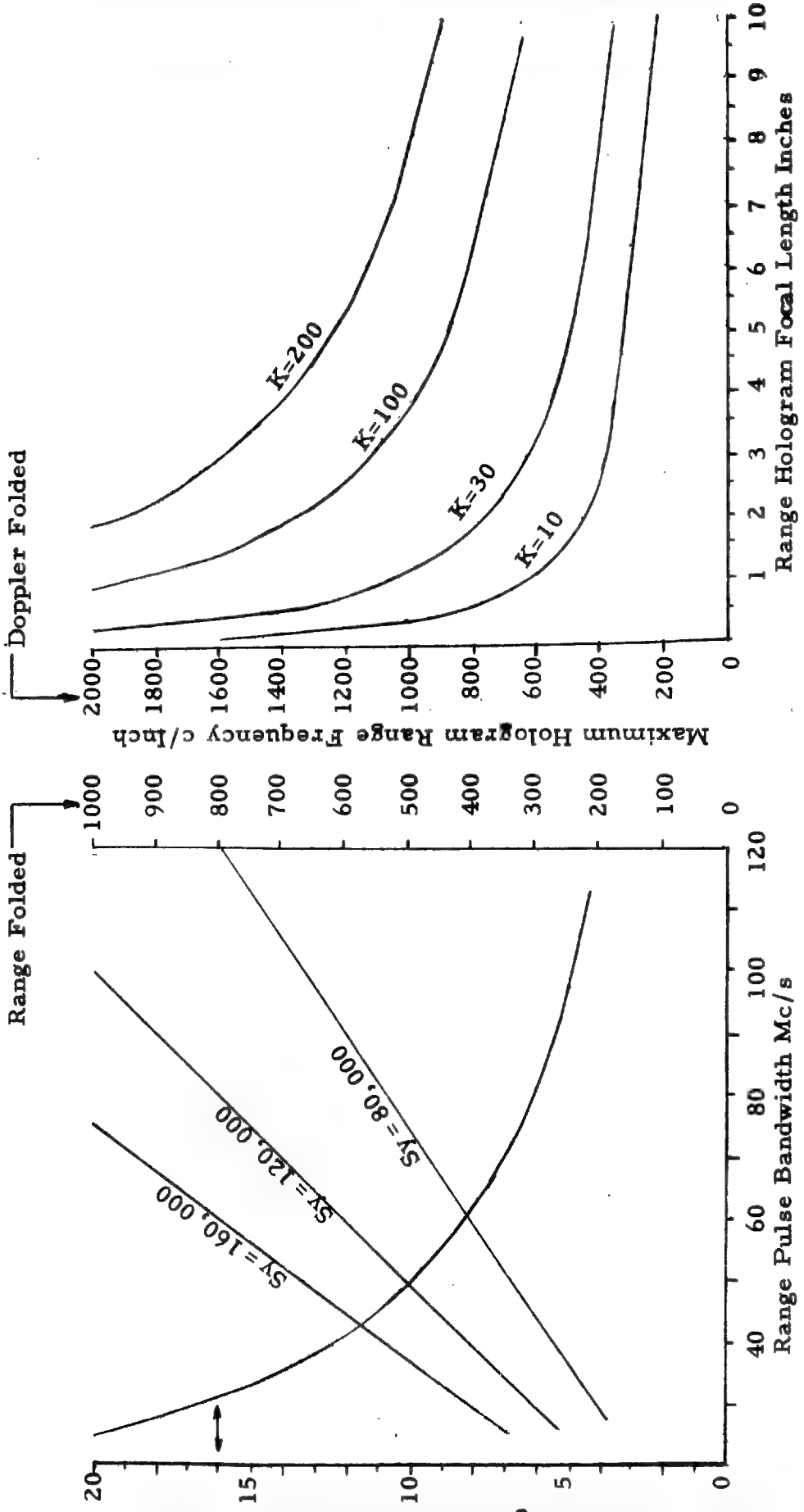

Figure 7

Chirp System Parameters

RF pulse bandwidth, B. When the range scale factor Sy is fixed, the hologram frequency depends on whether the spectrum is folded in range or azimuth. Finally, on the right hand graph the range hologram focal length can be found opposite the curve corresponding to the pulse compression factor K in use.

The FM sweep rate is equal to $\frac{B}{T} = \frac{B^2}{K}$.

For example, given a range resolution requirement of 5 feet, range scale factor Sy of 80,000 and chirp stretchout ratio of 100 we find that

(1) RF pulse bandwidth is approximately 100 Mc/s.

(2) Maximum range hologram frequency is 665 cycles/inch if folded in range of 1330 cycles/inch if folded in azimuth.

(3) Range hologram focal length is 2.15 inches.

(4) FM sweep rate is 100 Mc/s per second.

4.2 Short Pulse System

At small values of the pulse compression ratio K, the chirp pulse bandwidth is no longer independent of the pulse duration, but depends on the reciprocal of the pulse duration T.

This can be seen from Fig. 8, which shows the half-power bandwidth of rectangular pulses at different values of K. At K = 1, corresponding to a non-chirped pulse radar, the bandwidth is determined solely by the pulse envelope. When $K > 1$ an additional bandwidth is contributed by the FM sweep. At a compression ratio of $K \geq 100$, the pulse envelope spectrum becomes an insignificant part of the total bandwidth and can be ignored as in Section 4.1.

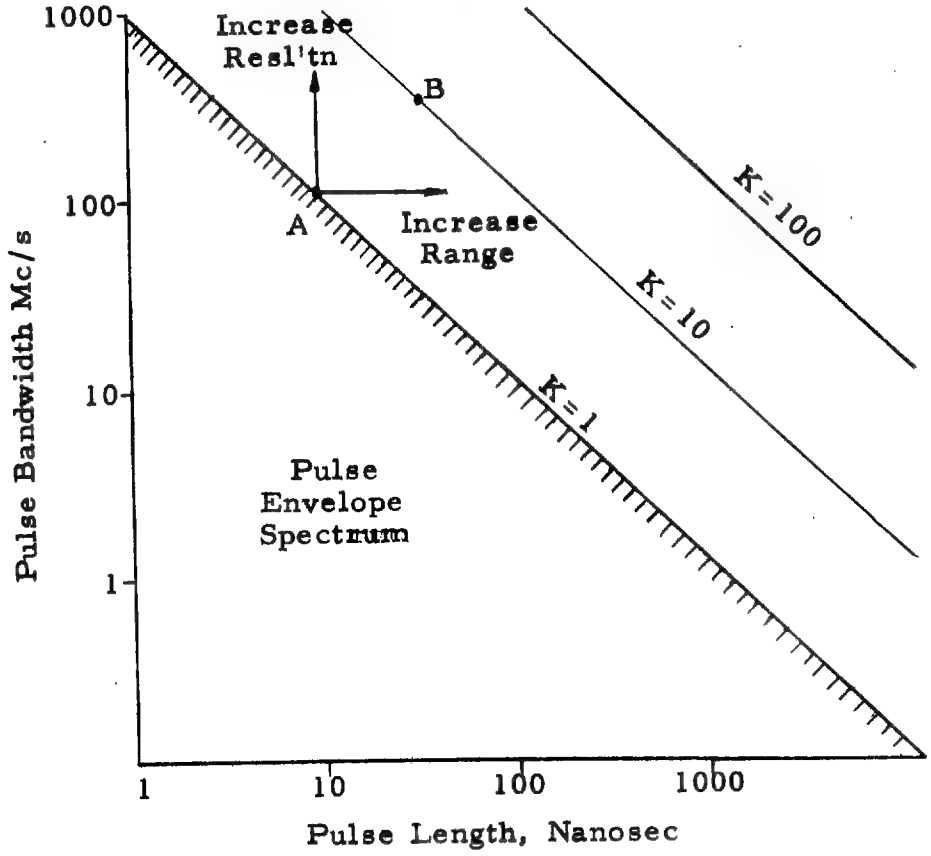

Figure 8

Pulse Bandwidth

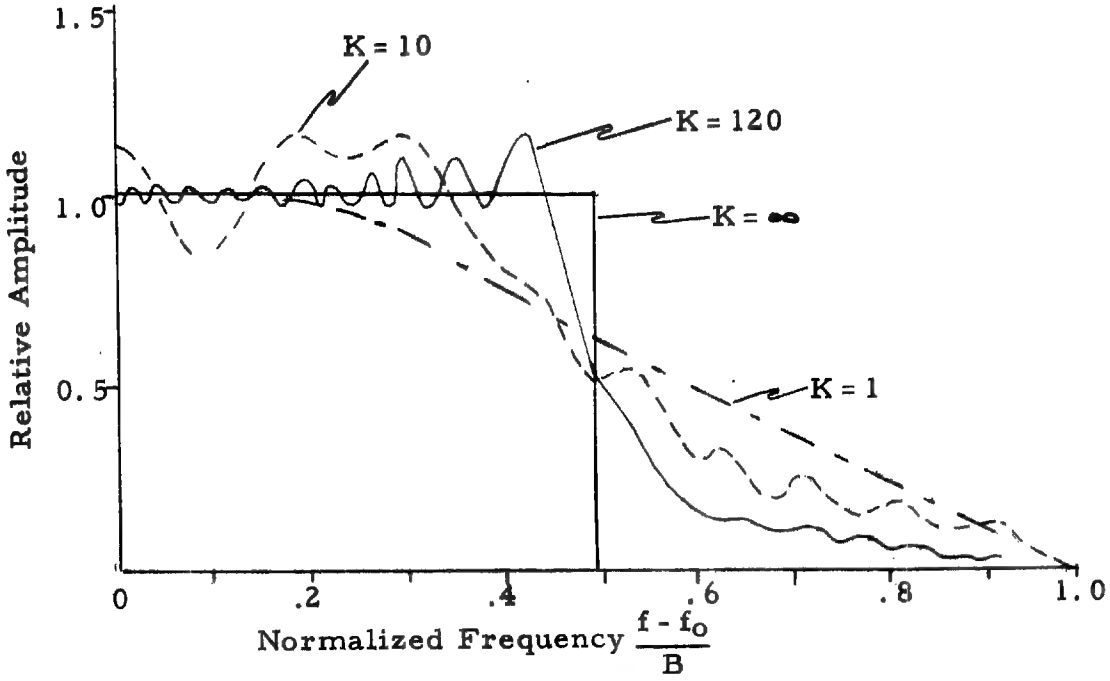

Figure 9

Pulse Frequency Spectra

In this section we are concerned with compression ratios in the region between 1 and 100, in which both pulse duration and FM sweep contribute to the total bandwidth. This is a case of practical interest if, for example, the performance of an existing pulse radar were to be increased by the addition of a small amount of chirp. If the existing pulse were specified by point A on Fig. 8, then the range, or resolution, or both could be increased by increasing K as shown. By using K = 10 and operating at point B for example, both resolution and pulse power would be improved by a factor of $\sqrt{10}$.

Figure 9 shows the frequency spectra of chirped pulses at several values of K. The ideal rectangular spectrum is obtained when $K = \infty$. The spectrum closely approximates the rectangular shape when K = 100, but when K = 10 it is very irregular in shape. As K approaches 1, the spectrum tends toward the sin x/x shape of a pure pulse radar.

It is instructive to note that the number of cycles N in the range dimension of the hologram is given by $N = a \cdot fy = W \cdot T$: If the hologram is folded in range, $W = \frac{B}{2}$ so that $N = \frac{K}{2}$. If the hologram extends to zero frequency then N = K. In other words the number of cycles in the hologram is equal to the compression ratio if a squinted system is used, or half the compression ratio if a folded system is used.

If K = 10 for example, the holograms appear as in Fig. 10(a) and (b). The correlated image width is the same in each case and is approximately equal to 1 cycle of the highest hologram frequency in a squinted system, or $\frac{1}{2}$ cycle of the highest hologram frequency in a folded system. At small values of K, however, the image will no longer be of the sin x/x form produced by a hologram containing a large number of cycles, but will be modified by the Fresnel diffraction pattern of the aperture.

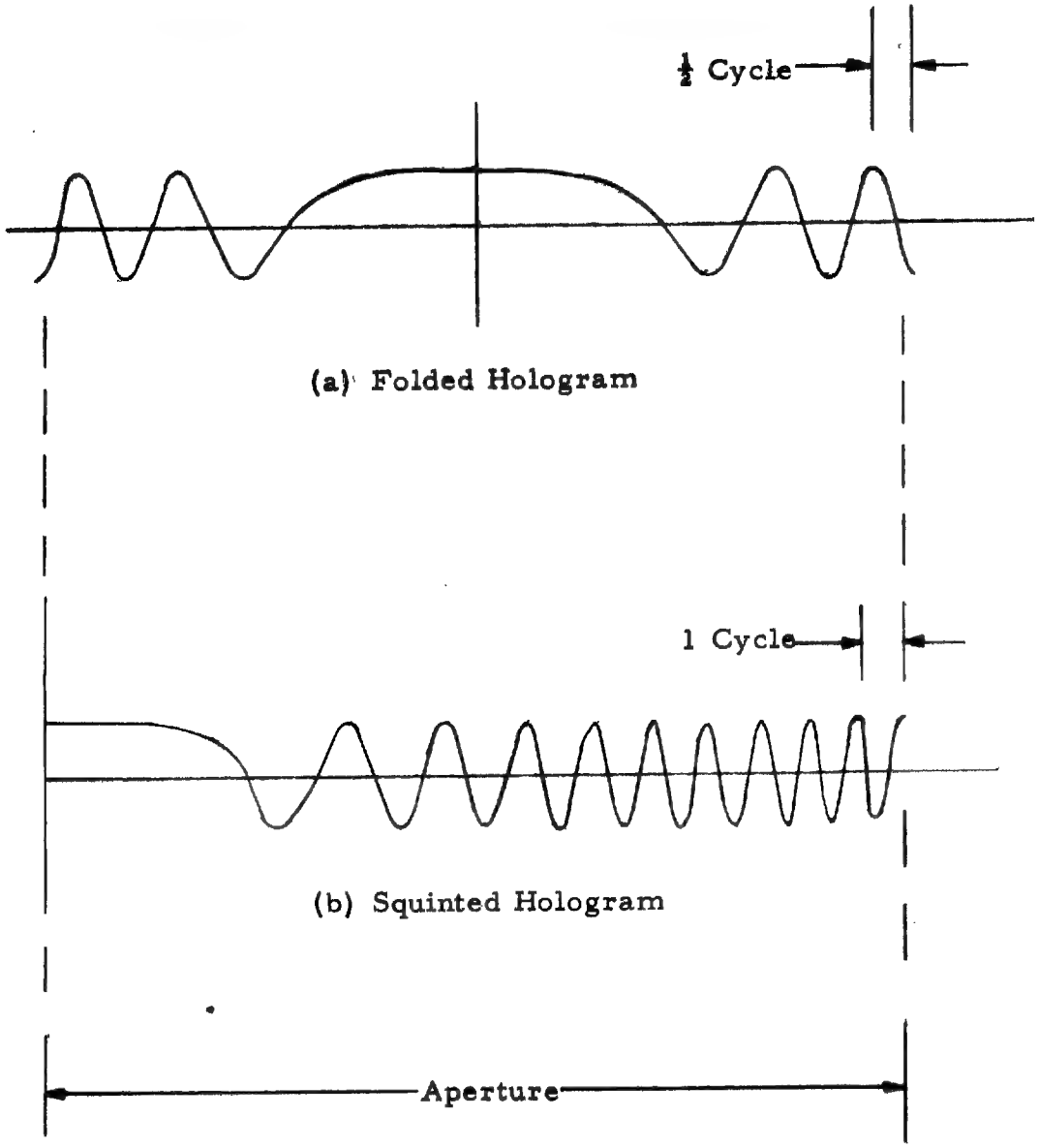

Figure 10

Comparison of Folded and Squinted
Holograms of Same Aperture and Focal Length

Appendix XV

SPECTRUM AND OUTPUT FOR OPTICALLY CORRELATED CHIRP SYSTEM

Appendix XV

SPECTRUM AND OUTPUT FOR OPTICALLY CORRELATED CHIRP SYSTEM

1.0 Spectrum

In the "chirp" system the radar resolution is increased by leaving the pulse length constant and using a "sinusoid" of linearly increasing rather than constant frequency. The purpose of this scheme is to increase resolution without sacrificing power.

The spectrum of the signal is found as follows. If the pulse starts at time -T and ends at time +T, and the frequency varies from w_o to $(w_o + \Delta w)$, during that interval, the function whose transform is to be taken is

$$f(t) = E_o e^{i(w_o + \frac{\Delta w}{T} t)t}, \quad |t| < T.$$

Taking the transform,

$$F(w) = E_o \int_{t=-T}^{t=T} e^{i\left[\frac{\Delta w}{T} t^2 + (w_o - w)\right] t} dt$$

Completing the square in the exponential and substituting

$$v_1 = \sqrt{\Delta w T} \left[-1 + \frac{w_o - w}{2\Delta w} \right]$$

and

$$v_2 = \sqrt{\Delta w T}\quad\left[1 + \frac{w_o - w}{2\Delta w}\right],$$

$$F(w) = \sqrt{\frac{T}{w_1}}\quad E_o\, e^{-\frac{(w_o - w)^2 T}{4\Delta w}} \int_{v_1}^{v_2} e^{i\xi^2}\, d\xi.$$

Letting the Fresnel Integral

$$\int_o^a e^{ix^2}\, dx$$

be denoted by $\Phi(a)$. the spectrum becomes,

$$F(w) = E_o \sqrt{\frac{T}{\Delta w}}\quad e^{-\frac{i(w_o - w)^2 T}{4\Delta w}}\quad \left[\Phi(v_2) - \Phi(v_1)\right].$$

Plots of the spectrum for various values of w_o and $\frac{\Delta w_1}{T}$ would involve the use of tables for the values of the Fresnel integral.

2.0 Output of Optical Correlator

If the data is recorded on film, the signals can be processed optically. The "chirp" signal is simply a zone plate and acts like a lens; the pulse acts like a mask which blocks out all but that portion of the zone plate for which the instantaneous signal is between w_o and w_1. The output taken in the focal plane of the zone plate consists of the interference of waves diffracted by the aperture (pulse) and focused by the zone plate. In the focal plane, this pattern

is the transform of the aperture.

3.0 System Resolution

Suppose that two targets are such that the data resulting from them is a pair of chirped pulses separated by a distance d. The question arises, what is the smallest value of d for which the correlated output can still distinguish the two targets.

To find the system resolution, consider first, the output of a single pulse. The zone plate intensity pattern is proportional to

$$1 + \cos \frac{\pi x^2}{\lambda f},$$

where x is distance from the zone plate center and f is the focal length of the plate for light of wavelength λ. Since the pulse extends from x_o to $(x_o + 2T)$, w_o and Δw are given by

$$w_o = \frac{\pi x_o}{\lambda f}$$

$$\Delta w = \frac{2\pi T}{\lambda f},$$

or letting v_o and Δv be the corresponding frequencies meausred in cycles (rather than radians) per unit distance,

$$v_o = \frac{\pi x_o}{2\lambda f}$$

$$\text{and } \Delta v = \frac{T}{\lambda f}.$$

For a square pulse, the spectrum is a $\frac{\sin x}{x}$ function. For a pulse of

duration 2T whose transform is obtained by use of a focusing device of focal length f, the first zero in the output (transform) plane occurs at a distance ξ from the origin with

$$\xi = \frac{\lambda f}{2T}.$$

If there are two such pulses whose centers are displaced by a distance d, their outputs will be displaced by the same distance. The resolution limit is approached when d is of the order of ξ. Setting d equal to ξ, the minimum separation for which resolution is possible is found to be

$$d = \frac{\lambda f}{2T} = \frac{1}{2\Delta v},$$

or

$$d = \frac{\pi}{\Delta w}.$$

It should be noted that the resolution is independent of the pulse duration and depends only on the (instantaneous) frequency band swept. This was the original purpose of using the chirp system.